Protein-Mineral Interaction of Purified Nacre Proteins with Calcium Carbonate Crystals

Vom Fachbereich für Physik und Elektrotechnik
der Universität Bremen

zur Erlangung des akademischen Grades eines

Doktor der Naturwissenschaften (Dr. rer. nat.)

genehmigte Dissertation

von

Dipl.-Phys. Laura Treccani

aus Rezzato (Italien)

1. Gutachter: PD. Dr. Monika Fritz
2. Gutachter: Prof. Dr. Horst A. Diehl

Eingereicht am: 10.Juli.2006
Tag des Promotionskolloquiums: 26.Juli.2006

Die Natur schafft immer von dem was möglich ist das Beste

(Aristoteles)

Acknowledgments

PD. Dr. Monika Fritz,
for giving me the possibility to work in her group and to discover the fascinating world of biomineralization, for the scientific and personal help, for the effort to understand me also if “sehr holperig war“;

Prof. Dr. Horst A. Diehl,
for the very kind and quick help with my “Gutachten”;

Prof. Dr. Radmacher,
for the nice welcome in Göttingen, for “switching the Biophysical lecture from German to English”;

All the members of the Biophysics Department, in particularly:

Fabian Heinemann,
for the help with the “oligo concentration”; for supporting and motivating me during good and bad times ,-)

Meike Gummich,
for the help with our aquarium, for taking care of me and for becoming a good friend; (take care of the abalone babies)

Marcus Prass,
for our long talks about success and frustration; we started together in Göttingen end we finish together in Bremen…..I wish good luck

Ilona Bär,
for the “schnelle Bestellungen” and for the nice atmosphere in the lab;

Holger Dotschke,
for the help to solve all the daily problems especially with laser printers;

Steffi Praußе,
for the “Trockene Früchte”;

Stefan von Cölln,
for the nice atmosphere in the lab and for the “Teebeutel”;

Jan Christian Martens,
for the engagement with our “WM Tip Spiel”;

Barbel Bödeker,
for the friendliness and for the beautiful “Osterneier”

Anja Resemann (Bruker Daltonics GmbH, Bremem), Regina Knitter (Forschungszentrum Karlsruhe GmbH, Germany), Dietmar Schwahn and Vitaliy Pipich (Institut für Festkörperforschung Forschungszentrum Jülich, Germany)

Susanne Kemper (Institut für Keramische Werkstoffe und Bauteile, University of Bremen) for the very friendly help with all the measurements.

Ulrike Schulz, Kerstin von Roden, Arne Schäfer, Leif Riemenschneider, Sven Blank and Sabine Khoshnavaz for the nice atmosphere in Göttingen.

Last but not least I want to thank all my family for supporting me all these years, for sharing with me all the difficulties, for being always close to me although the great distance between us. Thanks to my parents for being a constant inspiration, my point of reference and for showing me that nothing is impossible.

Bremen, 10th July 2006

Contents

1 Summary

Nacre, the pearly lustrous inner surface of mollusc shells, is a biogenic polymer-mineral composite. It consists of calcium carbonate (more than 95% weight) and a small amount of organic molecules (less than 5% weight) distributed within as well as outside the mineral phase. This small amount of organic material, secreted by the mollusc, guides nucleation and growth of the mineral phase, through a well regulated self-organization process, taking place at ambient conditions. The final product is a composite material that presents superior physico-chemical properties like high mechanical toughness and resistance against corrosion in seawater. The unique features of nacre, arising from its composition, peculiar structure and interplay of the organic and mineral phase, make nacre a fascinating example for inspiring new synthetic composites.

Nacre is composed of calcium carbonate and organic macromolecules intimately associated. Mature nacre consists of pseudohexagonal platelets of aragonite (a calcium carbonate polymorph). The platelets (5 to 10 µm diameter and 500 nm height) are arranged in flat layers, parallel to each other in the vertical direction. The mineral layers are alternated with interlamellar, thin sheets (40 nm) of organic matrix that consists of water soluble and water-insoluble proteins as well as chitin (a polysaccharide).

Despite the central role of the organic matrix, which forms the mold for the nucleation and growth of the mineral phase, its composition and in particular its interactions with the mineral phase have not been completely understood.

The aim of this thesis was the characterization of the functions of water-soluble proteins extracted from the organic matrix of abalone (*Haliotis laevigata)* nacre on calcium carbonate mineralization. The influences at the molecular scale of a new group of proteins, the *intracrystalline proteins,* and two already sequenced water-soluble proteins, *perlucin* and *perlinhibin*, on calcium carbonate mineralization were investigated *in vitro*. Because the function of the proteins is closely related to their molecular properties biochemical investigations were carried out to obtain more

detailed information.

During this thesis a new group of proteins incorporated into single aragonite platelets, the *intracrystalline proteins,* has been isolated. Intracrystalline proteins are present in a low concentration and are supposed to be highly negatively charged. In the course of this thesis new strategies for isolation and purification of proteins from single aragonite platelets were developed. Three main proteins with a molecular weight of approximately 6, 14 and 25 kDa respectively have been identified. The biochemical analysis was carried out by precipitation (which turned out to be the most efficient method to obtain a sufficient amount of proteins for further investigation), by chromatographic techniques (ion exchange chromatography and high pressure liquid chromatography), mass spectroscopy and gel electrophoresis combined with differential staining.

The distribution of the intracrystalline proteins within single aragonite platelets was investigated with neutron scattering. Neutron scattering revealed the presence of domains with a size of 40 Å in the aragonite platelets. Furthermore a new substructure in nacre was identified; domains with a size of approximately 300 Å were detected. These domains are with high probability protein aggregates.

The influences of intracrystalline proteins on the growth of calcite surfaces were investigated *in vitro* by atomic force microscopy (AFM). AFM, chosen because of its ability to image *in real* time single proteins in solutions, revealed that intracrystalline proteins act as inhibitors of calcite growth. In addition this group of proteins is able to induce the formation of aragonite, the same calcium carbonate polymorph occurring in abalone nacre.

Furthermore the interactions of *perlucin* and *perlininhibin*, two already sequenced water-soluble proteins, with calcium carbonate were characterized.

The influence of perlucin, the most abundant water-soluble protein of *H. laevigata*, on calcium carbonate was investigated by the “ammonium carbonate vapour diffusion technique”, a crystallization technique. It could be shown that perlucin induces *in vitro* nucleation of calcium carbonate crystals. Crystals grown in the presence of perlucin presented a stepped habit indicating that perlucin induces the nucleation of new mineral layers. This result confirmed previous investigations performed by atomic force microscopy.

The effect of perlinhibin on calcium carbonate crystallization was investigated with AFM and ammonium carbonate vapour diffusion technique. AFM showed that the interaction of perlinhibin with calcium carbonate minerals is very specific. Perlinhibin interacts only at specific crystal sites, suppressing their growth at the binding site. X-ray investigation of a calcite surface grown in the presence perlinhibin revealed that this protein is able to induce the formation of aragonite at ambient conditions.

Parallel to the investigation of the influences of nacre proteins on calcium carbonate mineralization, the effects of the synthetic polymer, poly-γ-methyl-L-glutamate, on calcium carbonate crystallization were studied with the ammonium carbonate vapour diffusion technique. This investigation was aimed at a better understanding of the interactions between the natural nacre proteins and calcium carbonate minerals. Poly-γ-methyl-L-glutamate is supposed to resemble the structure and properties of nacre proteins and therefore to interact with calcium carbonate minerals like nacre proteins. The possibility to use easily available synthetic molecules to understand and nacre formation and synthesize composite materials similar to nacre was here initiated.

Poly-γ-methyl-L-glutamate added to calcium carbonate solutions induced precipitation of flat polygonal crystals, with a shape resembling that of natural nacre aragonite platelets. This result strengthened the hypothesis that synthetic polymers may be a valid candidate to substitute natural proteins and to produce composite material inspired by nacre.

The possibility to use easily available synthetic molecules to produce composite materials that mimic nacre would have a high impact on the development of new high performance materials.

2 Introduction

2.1 Biomineralization

Biological mineralization (biomineralization) is a widespread phenomenon among living systems [Lowenstam, 1989]. It indicates the formation of minerals regulated by a small amount of organic molecules, which exerts a substantial control on the whole process and leads to the formation of controlled inorganic-organic composites. Biominerals typically present substructures of uniform size, novel crystal morphology, specific crystallographic orientation and interesting physical properties [Mann, 2001].
Organisms mainly synthesize organic/inorganic composites for the generation of protective and sustaining structures and to provide themselves with major evolutionary adaptation. The first biomaterials have been produced 500 million years ago.
Biomaterials are usually produced very slowly by assembling available materials, normally in aqueous media at ambient conditions. The chemical composition is mainly dominated by calcium carbonate, calcium phosphate and silica. Calcium minerals represent some 50% of all known biogenic minerals, presumably reflecting the abundance of calcium in the ocean as well as its widespread use as cellular messenger molecule [Addadi and Weiner, 1992]. Nevertheless organisms are able to form more than sixty different types of minerals with shapes that defy the geometrical restrictions of the 230 classical space groups.
In general mineralized tissues are produced by cell-mediated processes. The small amount of organic molecules exerts a high level of control on the spatial regulation, growth of mineral phase and development of microarchitectures. The mechanisms of biofabrication are usually very complex at the molecular scale, they can be divided into two main categories: *biologically induced mineralization* and *biologically controlled mineralization*.

2.1.1 Biomineralization mechanisms

Biologically induced mineralization refers to processes by which an organism modifies its local microenvironment creating conditions suitable for the chemical precipitation of extracellular mineral phases. Mineral formation in aqueous environments is achieved by introducing small perturbations, as biologically produced metabolic end-products, or the release of particular ions by the cells, that will induce the mineral to precipitate [Mann, 2001]. Biologically induced mineralization appears to be the predominant process among fungi and protista, many forms of pathologic mineralization occur under similar circumstances. Some examples of biologically induced minerals are presented in fig. 2.1 (A-C).

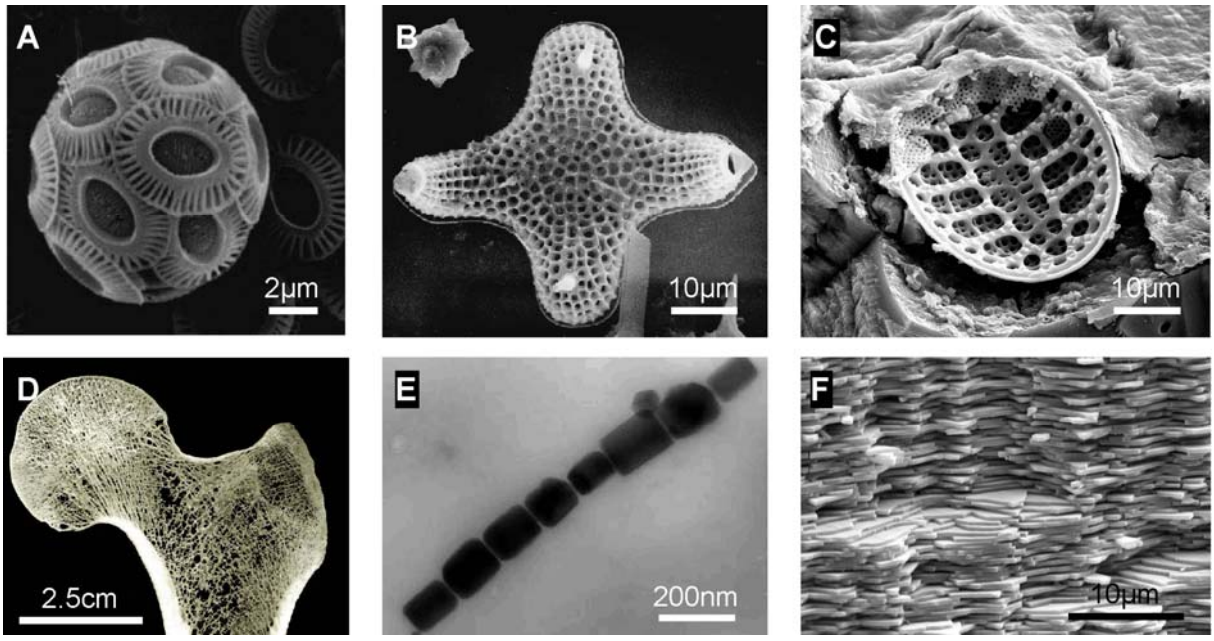

Fig. 2.1. A-C. Scanning electron microscopy (SEM) images of biologically induced minerals. A. Coccolith *Emiliana huxleyi*. Coccoliths are individual plates of calcium carbonate formed by coccolithophores, single-celled algae. B. Diatom Bacillariophyta *Odontella.* Diatoms are a group of eukaryotic algae. Most diatoms are unicellular organisms; the cells are encased within a unique cell wall made of silicate. C. Diatom incorporated into the calcite layer of shell of *H. laevigata.* D-F. Examples of biologically controlled minerals. D. SEM of a cross section of a bone. Bones are relatively hard and lightweight composite materials, consisting of calcium hydroxyapatite and collagen. E. Magnetite crystals in a magnetotactic bacterium. Magnetotactic bacteria are able to form iron magnetic crystals to orient themselves with the Earth magnetic field. F. Cross section of nacre of *Haliotis laevigata*.

The second mechanism is called biologically controlled biomineralization (or boundary organized biomineralization [Mann, 2001]), in which inorganic particles are grown within or on some organic matrix produced by the organism. The organic macromolecules do not just induce nucleation but control the growth pattern of the mineral phase, selecting the faces of the mineral crystallites, the packing of the crystallites and the microarchitecture. Furthermore the organic macromolecules influence the mechanical properties of the biomaterial.

A specialized cellular or macromolecular machinery is responsible for secretion of the biomolecules. The organic material, mostly composed of proteins, glycoproteins or polysaccharides, acts as nucleator, cooperative modifier and matrix for the mineral ions.

Typically in biological controlled mineralization the site of mineral formation is sealed off from the environment by a barrier of macromolecules through which ions cannot freely diffuse. The creation of closed compartments, termed *space delineation* [Wilbur, 1984], is fundamental for the control of mineralization and it is usually achieved by polymerization of water-insoluble macromolecules (proteins and/or polysaccharides). Space delineation as a mean of exerting control over the mineralization probably derives from the necessity to finely control the composition of the mother liquor from which mineral forms. It has been proposed that in molluscs the periostracum, a non-calcareous membrane covering the shell, shows selective ion-permeable properties that facilitate the mineral formation [Digby, 1965].

Controlled mineralization begins with the synthesis of an array of macromolecules (organic matrix) that are secreted by specialized cells into the extracellular space, where they self-assemble into a three-dimensional framework. The formation of a saturated solution, precondition for mineralization, is also a cell-regulated process. Cells can pump special ions into mineralizing compartments. Cations and anions are kept separated and are introduced in the solution in a controlled sequence. The composition of the ions for the mineralization is determined by the manner in which they are extracted from the environment, transported through the tissues, and introduced into the mineralization site [Lowenstam, 1989].

Once the local saturation in the delineated space is reached the crystallization can take place spontaneously (when a lower energy state is reached), or nucleation and growth of the mineral can be initiated by molecules in solution. Macromolecules have a dramatic influence on mineralization. They may specifically inhibit the formation of

nascent nuclei of one mineral phase and allow another form. It has been demonstrated that glycoproteins extracted from mollusc shell can inhibit calcite crystal nucleation *in vitro,* whereas absorbed on a solid substrate, they become efficient nucleators [Addadi and Weiner, 1985]. Examples of biological controlled minerals are shown in fig. 2.1 (D-F).

2.2 Calcium carbonate mineralization

Calcium carbonate ($CaCO_3$) is one of the most abundant mineral species in nature. It occurs in precipitated minerals and rocks (*e.g.* marble and chalk) and as biogenic composites (*e.g.* seashell and egg shell). The crystallization of calcium carbonate in aqueous solution is a complex process, influenced by external factors like supersaturation, temperature, pressure and presence of impurities (ions or macromolecules) in the solution. The intent of this chapter is to give an overview of the main aspects related to the formation of geological calcium carbonate minerals and of the shell of *Haliotis laevigata*, a sophisticated example of biologically controlled calcium carbonate mineral.

2.2.1 Precipitation of calcium carbonate in aqueous solutions

Distribution of carbonate species

Calcium carbonate precipitation in aqueous solution is strongly regulated by the pH-dependent acid-base equilibria of carbonic acid (H_2CO_3) in its different protonated states. Carbon dioxide (CO_2), the anhydrous form of carbonic acid, dissolves according to *Henry's law* and further reacts forming H_2CO_3 and hydrogen carbonate (HCO_3^-) [Mortimer, 1996].
The equilibria of the reactions can be summarized as follows

$$CO_{2(gas)} \Leftrightarrow CO_{2(aq)} \quad \textbf{(2-1)}$$

$$CO_{2(aq)} + H_2O \Leftrightarrow H_2CO_3 \quad \textbf{(2-2)}$$

$$H_2CO_3 \Leftrightarrow H^+ + HCO_3^- \quad \textbf{(2-3)}$$

$$HCO_3^- \Leftrightarrow H^+ + CO_3^{2-} \quad \textbf{(2-4)}$$

To calculate the pH-dependence of the concentrations the following dissociation

steps have to be considered

$$H_2CO_3 + H_2O \Leftrightarrow HCO_3^- + H_3O^+ \qquad pK_1=3.88 \qquad \textbf{(2-5)}$$

$$HCO_3^- + H_2O \Leftrightarrow CO_3^{2-} + H_3O^+ \qquad pK_2=10.33 \qquad \textbf{(2-6)}$$

Carbonic acid is an (highly instable) intermediate state of the reaction of dissolved carbon dioxide with water to hydrogen carbonate.

The first dissociation step (2-5), which depends on the hydration of dissolved CO_2 (2-2), can be considered a two-step reaction, with H_2CO_3 as intermediate highly instable product

$$2H_2O + CO_{2(aq)}(\Leftrightarrow H_2CO_3 + H_2O) \Leftrightarrow HCO_3^- + H_3O^+$$

$$H_2O + H_2CO_3^* \Leftrightarrow HCO_3^- + H_3O^+ \qquad pK_0=6.35 \qquad \textbf{(2-7)}$$

where pK_0 is the effective acid dissociation constant of the reaction (3-4). H_2CO_3* is defined as the sum of CO_2(aq) and dissociation of H_2CO_3 [Dreybrodt, 1988].

The species involved react according to the *law of mass action* that can be expressed in term of pH as follows

$$10^{(-pK_2+pH)} = \frac{[CO_3^{2-}]}{[HCO_3^-]} \qquad \textbf{(2-8)}$$

$$10^{(-pK_0+pH)} = \frac{[HCO_3^-]}{[H_2CO_3^*]} \qquad \textbf{(2-9)}$$

The overall concentration of the three different carbonate species ([H_2CO_3*], [HCO_3^-] and [CO_3^{2-}]) and their pH-dependency are shown in fig. 2.2 [Heinemann, 2005].

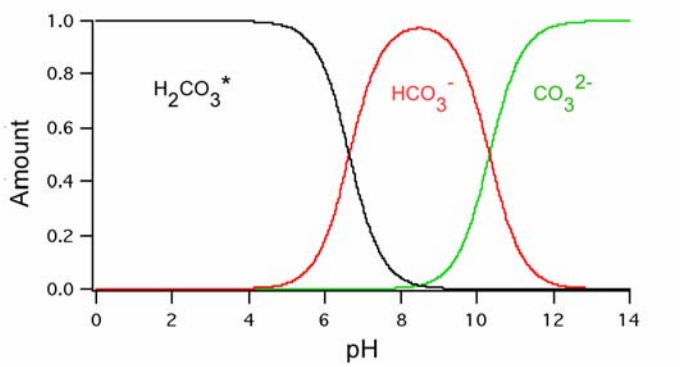

Fig. 2.2. Distributions of carbonate species in relation to the pH of the solution. H_2CO_3*, which represents the sum of dissolved CO_2 and H_2CO_3, predominates at low pH range. HCO^{3-} is the most abundant species at intermediate pH values; CO^{2-}_3 dominates at high pH values [Heinemann, 2005].

Dissolution and precipitation of calcium carbonate crystal in solution

Starting from the dissociation of calcium carbonate in Ca^{2+} and CO_3^{2-} (2-10), the *solubility* of calcium carbonate (*K)*, derived from the *laws of mass action,* the *solubility product (L)* and the *relative saturation* (σ) of a $CaCO_3$ solution are defined as follows

$$CaCO_3 \Leftrightarrow Ca^{2+} + CO_3^{2-} \quad \textbf{(2-10)}$$

$$K = \frac{[Ca^{2+}][CO_3^{2-}]}{[CaCO_3]} \quad \textbf{(2-11)}$$

$$L_{CaCO_3} = [Ca^{2+}][CO_3^{2-}] \quad \textbf{(2-12)}$$

$$\sigma = \sqrt{\frac{[Ca^{2+}][CO_3^{2-}]}{L_{CaCO_3}}} \quad \textbf{(2-13)}$$

According to (2-13) calcium carbonate minerals in solution can form if Ca^{2+} is available in solution and if the product of the concentration of Ca^{2+} and CO_3^{2-} is higher than the solubility product ($[Ca^{2+}]$ $[CO_3^{2-}]$ > L). The *solubility value* (square root of (2-12)) is about 5.9 x 10^{-5} mol/L for calcite and 7.7 x 10^{-5} mol/L for aragonite [Chou et al., 1989].

Dissolution and precipitation of calcium carbonate minerals are pH-dependent reactions. At acidic pH (pH < 3.5) calcium carbonate strongly dissolves; at intermediate pH values (between 3.5 and 7.8) nearly no dissolution or precipitation

occurs, whereas at pH values above 7.8, calcium carbonate spontaneously precipitates [Chou et al., 1989].

The reactions regulating the precipitation and/or dissolution of $CaCO_3$ minerals in solution can be summarized as follows

$$CaCO_3 + H^+ \Leftrightarrow Ca^{2+} + HCO_3^- \quad \textbf{(2-14)}$$

$$CaCO_3 + H_2CO_3^* \Leftrightarrow Ca^{2+} + 2HCO_3^- \quad \textbf{(2-15)}$$

$$CaCO_3 \Leftrightarrow Ca^{2+} + CO_3^- \quad \textbf{(2-16)}$$

The dissolution of carbonate can take place at moderate pH values and is regulated by reactions (2-14) and (2-15). When the reaction (2-14) dominates the dissolution of carbonate takes place with relative pH-increment. Reaction (2-16) represents the precipitation of calcium carbonate and its equilibrium is shifted to the left. If carbonate ions are used, the equilibrium of (2-6) and (2-7) modifies inducing dissociation of H^+ and consequent pH decreasing [Otaki, 1988].

2.3 Calcium carbonate polymorphs

Calcium carbonate precipitates in three crystalline anhydrous polymorphs: *calcite, aragonite* and *vaterite*[1] (fig. 2.3). The polymorphs present the same chemical composition but a different arrangement and/or conformation of the ions in the crystal lattice.

[1] Calcium carbonate forms also two crystalline hydrous polymorphs (*$CaCO_3$ monohydrate and $CaCO_3$ hexahydrate*) and amorphous precipitates.

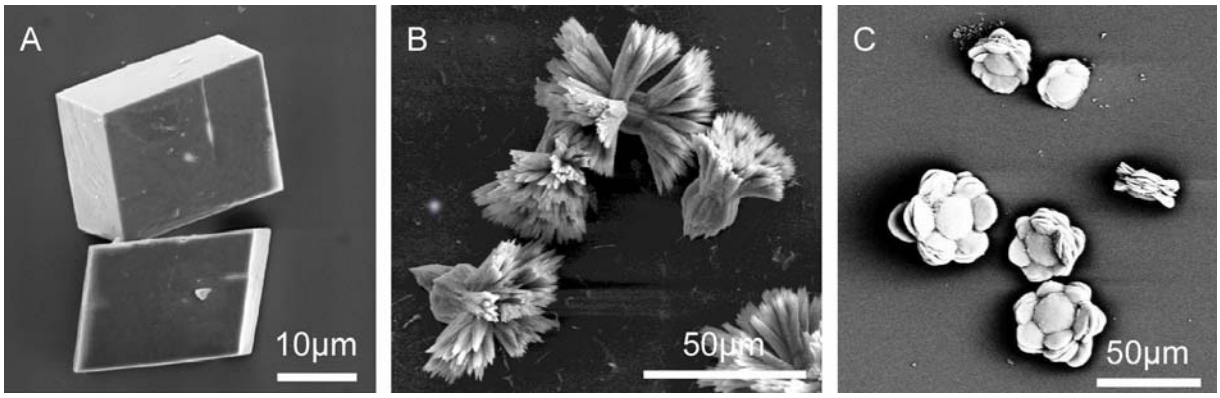

Fig. 2.3. SEM images of allotropic calcium carbonate crystals precipitated from saturated calcium carbonate solutions. A. Calcite crystals are characterized by a rhombohedral shape. Calcite is the most abundant and thermodynamically stable polymorph at ambient conditions. B. Aragonite typically forms needle-like crystals. C. Vaterite florets. Vaterite is the most thermodynamically unstable polymorph.

Calcite is the most abundant and thermodynamically stable polymorph at ambient conditions and it is well known for its double diffraction properties. The smallest unit cell is an acute rhombohedron containing two $CaCO_3$ units. The calcite structure consists of alternating sheets of Ca^{2+} and CO_3^{2-} perpendicular to the *c*-axis (*ab*-plane) of the crystal and spaced at intervals of *c*/12 (fig. 2.4).

Each CO_3^{2-} consists of a carbon ion at the centre of a planar group of oxygen atoms, whose centres define an equilateral triangle (the O-C-O bond angle is 120°). The CO_3^{2-} groups are identically oriented within one layer and the orientation reverses between adjacent layers. Each Ca^{2+} ion has six immediate CO_3^{2-} neighbours, oriented such that one oxygen from each CO_3^{2-} forms the immediate neighbour of calcium. Each Ca^{2+} ion thus occupies an octahedral environment of oxygen atoms [Meldrum, 2003].

Aragonite presents the same alternating structures of Ca^{2+} and CO_3^{2-} perpendicular to the *c*-axis of the crystal (fig. 2.4). The carbonate ions do not lie in a single plane, some CO_3^{2+} are raised in the vertical direction to form a second layer. The CO_3^{2-} groups lie in two planes parallel to the *a*-axis that point in opposite directions while in calcite they point in the same direction.

Each Ca^{2+} is surrounded by six CO_3^{2-} groups bound via two oxygens, while the remaining three CO_3^{2-} are bound by one oxygen, leading to nine immediate oxygen neighbours [Meldrum, 2003].

Vaterite, the most thermodynamically unstable polymorph, shows a hexagonal

symmetry. The Ca^{2+} and CO_3^{2-} groups are organized in alternating layers parallel to the *c*-axis (fig. 2.4), but in contrast to calcite and aragonite, the plane of CO_3^{2-} groups is parallel to the *c*-axis. Vaterite is very rare in nature, it is a common synthetic product of solution precipitations and mostly found in calcareous biomaterials [Meldrum, 2003].

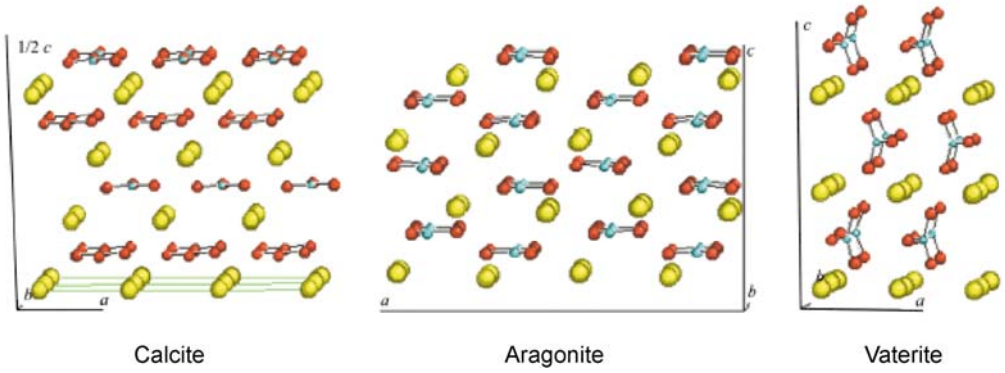

Fig. 2.4. Schematic representation of the crystal structure of calcite, aragonite and vaterite. Calcium atoms (yellow), carbon (blue), oxygen red. Calcium carbonate polymorphs consist of alternating layers of calcium ions (Ca^{2+}) and carbonate groups (CO_3^{2-}). In calcite the layers are perpendicular to the *c*-axis and spaced at intervals of *c*/12. In aragonite the Ca^{2+} and CO_3^{2-} are perpendicular to the *c*-axis, but all the CO_3^{2-} groups do not lie in a single plane, as in calcite. In aragonite some CO_3^{2+} are raised in the vertical direction to form a second layer. In vaterite CO_3^{2-} groups is parallel to the *c*-axis [Meldrum, 2003; Falini et al., 2000].

Some physical properties of calcium carbonate polymorphs are summarized in the following table.

	Density [g/cm^3]	Hardness (Mohs scale)
Calcite	2.71	3
Aragonite	2.93	3.5 - 4
Vaterite	2.54	3

Table 1. Some physical properties of calcite, aragonite and vaterite. The hardness is calculated according to the Moh´s scale. The Moh´s scale is a scale for classifying minerals based on relative hardness, determined by the ability of harder minerals to scratch softer ones. The scale includes (in order from softest to hardest): 1. talc; 2. gypsum; 3. calcite; 4. fluorite; 5. apatite; 6. orthoclase; 7. quartz; 8. topaz; 9. corundum; 10. diamond [www.webmineral.com].

2.3.1 Polymorph formation and crystal morphology modification

The formation of a certain polymorph and the morphology of a crystal are determined by intermolecular interactions between molecules in the crystal as well as by a number of external parameters such as solvent supersaturation, temperature and presence of impurities (foreign ions or macromolecules). Changes in any of these factors may lead to dramatic modifications in crystal morphology. In particular minute amounts of impurities present in solution during crystallization, may induce morphological changes when they are selectively adsorbed at specific surfaces of the growing crystal.

Influence of temperature

The abundance of $CaCO_3$ polymorphs formed by precipitation in aqueous solution depends strongly on the temperature.
At ambient temperature calcite is the most dominant polymorph whilst aragonite is the most dominant species at T > 50°C (fig. 2.5). Vaterite is metastable and presents a higher solubility than the other forms of calcium carbonate; vaterite usually converts by exothermical process into calcite (at low temperature) or aragonite (at above 40°C) [Otaki, 1988].

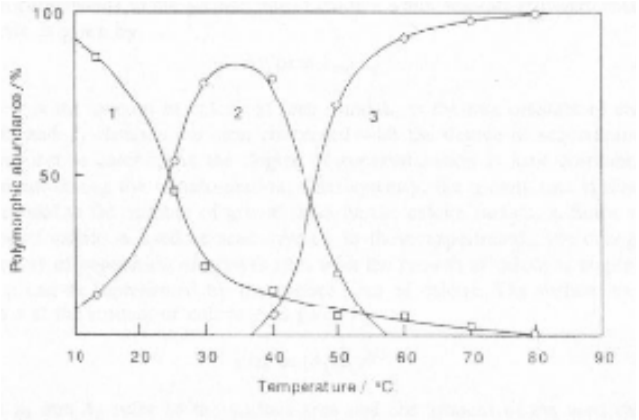

Fig. 2.5. Abundance of crystalline calcium carbonates as a function of temperature. Calcite (curve 1) is the most abundant polymorph at lower temperatures. Vaterite (curve 2) predominates at intermediate temperatures. Vaterite is metastable and usually converts into calcite (at low temperature) or aragonite (at above 40°C). Aragonite (curve 3) is the most abundant polymorph at temperatures higher at 50° C [Otaki, 1988].

Aragonite is stable at higher temperature and pressure (fig. 2.6). If aragonite is heated up to 400° C, it converts endothermically into calcite if the pressure is not increased. The aragonite-calcite transformation is a *reconstructive transformation* involving breaking and formation of chemical bonds and large translations of calcium and the carbonate ions in the *ab*-plane [Redfern et al., 1989].

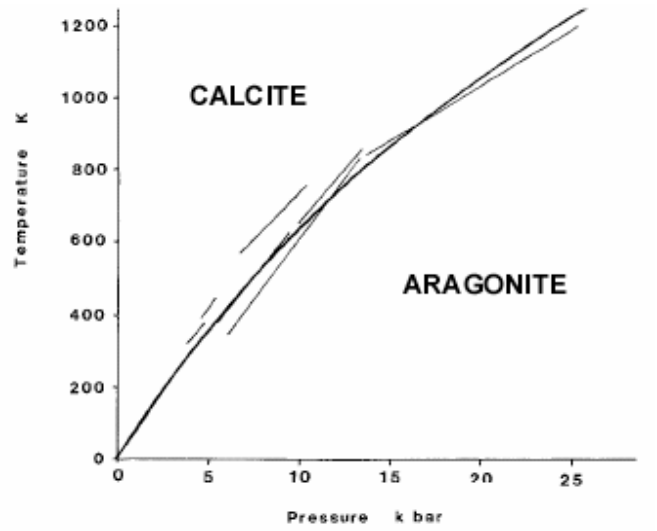

Fig. 2.6. Calcite-aragonite phase transition diagram. Calculated (thick line) and experimental (thin lines) equilibrium curves between the two mineral phases. Calcite is stable at higher temperatures, whereas aragonite converts endothermically into calcite at temperatures higher than 400° C, if the pressure is not increased. Adapted from [Redfern et al., 1989; Salje and Viswanathan, 1976].

Influence of magnesium ions

Polymorph formation or modification of polymorph morphology is highly influenced by the presence of metal foreign ions (*metal dopants*).

In natural seawater magnesium is the principal modifier of calcite morphology. Incorporation of magnesium ions (Mg^{2+}) inhibits calcite growth by destabilizing the crystal lattice and increasing its solubility. Absorption of magnesium ions, which have a smaller radius than calcium ions (0.65 Å and 0.99 Å respectively), takes place into non-equivalent calcite step-types resulting in strain at the intersection of these steps and further creation of new step directions. The development of these new step directions is responsible for the modification of calcite crystals along the *c*-axis (fig. 2.7), which results to be elongated in this direction [Davis et al., 2004].

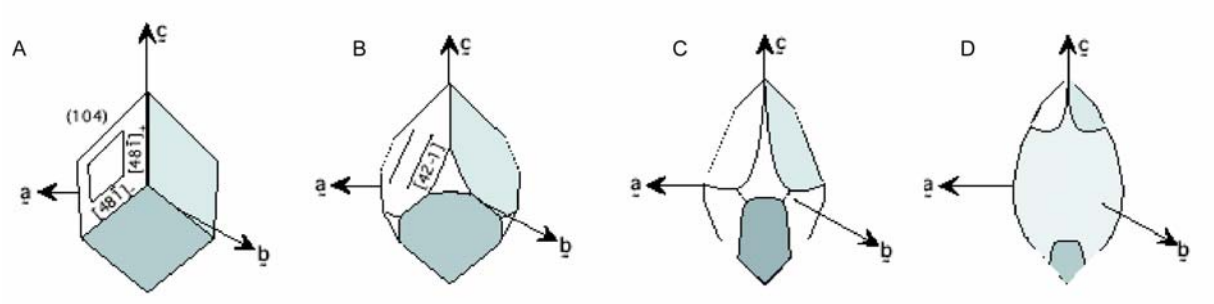

Fig. 2.7. Schematic representation of the effect of magnesium ions on calcite morphology. A. Unaffected rhombohedral calcite. B. Incorporation of magnesium ions leads to the development of a new crystal face. C. Further development of the newly nucleated crystal faces. D. The final crystal shows an elongated structure with a roughened rounded shape and elongated form [Davis et al., 2004].

Influence of organic additives

The morphology of crystals can be strongly influenced by biomolecules that can be adsorbed stereospecifically on certain crystal surfaces. Macromolecules binding to unstable faces of a crystal lead to their stabilization presumably because the surface energies are lowered. Vaterite stabilization by organic molecules is a typical example. Furthermore occlusion of additives into the atomic lattice may affect the mechanical properties of the crystal [Addadi and Weiner, 1985].

Additives containing chemical groups or moieties that mimic the solute or substrate molecules are defined as *tailor-made additives or auxiliaries* [Addadi et al., 1985]. Tailor-made additives interact in very specific ways with selected faces of a particular crystalline phase. The molecular similarity implies that the additives are readily adsorbed at growth sites on the crystal surface (fig. 2.8). The adsorbed molecule disturbs the regular deposition of oncoming crystal layers causing a retardation of the growth normal to these faces. Retardation of the growth in a certain direction implies a relative increase in its surface area. A fast growth in a given direction implies a small face development perpendicular to this direction. When the growth is inhibited in a direction perpendicular to a given face, the area of this face is expected to increase relative to the areas of other faces of the same crystal [Shimon et al., 1985; Shimon et al., 1986].

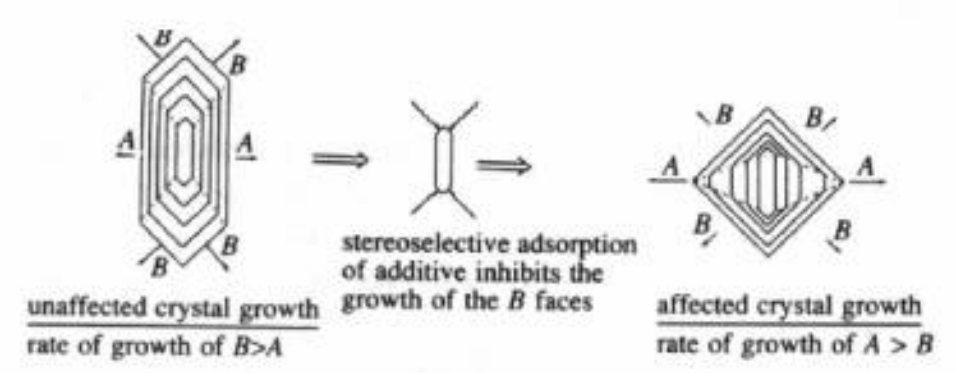

Fig. 2.8. Schematic representation of the interaction of tailor-made additives with crystal faces and relative modification of the crystal face growth rate. The growth directions are indicated as *A* and *B,* whereas *A* indicates the slower growth direction and B refers to the faster growth direction. Unaffected crystals are characterized by the formation of relative small faces perpendicular to the fastest growth direction *B*. Inhibition of the growth in the *B* direction, due to stereoselective additives binding, induces an enhancement of the growth rate in the slower growth direction *A* [Addadi and Weiner, 1985].

In aqueous solution the selective adsorption of molecules like amino acids on certain crystal faces is strongly influenced by electrostatic-ionic interactions depending on the surface charge of a mineral face and the isoelectric point (pI) values of amino acids.

The charge of an exposed mineral surface in aqueous environments is the result of surface complexation: water molecules form chemical bonds with surface ions via chemisorptions and are subjected to a proton transfer process that shifts hydrogen ions onto neighbouring surface anions [Churchill et al., 2004].

The pH, at which an equal amount of positive and negative charged surface species are present, is defined as the *point of zero charge (pH_{pzc})*, specific for each crystal surface. Above the pH_{pzc} mineral faces display negative surface charge, whereas below the pH_{pzc} a positive charge occurs.

Additives as amino acids are zwitterions and exhibit pH-dependent electrical properties analogous to those of mineral surfaces. Amino acids present no net charge at the isoelectric point; at pH above the pI the amino acids become anionic, whereas below the pI-value they become cationic. Typically amino acids with pIs differing greatly from the pH_{pzc} of a mineral surface are adsorbed in greater abundance onto the mineral surface than amino acids for which pI-value and pH_{pzc} value are similar [Churchill et al., 2004].

Calcite has a relatively high pH_{pzc} of 9.5 and shows preferential adsorption of aspartic acid and glutamic acid [Churchill et al., 2004]. These amino acids are characterized by a relatively low pI. Aspartic acid has a pI value of 2.98, whilst glutamic acid has a pI value of 3.5. Aspartic acid and glutamic acid presents similar properties. They carry a hydrophilic acidic group with strong negative charge at pH > pI and they are usually located on the outer surface of the protein, making it water-soluble. Aspartic and glutamic acid both bind to positively charged molecules and ions. Glutamic acid presents a longer, slightly more flexible side chain than aspartic acid [Lowenstam and Weiner, 1989; Weiner and Addadi, 1997].

2.4 Abalone nacre

Mollusc shells are examples of sophisticated composite materials consisting of crystallized inorganic molecules concentrated from the seawater and bound with organic material secreted by the animal. Mollusc shells show remarkable physical and biochemical properties developed during evolution.

The shell of *Haliotis laevigata* (class gastropoda: *Haliotidae*) consists of two distinct calcified layers (fig. 2.9), an outer layer consisting of calcite and a shining inner layer made of aragonite. The amount of calcium carbonate comprises 95% (weight), whereas the remaining 5% consist of organic material as polysaccharides and several different proteins.

Fig. 2.9. Shell of the seawater snail *Haliotis laevigata*. Left. Outer calcite layer. Right. Inner nacreous layer.

2.4.1 Nacre structure

Mature nacre consists of single polygonal shaped aragonite crystals (aragonite platelets) which present a size of 5 to 15 µm diameter (*a*- and *b*-direction) and thickness of 500 nm (*c*-direction). The tablets are aligned in horizontal lamellae and arranged in the vertical direction (fig. 2.10, A). The growth front of nacre is characterized by pyramidal micro-architectures, defined as “stacks of coins” (fig. 2.10, B and C). “Stacks of coins” are formed by several aragonite platelets stacked in the vertical direction. The conical surface of each stack presents a marked indentation due to the uneven growth rate of each tablet [Nakahara, 1983].

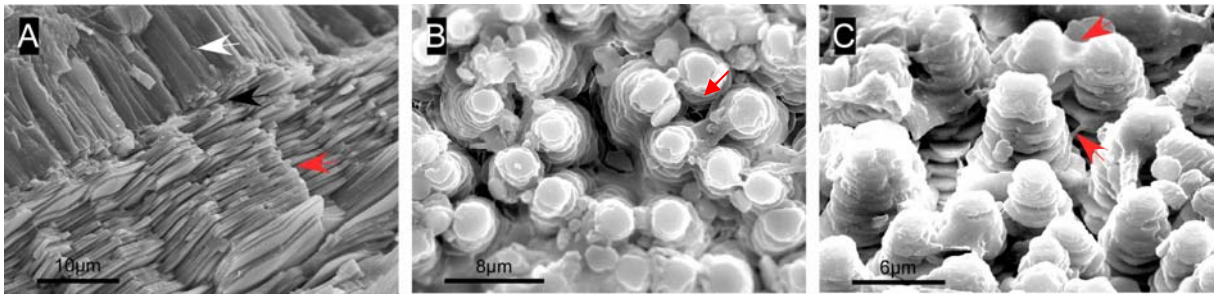

Fig. 2.10. A. SEM image of the cross section of the shell of *Haliotis laevigata*. Both calcium carbonate polymorphs, calcite (white arrow) and aragonite (red arrow) are visible. The two polymorphs are separated by a sharp transition region (black arrow). The roughness of the calcite layer is evened by the flat aragonite platelets. Nacre aragonite platelets (5 - 10 µm in diameter and 500 nm vertical direction) are arranged in flat layers, parallel to each other and well ordered in the vertical direction. B-C. SEM images of nacre growth front. B. Nacre growth front of abalone shells (top view) is characterized by typical pyramidal structures, defined as “stacks of coins”. Stacks of coins are formed by several aragonite platelets (red arrow) stacked in the vertical direction. C. Stacks of coins (side view). The characteristic pyramidal shape is more visible. Rests of organic material between the mineral platelets are visible (red arrows).

Recent studies on the nacre of some bivalves (*Pinctada* species) indicate that aragonite platelets present a further substructure (fig. 2.11). Single tablet consists of “nanobuilding blocks” (approximately 10 nm length), which show a flat pseudohexagonal habit similar to that of aragonite platelets. The nanobuilding blocks present the same orientation of the aragonite platelets [Oaki et al., 2005] and they are maybe divided by a continuous organic framework [Rousseau et al., 2005].

Due to the high similarity of bivalve nacre with gastropod nacre the existence of the same substructure in abalone nacre is hypothesized. Unfortunately no clear evidence is available.

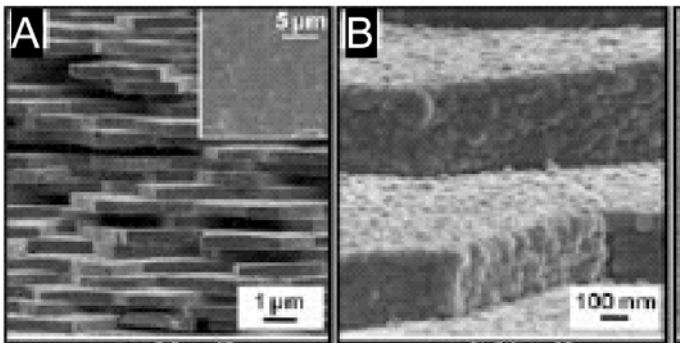

Fig. 2.11. A. Field-emission scanning electron microscopy image of the nacre of the oyster shell *Pinctada fucata*. Nacre of the oyster shell present a well ordered layered structure consisting of aragonite platelets (1 – 5 µm wide and 200 – 700 nm vertical direction). B. Magnification of A. The presence of smaller components ("nanobuilding block") in each aragonite platelet can be individuated. Each nanobuilding block presents a size of 10 nm [Oaki et al., 2005].

2.4.2 Nacre organic matrix

The organic matrix, representing only about 5 % (weight) of the total shell material [Hare, 1965], is distributed between the aragonite platelets (*interlamellar*) and within single aragonite platelets (*intracrystalline*) [Nakahara et al., 1982; Belcher et al., 1986]. The organic matrix has been conventionally classified as *water-insoluble* and *water-soluble*, based on its solubility in aqueous media after decalcification of the mineral phase. The organic matrix between the mineral layers forms interlamellar horizontal sheets of 40 nm thickness, which are composed of sublayers. The core is a highly ordered β-chitin on which proteins are bound.

Chitin is the major component of the interlamellar matrix, it is a nitrogen containing polysaccharide consisting of units of acetylglucosamine (N-acetyl-D-glucos-2-amine), linked together with ß-1,4 glycosilic bonds (fig. 2.12, A). β-chitin consists of parallel polymers chains[2], it shows a highly ordered conformation, a preferred orientation over length scales of several microns [Falini et al., 2003]. Chitin, obtained after dissolution of the nacreous mineral phase, presents a peculiar honeycomb pattern

[2] α-chitin is characterized by anti-parallel chains [Falini et al., 2003].

(fig. 2.12, B). The chitin honeycombs, which have diameter of 7 - 12 µm, are delimited by twisted proteinaceous filaments that form a network along the interspace between the aragonite tablets. In the middle of each comb pores of 150 nm in diameter are present (fig. 2.12, C). Chitin is permeable to ions and proteins that can easily diffuse during the shell growth [Weiss et al., 2002; Blank et al., 2003].

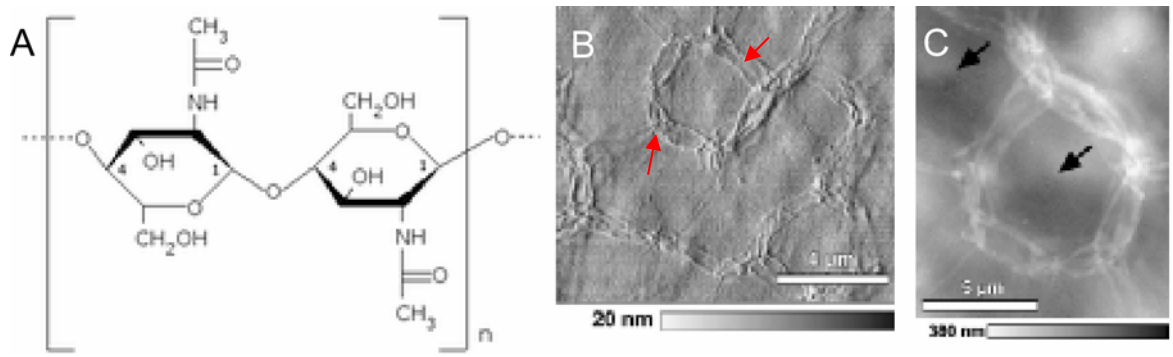

Fig. 2.12. A. Schematic representation of chitin molecule. B. Atomic force microscopy (AFM) deflection image of demineralized nacre ground parallel to the aragonite layers. The organic matrix shows a honeycomb-like structure. Each comb is delimited by twisted proteinaceous filaments (collagen-like) that form a network along the interspaces between the aragonite tablets (red arrows). These proteinaceous filaments extend along several tablets and cross each other or end at the edges of the tablets. C. Enlargement of B. Black arrows point to the holes (150 nm in diameter) in the organic sheet [Blank et al., 2003].

It is hypothesized that the surface of the insoluble chitin matrix is coated with hydrophilic proteins, some of them in contact with the mineral phase. These proteins may adopt a β-sheet conformation similar to that of silk-fibroin protein and they may be orthogonally aligned with the chitin layer forming a plywood-like construction [Levi-Kalisman et al., 2001].

The intracrystalline organic matrix is mainly composed of proteins, typically rich in aspartic acid, glycine or serine and in many cases glycosylated. The intracrystalline proteins seem to influence and regulate the mineralization process inducing oriented nucleation, inhibition of crystal growth and control of polymorph selection. *In vitro* experiments have demonstrated that proteins in solution specifically interact with different steps of a calcite crystal and induce the oriented nucleation of aragonite [Thompson et al., 2000].

2.4.3 Water-soluble nacre proteins of *Haliotis laevigata*

Up to ten different water-soluble proteins have been individuated in the nacre of *Haliotis laevigata*. Only five of them, *perlucin, perlwapin, perlinhibin, perlustrin and perlbikunin*, have been sequenced.

Perlucin

Perlucin is the first water-soluble protein isolated from the nacre of *H. laevigata*, it shows a molecular weight of ~17 kDa and contains 155 amino acids (fig. 2.13), including a glycosylated asparagines [Mann et al., 2000]. Perlucin is a functional C-type lectin protein with broad carbohydrate-binding specificity. The C-type domain consists of ~135 amino acids followed by a short C-terminal domain of ~20 amino acids containing almost two identical repeats of 10 amino acids. The lectine domain contains six cysteines that may form disulfide bonds [Weiss et al., 2000].

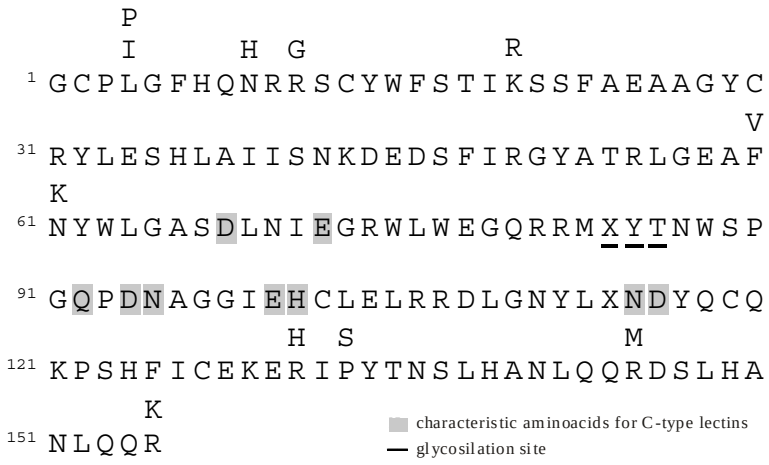

Fig. 2.13. The complete amino acid sequence of perlucin. Grey: characteristic amino acids for C-type lectins; underlined: glycosylation site. The protein sequence of perlucin is submitted to the database Uniprot Knowledgebase-SwissProt, with accession number P82596.

Perlucin has an amino acid sequence similar to the C-type carbohydrate-recognition domains of asialoglycoprotein receptors of various organisms and lithostathine, a human pancreatic stone protein. Both are involved in calcium carbonate precipitation. In particular lithostathine seems to inhibit the calcium carbonate precipitation in the pancreatic fluid, but to induce stone formation after proteolytic processing in pancreatitis [Bimmler et al., 1997; Gerbaud et al., 2000].

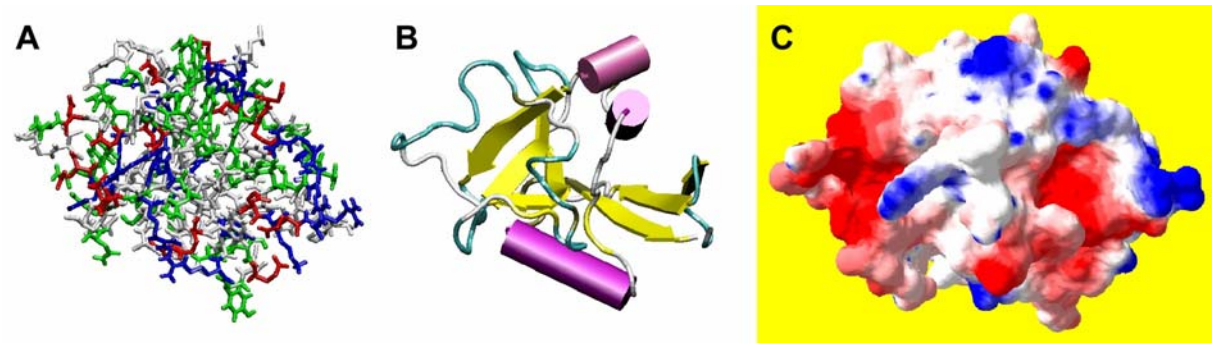

Fig. 2.14. Computer simulated structure of perlucin. The structure and surface potential of perlucin have been calculated by computer simulation using the known X-ray structures of asialoglycoprotein receptor and lithostathine as templates. A. Molecular structure of perlucin. Red: negatively charged residue; blue: positively charged; green: polar, grey: non-polar. B. Schematic diagram of perlucin showing the α-helixes (purple cylinders) and β-sheets (yellow arrows). C. Surface potential of perlucin: red area: negatively charged, blue area: positively charged. In cooperation with Prof. Martin Zaccharias, International University Bremen, Germany.

Studies *in vitro* have shown that perlucin is a nucleation promoter of calcium carbonate in solutions [Weiss et al., 2001] and modifies the morphology of a calcite crystal surface inducing the epitactic growth of new mineral layers, which show a peculiar round shape [Treccani et al., 2003; Blank et al., 2003].

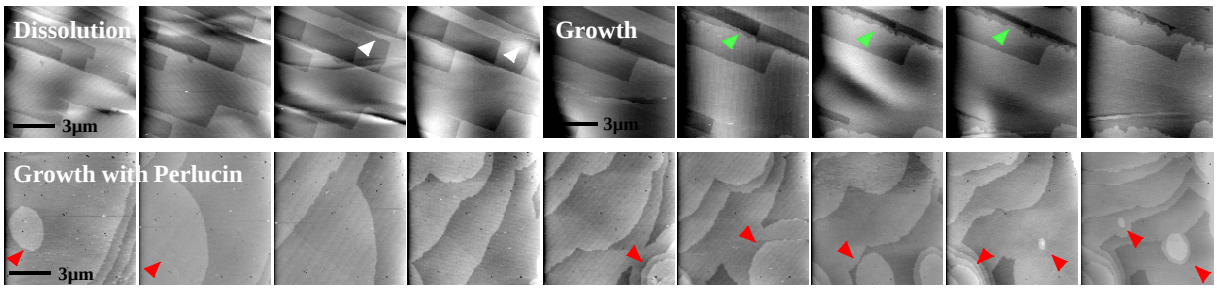

Fig. 2.15. AFM images of the interactions of perlucin with geological calcite (3 min interval between two images). Upper row. Dissolution layer by layer of the [4 4 1] calcite surface immersed in deionized water (white arrows) growth of the same surface in a saturated calcium carbonate solution. Note the growth of the molecular layers (green arrows). Bottom row. AFM images of the growth of a [4 4 1] calcite surface with perlucin (0.01 mg/ml). Perlucin nucleates small islands (red arrows) for the next molecular layer. The new layers merge without detectable defects. This suggests that perlucin induces epitactic growth of new mineral layers in the orientation of the crystal lattice [Treccani et al., 2003].

Perlwapin

Perlwapin is a recently sequenced soluble protein from the abalone shell *Haliotis laevigata*. The amino acid sequence analysis showed that perlwapin consists of 134 amino acids (fig 2.16), it presents a molecular weight of ~18 kDa and consists of three WAP domains of four-disulphide core domains. The amino acid sequence of perlwapin compared with the amino acid sequences of other proteins shows a high relation with whey acidic protein (WAP).

WAP domains are small domains consisting of 40 - 50 amino acid residues with a characteristic four disulphide-core pattern. This motif was first identified in the whey acidic protein (WAP), a predominant protein in milk whey of lactating mice [Simpson, 2002]. WAP-domain proteins belong to serine protease inhibitors that vary in specificity and inhibitory capacity. Some WAP domain protease inhibitors present a microbial activity [Hagiwara et al., 2003] and others inhibit ion transport [Araki et al., 1989].

A WAP domain has been also identified in lustrin A, a multidomain protein isolated from the nacre of *Haliotis rufescens* [Shen et al., 1997]. Lustrin A is thought to act as a part of the adhesive between the nacre tablets [Smith et al., 1999].

Perlwapin shows a specific binding affinity on certain steps of a calcite surface with consequent inhibition of crystal growth. Therefore perlwapin may be involved in the regulation of the growth if single aragonite platelets, which present uniform size in the three spatial directions. Perlwapin could also play a role in the polymorph transition, inhibiting calcite growth to allow aragonite formation [Treccani et al., 2006].

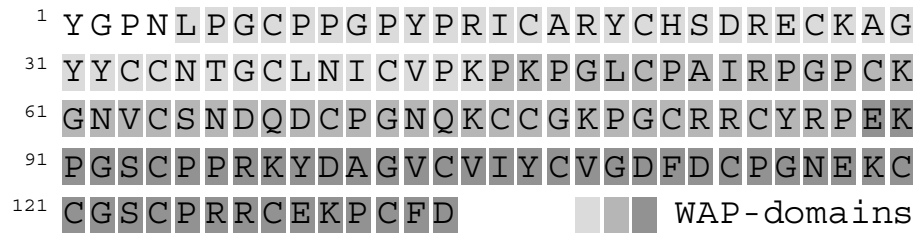

Fig. 2.16. The complete amino acid sequence of perlwapin. Highlighted the three consecutive WAP-domains. The last domain presents a high percentage of identical amino acids (61.4%) with the WAP domain of lustrin A, a protein isolated from the nacre of *Haliotis rufescens*. The protein sequence of perlwapin is submitted to the Uniprot Knowledgebase, accession number P84811.

Perlinhibin

Perlinhibin is a minor component of the water-soluble protein fraction (approximately 3 µg/shell). It consists of 41 amino acids (fig. 2.17) and shows a high content of arginine (14.6%), histidine (17%) and cysteine (19.5%). The eight cysteines form four cystein-bridges that stabilize the protein.
Perlinhibin inhibits *in vitro* the growth of calcium carbonate crystals. Perlinhibin binds specifically to certain faces of a calcite crystal and inhibits at its binding site the growth of new crystal layers. The influence of perlinhibin on calcium carbonate crystallization, investigated during this thesis, is presented in chapter 4.

Fig. 2.17. The complete amino acid sequence of perlinhibin. The sequence is formed from 41 amino acids. Highlighted the eight cysteines.

Perlustrin

Perlustrin is also a minor component of the soluble protein fraction isolated from the aragonite layer of the abalone *Haliotis laevigata* (approximately 10 µg/shell). This protein has a molecular weight of 13 kDa and the polymer chain is formed from 84 amino acids (fig. 2.18). Perlustrin presents a high sequence identity with the insuline-like growth factor binding proteins (IGFBP). Perlustrin is the first member of the IGFBP superfamily isolated from an invertebrate. The presence of an IGFBP in nacre could support the idea that phylogenetically distant biominerals as nacre and bone may contain components inherited from common ancestors [Weiss et al., 2001].

```
 1 LSCASCENAACPAIGLPCKPSEYVYTPCGC
31 CPQCPLELGQPCGSFTQRCQFDLWCLRRKG
61 NKIEAYKYVPWKLDFKKGVCARDDV
```

Fig. 2.18. The complete amino acid sequence of perlustrin. The protein sequence of perlustrin is submitted in the Uniprot Knowledgebase-SwissProt, accession number P82595.

Perlbikunin

Perlbikunin is a very minor component of the water-soluble nacre proteins (approximately 0.1 µg/shell). Analysis of the first 65 amino acids (fig. 2.19) revealed similarities to Kunitz-type proteinase inhibitor (BPTI). Perlbikunin seems involved in the stabilization of the nacre organic matrix and control of mineralization processes [Mann et al., in preparation] but its role is still under investigation.

```
 1 KYHDVCQLPKDPGPCRAYFPKYYFNSRTCL
31 CEKFVYGGCLGNANRFETLEDCRRRCGGDD
61 LCNLPK
```

Fig. 2.19. First 66 amino acid of perlbikunin. Perlbikunin is a very minor component of the water-soluble nacre proteins.

2.4.4 Nacre growth

The growth of nacre takes place in a closed compartment shielded from the external environment to maintain a defined ionic composition. An array of organic molecules differentially secreted by the *mantle*[3]*,* mediates the whole process, influencing polymorph selection and atomic lattice orientation.

The growth of the shell begins with the nucleation of prismatic calcite into a proteinaceous matrix (*periostracum*), followed by the deposition of nacreous aragonite on the top of the calcitic primer [Fritz and Morse, 1998]. Aragonite crystals are supposed to grow from one layer to the next through nanopores in the interlamellar organic sheets. The nanopores (5 - 50 nm in diameter and a hole-to-hole spacing of 50 nm) facilitate the ion flux, the diffusion of proteins and guide the

[3] The *mantle* is responsible for the shell building. It covers the body of the molluscs with a thin sheet of tissue lining the inner surface of the shell.

c-axis growth of nacre from the layer beneath into the next succeeding layers. Aragonite platelets in different layers are connected together by “mineral bridges” and form domains of 10 - 20 tablets [Schaeffer et al., 1997]. This continuous growth seems to be responsible for the almost perfect alignment of aragonite tablets in the vertical direction.

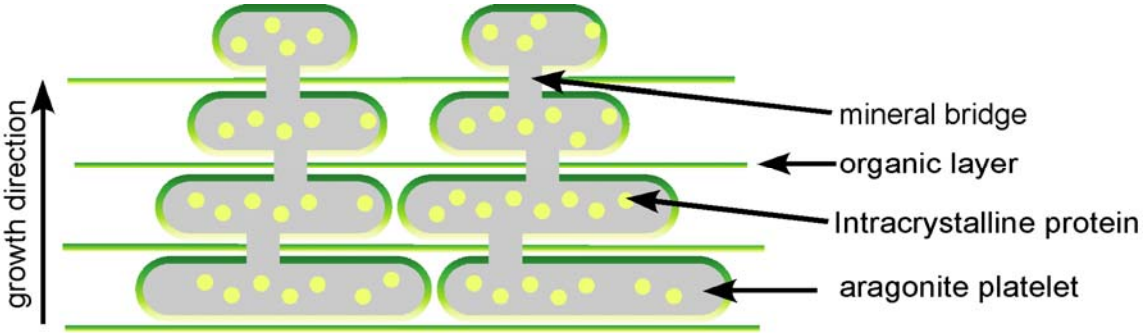

Fig. 2.20. Schematic representation of nacre growth through mineral bridges. Aragonite tablets might grow from one layer to the succeeding one through nanopores (5 – 50 nm in diameter) in the interlamellar organic sheets. The pores facilitate the diffusion of ions and proteins and allow the growth of single crystal from one layer to each other. Aragonite platelets in different layers are connected by mineral bridges, which are maybe responsible for the perfect alignment of the aragonite tablets.

2.4.5 Nacre physical and chemical properties

Nacre presents remarkable mechanical properties, like stability and elasticity, high resistance against corrosion and a beautiful appearance shining in all rainbow colours.

The mechanical stability of nacre is the result of its extremely well ordered microstructure and the presence of organic material intimately connected to the mineral phase. The staggered arrangement of the aragonite platelets deviates the propagation of cracks and the platelets tend to spring apart. The organic matrix acts like a flexible glue that prevents the pull-out of the platelets (fig. 2.20). Mechanical tests on nacre showed that the fracture toughness of nacre is several orders of magnitude higher than one would expect from the pure crystalline aragonite. The fracture toughness is about 350 - 1240 J/m^2 depending on the degree of hydration. The tensile strength is of the order of 140 – 170 MPa (wet/dry) and the Young’s

modulus is about 60 - 70 GPa [Jackson et al., 1988].

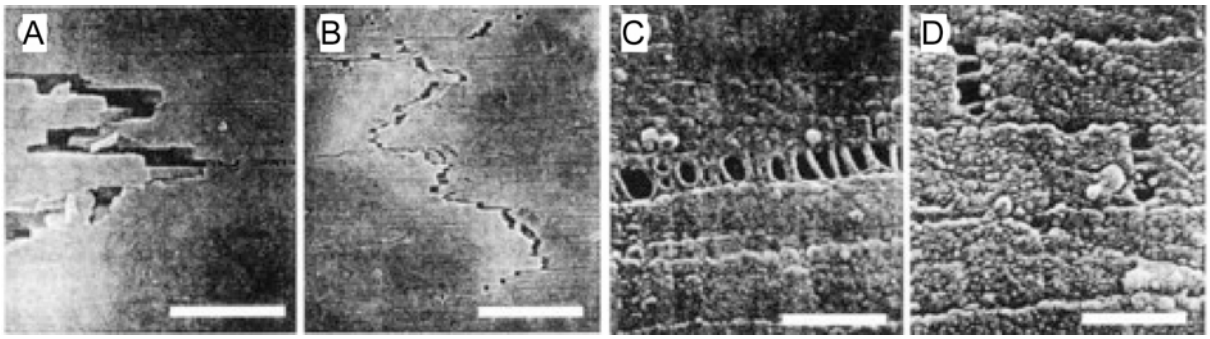

Fig. 2.20. SEM images of crack propagation in nacre of the bivalve *Pinctada fucata* tested in a wet stage [Currey, 1980]. A. SEM of a cross section of nacre in the vicinity of a propagating crack. The delamination cracks extend laterally from the main crack. Scale bar: 2.7 µm. B. The delamination cracks just ahead of the main crack tip. Scale bar: 7.5 µm. C. Fibrils of organic matrix between the tablets become more visible during crack propagation. Scale bar: 0.6 µm. D. Fibrils of the organic matrix extending between the ends of a tablet to prevent the pullout. Scale bar: 0.43 µm.

Within the organic components chitin is particular important for the mechanical and chemical stability of the shell. Chitin forms long straight polymer chains that enhance the elasticity of the shell while chitin rigidity augments with increasing mineralization of the matrix material. The chemical stability of nacre, insolubility in water and high resistance to acids and alkalis, seems to be directly related to chitin properties.

Abalone nacre shows unique rainbow colours and a lustrous iridescence that can be explained in terms of diffraction and interference phenomena of light passing through alternating uniform layers of organic material and aragonite platelets. The refractive index *n* of the aragonite platelets is 1.53 in the [001] direction and 1.68 in the other two axial directions, the organic layer presents *n*=1.43 [Snow et al., 2004].

3 Materials and methods

3.1 Protein extraction and biochemical characterization

In this section the techniques used to purify and investigate nacre proteins are presented. In the first part the most relevant techniques used for the biochemical analysis for nacre protein extraction and purification are introduced. In the second part, the physico-chemical techniques for characterization of the protein functions in term of calcium carbonate mineralization are introduced.

3.1.1 Demineralization of nacre

Nacre proteins are accessible for biochemical analysis only after complete demineralization of the mineral phase. Calcareous materials, as nacre, can be demineralized using specific chelating agents as ethylenediaminetetraacetic acid (EDTA) or diluted acid solutions as acetic acid.

EDTA

EDTA (ethylenediaminetetraacetic acid, $C_{10}H_{16}N_2O_8$) is a tetraprotic acid (pK_1=2.0, pK_2=2.8, pK_3=6.2, pK_4=10.3) containing four carboxylic groups and two amine groups. The fully deprotonated form of EDTA binds to the metal ions forming chelates or complexes. EDTA can form four or six bonds with two- or trivalent metal ions, forming coordination binding at the four oxygen and the two nitrogen sites.

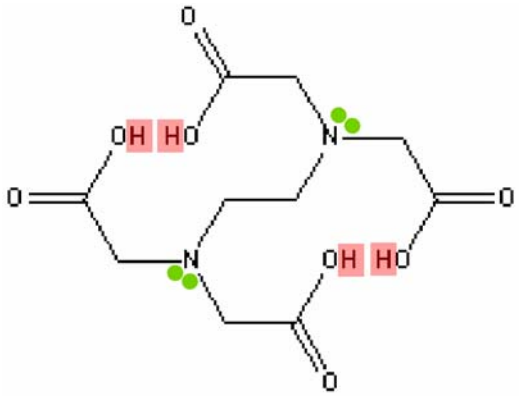

Fig. 3.1. Structural formula of EDTA molecule. Carboxylic groups (red), pair electrons of amine groups (green dots).

In the calcium complex, $[Ca(EDTA)]^2$, EDTA is a tetradentate ligand. The equilibrium or formation constants for most metals are very large; hence the reactions are shifted to the complex. The complexation reaction of EDTA with Ca^{2+} or Mg^{2+} can be represented as follows

$$M^{2+} + HY^{3-} \Leftrightarrow HY^{2-} + H^{+} \quad \textbf{(3-1)}$$

$$M^{2+} + Y^{4-} \Leftrightarrow MY^{2-} \quad \textbf{(3-2)}$$

where M^{2+} represents a metal ion and the EDTA molecule is represented as H_4Y.
The reactions for the weaker forming complexes with Ca^{2+} and Mg^{2+} are pH dependent [Kellner, 1998].
Demineralization of calcified structures with EDTA is most effective at neutral pH and hence under conditions, which are not causing protein denaturation.

Acetic acid

Acetic acid (or ethanoic acid) is a weak acid (pK_a= 4.75)[4] and can be used to dissolve the mineral phase of nacre.
The acid-base reaction of acetic acid (CH_3COOH) with calcium carbonate forms carbonic acid (H_2CO_3) and calcium acetate, $Ca(CH_3O_2)_2$, in solution:

$$CaCO_{3(s)} + 2CH_3COOH_{(aq)} \Leftrightarrow Ca(CH_3O_2)_{2(aq)} + H_2CO_{3(aq)} \quad \textbf{(3-3)}$$

Carbonic acid is unstable at room temperature decomposes to carbon dioxide (CO_2)

[4] pK_a indicates the acid dissociation constant. pK_a is defined as pK_a= -logK_a [Atkins, 2002].

and water

$$H_2CO_{3(aq)} \Leftrightarrow H_2O_{(aq)} + CO_{2(g)} \quad \textbf{(3-4)}$$

The formation of gaseous CO_2 tends to drive the overall reaction by removing the product, according to the Le Chatelier principle [Mortimer, 1996].
The use of a weak acid for protein extraction prevents in most cases from protein hydrolysis.

3.1.2 Ion exchange chromatography

Chromatographic analysis is used for separation and detection of analytes in a solution, based on different physicochemical and chemical interactions between the sample components dissolved in a liquid phase (*mobile phase*) and a stationary matrix (*stationary phase).* Ion exchange chromatography (IEC) is a method for the fractionation of proteins based on differences in their anionic or cationic charge characteristics.
Proteins are complex organic polymers made of a chain of amino acids[5]. The charge of a protein depends on charge carrying the side groups of the amino acids at the surface. According to the pH value of the surrounding solution, these groups may exist in protonated or deprotonated states, thus modifying the net charge of the protein. There are five charged amino acids, two negatively charged (aspartic and glutamic acid) and three positively charged (lysine, arginine and histidine). In the acidic pH region the amino groups of lysine, arginine and histidine are protonated, resulting in a cationic behaviour of the protein. Whereas in the basic pH region, the carboxylic groups of aspartic and glutamic acid are deprotonated and proteins show anionic behaviour [Lottspeich and Zorbas, 1998].
The pH, at which the charged side groups of a protein compensate each other, is defined as *isoelectric point* (*pI*). At this pH = pI the molecule carries no charge.

[5] There are twenty different amino acids, which differ in their side chains. The amino acids are listed in appendix 6.3.

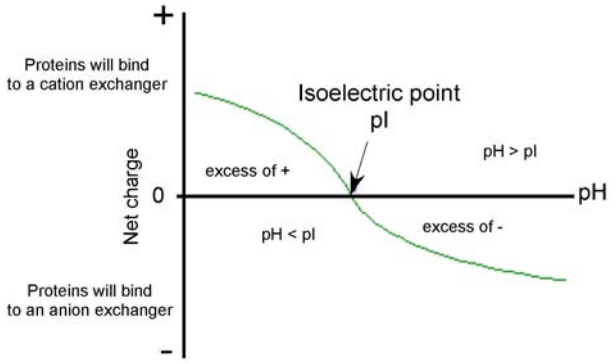

Fig. 3.3. Schematic representation of the variation of the protein net charge as a function of the pH. The pH, at which a protein carries no charge, is defined as isoelectric point (pI). At low pH values (pH < pI) proteins are positively charged and therefore will bind to a cation exchanger. At pH > pI proteins are negatively charged and bind to an anion exchanger. Adapted from [www.chromatography.amershambiosciences.com].

During ion exchange chromatography proteins dissolved in a buffer solution are loaded on the stationary matrix of a column that carries an opposite charge with respect to the protein charge. The ionic groups of exchanger columns are covalently bound to a gel matrix and are compensated by small concentrations of counter ions present in the buffer solution.

The proteins will attach themselves on the stationary matrix by ion-pairing between their charged side chains and the charged groups of the matrix. Proteins are desorbed in order of their affinity for the matrix by buffers of increasing ionic strength. Addition of proper ions, which compete with the binding sites of the proteins on the matrix, provides a mean of desorbing the sample molecules in order of increasing net charges; the higher the protein net charge, the higher the salt concentration required for desorption. Neutral monovalent salts, as sodium chloride, are used as desorbing agents because they have little or no effect on the running pH[6].

Ion exchange chromatographic separation is carried out in columns packed with an ion-exchanger. Ion exchange chromatographers require a matrix of an insoluble swollen polymer containing charged groups. The polymer can be chemically modified cellulose or chemically cross-linked dextranes. There are two types of ion-exchangers namely *cation* and *anion exchanger*. Cation exchangers (or *acidic ion-exchange materials*) possess negatively charged groups and they will attract positively charged molecules. On the contrary anion exchangers (or *basic ion-*

[6] Proteins may also be eluted by changing the pH of the eluting buffer.

exchange materials) show positive charges and they will attract negatively charged proteins.

Depending on the pK_a value of the charged ligand, the ion exchangers are further divided into strong and weak. The weakly basic types consist of secondary and tertiary amino functional groups. Weakly basic exchangers should only be used at pH values below 8.5, weakly acidic exchangers only at pH values above 6. Outside these ranges strongly basic, or strongly acidic exchangers should be used. Many proteins can be separated as polyanions (pH > pI) or as polycations (pH < pI), as long as the pH stability of the protein of interest allows this selection. The most common ion exchanger groups are summarized in fig. 3.4 [Lottspeich and Zorbas, 1998].

Anion Exchangers	Functional group
Diethylaminoethyl (DEAE)	$-O-CH_2-CH_2-N^+H(CH_2-CH_3)_2$
Quaternary aminoethyl (QAE)	$-O-CH_2-CH_2-N^+(C_2H_5)_2-CH_2-CHOH-CH_3$
Quaternary ammonium (Q)	$-O-CH_2-CHOH-CH_2-O-CH_2-CHOH-CH_2N^+(CH_3)_3$
Cation Exchangers	**Functional group**
Carboxymethyl (CM)	$-O-CH_2-COO^-$
Sulfopropyl (SP)	$-O-CH_2-CHOH-CH_2-O-CH_2-CH_2SO_3^-$
Methyl sulfonate (S)	$-O-CH_2-CHOH-CH_2-CH_2-CHOH-CH_2SO_3^-$

Fig. 3.4. Common types of ion exchangers. Quaternary ammonium-exchangers (strong anion exchanger) are fully charged over a broad pH range (pH 2 - 12), whilst carboxymethyl-exchangers (weak cation exchanger) are fully charged over a narrower pH range (pH 6 - 10).

3.1.3 High performance liquid chromatography

High performance liquid chromatography (HPLC) separates proteins and peptides with different hydrophobicity, based on their reversible interaction with the hydrophobic surface of a chromatographic medium. The sample binds to a non-polar stationary phase, a decrease in the polarity of the mobile phase lead to a decrease in solute retention and the bound substances are eluted differentially. Due to the nature of the reversed phase matrices, the binding is usually very strong and for desorption organic solvents are needed [Lottspeich and Zorbas, 1998].

Desorption and elution of polypeptides from HPLC columns are accomplished with

aqueous solvents containing an organic modifier and an ion-pair reagent. The organic modifier solubilizes and desorbs the polypeptide from the hydrophobic surface while the ion-pair agent sets the eluent pH and interacts with the polypeptide to enhance the separation. Elution is accomplished by gradually raising the concentration of organic solvent during the chromatographic run (solvent gradient). When the solvent reaches the precise concentration necessary to cause desorption, the polypeptide is desorbed and elutes from the column [Lottspeich and Zorbas, 1998].

The most common stationary phases have functionally groups chemically attached to a silica support, like alkyl groups as $–CH_3$, $–C_4H_9$, $–C_{18}H_{37}$, with retention increasing exponentially with the chain length. The silanol groups on the silica surface are altered by changing the functional group, which influences the selectivity and the column efficiency. Typically $–C_{18}H_{37}$ columns (C-18 column) are used for small molecule separations, (*e.g.* for peptides), whereas $–C_4H_9$ columns (C-4 column) are more suitable for large proteins [Szepesi, 1992].

The mobile phase is a polar solvent, typically water (polarity index[7] P = 10.2) to which a less polar solvent as acetonitrile (P = 5.8) or methanol (P = 5.1) is added. The hydrophobicity of the solute molecules is increased by ion-pairing agents, which neutralize the charge of the molecules. This is typically obtained by decreasing the pH of the solution in which the proteins are dissolved. The low pH is necessary in order to protonate the solute molecules and to enhance their hydrophobicity.

Acetonitrile (C_2H_3N) is the most commonly used organic modifier because it is volatile and can be easily removed from collected fractions. Acetonitrile has a low viscosity (0.38 cP[8] at 15 °C) and little UV absorption at low wavelengths (UV cut-off at 190 nm).

Trifluoroacetic acid ($CH_2F_3O_2$) is a weak hydrophobic ion-pairing reagent. Trifluoroacetic acid (TFA) is typically used at a concentration of 0.1% (w/v); at this concentration TFA presents a low UV absorption at low wavelengths (UV cut-off at 205 nm).

[7] A higher value of the polarity index P indicates a more polar eluent. An exhaustive list of P values and other physico-chemical properties of several solvents can be found at the following website: http://home.planet.nl/~skok/techniques/hplc/eluotropic_series_extended.html.

[8] cP= centipoises. 1 centipoise = 1 mPa·s. The cgs physical unit for dynamic viscosity is the *poise* (P), more commonly expressed as *centipoise* (cP). Water has a viscosity of 1.0020 cP at 20 °C.

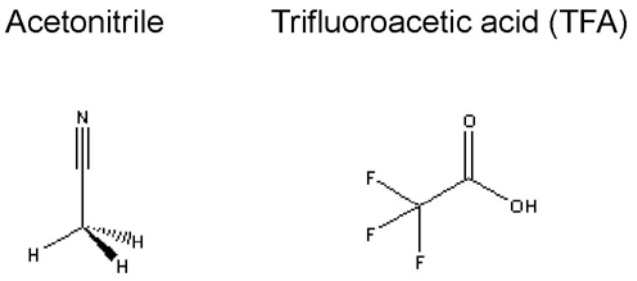

Fig. 3.5. Structural formula of acetonitrile (C_2H_3N) and trifluoroacetic acid ($CH_2F_3O_2$). Acetonitrile and trifluoroacetic acid (TFA) are two of the most common HPLC solvents.

3.1.4 Gel electrophoresis

Gel electrophoresis is a technique to separate proteins and nucleic acids on the basis of physical characteristics as size, shape and isoelectric point. The working principle exploits the fact that molecules with a net electric charge z can move when immersed in an electrical field E. The velocity of migration v in the field depends on the electric field strength E, on the net charge on the protein and the frictional coefficient η

$$v = \frac{Ez}{\eta}$$

The force $F = Ez$ driving the charged molecule toward an electrode (with an opposite charge respect to the molecule) is opposed by the viscous drag ηv arising from the friction between the moving molecule and the medium[9]. Electrophoresis separation is typically performed in gels in the form of thin slabs [Cooper, 1980; Lottspeich and Zorbas, 1998]. Sodium dodecyl sulfate polyacrylamide gel electrophoresis (SDS-PAGE) is one of the most used electrophoretic methods to separate proteins according to their mass [Raymond and Weintraub, 1959]. Proteins are dissolved in a solution of sodium dodecyl sulfate (SDS), mercaptoethanol and dithiothreitol. SDS is an anionic detergent that denatures secondary and non–disulfide–linked tertiary structures. The negative charge acquired on binding SDS is usually much greater than the overall charge on the native protein. 2-mercapthoetanol and dithiothreitol (DTT) are used as reducing agents. They further denature the proteins by reducing

[9] For small spherical molecules the Stoke´s law can be used to calculate the frictional force.

disulfide linkages, thus overcoming some forms of tertiary protein folding, and breaking up quaternary protein structure (oligomeric subunits).

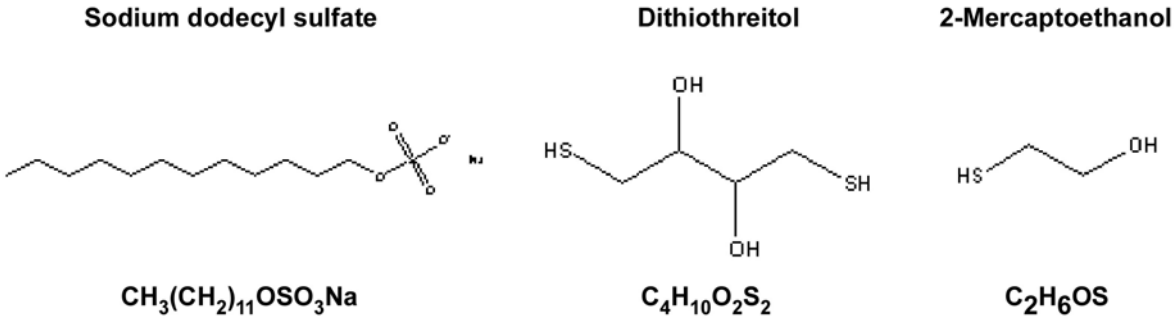

Fig. 3.6. Structural formula of sodium dodecyl sulfate, dithiothreitol and 2-mercaptoethanol.

The SDS complexes with the denaturated proteins are then electrophoresed on a polyacrylamide gel. Polyacrylamide gels (PAGE) are chemically inert and can be easily obtained by polymerization of acrylamide [Raymond and Weintraub, 1959].

3.1.5 Gel staining

After electrophoresis the proteins in the gel can be visualized by chemical staining (or dyes). Chemical stains operate by binding to proteins with a higher affinity than to the gel matrix. The result is a local increase in concentration of the dye in the protein bands [Lottspeich and Zorbas, 1998].

The most common method for visualizing proteins within the gel is staining with Coomassie Brilliant Blue dye. Coomassie dye binds to proteins through ionic interactions between dye sulfonic acid groups and positive protein amine groups as well as through van der Waals attractions [Lottspeich and Zorbas, 1998]. Coomassie dye is an integral component of the *Bradford protein assay* [Bradford, 1976], a spectroscopic analytical method for determining protein concentration in a solution (see section 3.1.6).

"Stains-all"(1-ethyl-2-[3-(1-ethyl-naphtho [1,2d] thiazolin-2-ylidene)-2 methylpropenyl naptho [1,2d] thiazolium bromide) is a cationic carbocyanine dye that allows the visualization and identification of acidic proteins due to their differential staining [Kevin et al., 1983].

Stains-all is particularly useful to detect proteoglycans and mucins, which contain high levels of sulfated sugar residues, acidic proteins and phosphoproteins found in mineralized tissues (*e.g.* osteopontin, bone sialoprotein, dentin phosphophoryn), proteins with high levels of acidic amino acids, phosphate and in some cases, sialic acid and sulfate residues. Typically sialoproteins and phosphoproteins and highly acidic proteins stain blue. Intact proteoglycans stain purple, whereas less acidic proteins stain pink. Furthermore Stains-all has a wide application for staining all type of calcium-binding proteins (*e.g.* calsequestrin, calmodulin, and troponin C [Goldberg et al., 1983]). Ca^{2+}- binding proteins stain blue, presumably through an interaction within the Ca^{2+}- binding domains. However the use of Stains-all for labelling acidic proteins is limited by photobleaching or lack of stability toward light. Stained bands fade within few hours [Goldberg et al., 1997].

A **B**

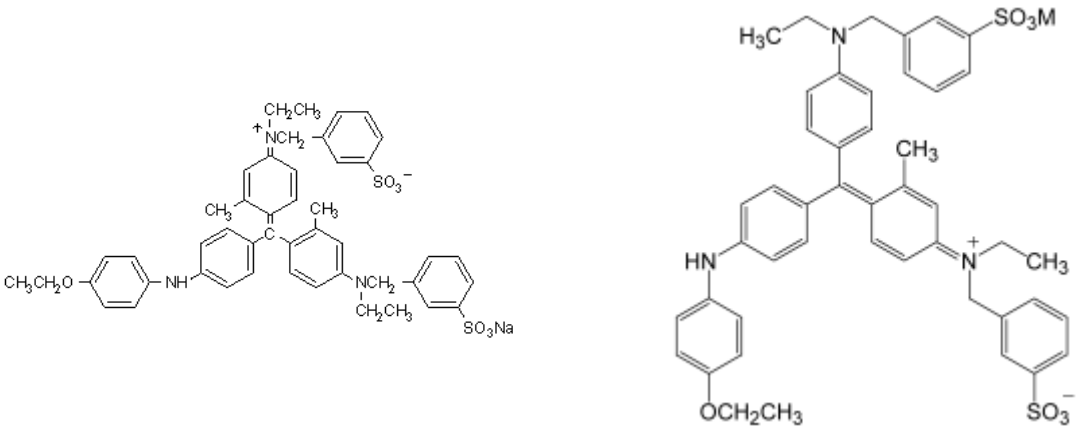

Fig. 3.7. A. Structural formula of Coomassie Blue G-250 molecule. B. Structural formula of Stains-all molecule.

3.1.6 Determination of protein concentration

The quantification of protein concentration in solutions can be determined with the so-called Bradford assay [Bradford, 1976]. This method is based on the fact that Coomassie Brilliant Blue G-250, in its deprotonated anionic sulfonate state, forms complexes with proteins mainly at cationic or hydrophobic side chains in a rather unspecific reaction. The interactions are strong with arginine, followed by those with lysine, histidine, tryptophan, tyrosine and phenylalanine [Lottspeich and Zorbas, 1998].

Coomassie Blue in acidic solutions has an absorbance shift when complexes with proteins are formed. The anionic form (bound) of the dye has an absorption maximum at 595 nm whereas the cationic form (unbound) has an absorbance maximum at 470 nm. The increase of absorbance at 595 nm is proportional to the amount of bound dye and therefore to the concentration of the protein in the sample. The absorbance is measured photometrically and is related to the sample concentration by the *Beer's law*

$$A = \varepsilon c d \qquad \textbf{(3-5)}$$

where d [cm] is the cell thickness (dimension of a cuvette), c the concentration of the solution [mol/l] and ε the extinction coefficient. A linear relationship between absorbance and the sample concentration is maintained only in diluted solutions (c < 0.1 mol/l), at higher concentrations changes of ε may deviate from the linear range [Lottspeich and Zorbas, 1998].

Estimation of protein concentration with Bradford microassay

Protein concentration was determined by the so-called Bradford microassay using a commercially available Coomassie dye stock solution (Bio-Rad Laboratories GmbH, Germany). Lysozyme (molecular weight ~14.3 kDa), immunglobuline G (molecular weight 150 kDa) and bovine serum albumin (molecular weight 66 kDa) were used as protein standards. Protein standards were purchased from Sigma Aldrich Chemie GmbH, Germany).

For spectrometer calibration 800 µl reference buffer solution were mixed with 200 µl Coomassie dye stock solution (as purchased). 800 µl of standard proteins at different concentrations (from 1 to 20 µg/ml) were mixed with 200 µl Coomassie dye solution. 800 µl of protein sample solution were mixed with 200 µl Coomassie dye solution. Solutions were gently mixed and incubated for 5 min at room temperature in one-way cuvettes (Plastibrand, Brand, Germany). The absorption was measured at 595 nm with a UV-VIS spectrometer (Perkin-Elmer, Germany).

3.1.7 Matrix assisted laser desorption ionization (MALDI)

Matrix-assisted laser desorption ionization (MALDI) is a soft ionization technique used in mass spectrometry, allowing the characterization of biomolecules. MALDI furnishes several information about the physico-chemical properties of the sample as molecular weight estimation, purity of a sample, amino acid substitutions, post-translational modifications and number of disulphide bridges. MALDI allows amino acid sequencing, *de novo* characterization of peptides and identification of proteins by database searching.

Molecules are ionized by a beam of electrons produced by a laser source[10], which removes electrons from the molecules and breaks the samples down into small-ionized fragments. The charged fragments are removed and accelerated to high velocity by an electric field towards a magnetic field. Ions are deflected by the magnetic field and collected to a detector and the sample molecules are separated according to their mass-to-charge ratios (*m/z* - ratio). MALDI with *time-of-flight* (MALDI-TOF) analyzers are typically used. Ions are boosted with the same kinetic energy by passage through an electric field and the times they take to reach the detector are measured. While the nominal kinetic energy of all the ions is the same, the resultant velocity is different, causing lighter ions (and also more highly charged ions) to reach the detector first [Lottspeich and Zorbas, 1998].

In MALDI analysis a matrix is used to protect the biomolecules in the sample from being destroyed by the direct laser beam. The matrix consists of crystallized molecules, the most commonly used are 3,5-dimethoxy-4-hydroxycinnamic acid (sinapinic acid), α-cyano-4-hydroxycinnamic acid (α-cyano or α-matrix) and 2,5-dihydroxybenzoic acid (DHB). The matrix molecules are typically mixed with ultrapure water or organic compound (*e.g*. acetonitrile), or trifluoroacetic acid. The organic compound allows the hydrophobic proteins in the sample to be dissolved, while the water allows hydrophilic proteins to do the same [Lottspeich and Zorbas, 1998].

Proteins separated by gel electrophoresis can be used for *peptide finger printing*. Peptides are extracted from the gels after enzymatic digestion, usually with trypsin, which yields peptides with C-terminal basic residues (arginine and lysine).

The resulting peptides with relative molecular weights can be used for database

[10] In UV-range nitrogen-lasers (N_2-laser) with wavelength of 337 nm and pulse duration of 2-5 ns, or neodymium-yttrium aluminium garnate lasers (Nd-YAG-laser) with wavelengths of 355 nm or 266 nm and pulse duration of 5-15 ns [Lottspeich and Zorbas, 1998].

search typically by *peptide mass mapping (PMM)*[11], s*equence tag*[12] and *tandem mass spectrometry (MS/MS) fragmentation ion search*[13].
The above three searches allow to identify all known proteins (present in data bases), but cannot be applied for identification of any unknown protein. For unknown proteins, the amino acid sequence is obtained by interpreting the MS/MS data (*de novo sequencing by MS/MS*) and used for sequence homology search (FASTA or BLAST search)[14].

3.1.8 Extraction and purification of nacre intracrystalline proteins

Intracrystalline proteins were extracted by demineralization of single aragonite platelets from abalone nacre (*H. laevigata*). Proteins were further investigated by precipitation techniques, ion exchange chromatography, high performance liquid chromatography and MALDI. Gel electrophoresis was performed in combination with differential gel staining. Each step is presented as follows.

Nacre preparation

Green lip abalone (*Haliotis laevigata*) specimens of 10 - 20 cm in diameter were obtained from Abalone Exports (Laverton North, Victoria, Australia). The outer calcitic layer of the shells was removed by sand blasting (Hommel, Heinrich-Schlick-KG GmbH, Germany) working with a pressure of 7 bar (sandblasting agent: aluminium silicate grains, 0.2 - 0.5 mm Ø, Asilikos GmbH, Germany).
Nacre was incubated for 2 minutes in a solution of 50% sodium hypochlorite (NaOCl) (Sigma Aldrich Chemie GmbH, Germany) and ultrapure water to completely remove any organic contaminations from the surface. Sodiumhypochlorite and dissolved organic contaminants were removed by extensive washing with ultrapure water. Nacre was dried at 4° C and crushed into small pieces (approx. 0.5 - 1 cm Ø) with a hammer.

[11]PMM is a method of identifying proteins by comparing observed mass (m/z) with predicted masses of digested proteins contained in a database.
[12] Mass values are combined with partial amino acid sequence.
[13] Only a list of the ions contained in a MS/MS spectrum is employed for data base search.
[14] FASTA can be very specific for identifying long regions of low similarity especially for highly diverged sequences. Basic Local Alignment Search Tool (BLAST) finds regions of local similarity between sequences.

Extraction of intact aragonite platelets from nacre

Crushed nacre was immersed in a 3% NaOCl solution, constantly stirring at 4° C. The supernatant (a white foggy solution) containing aragonite platelets was daily removed and fresh 3% NaOCl solution added.
Aragonite platelets in 3% NaOCl solution were washed extensively with 10 mM TRIS buffer solution (Carl Roth GmbH, Germany) with 0.02% NaN_3 (pH 8.5) at 4° C to remove any rest of NaOCl. Aragonite platelets were stored in glass bottles at 4° C.

Extraction of intracrystalline proteins by demineralization of aragonite platelets with EDTA

Demineralization of aragonite platelets with EDTA (Merck KGaA, Germany) was performed in dialysis tubes, which where boiled for 5 min with 7 mM EDTA and rinsed several times with ultrapure water before use to remove any contaminations and heavy metal ions.
Aragonite platelets were filled into a dialysis bag of regenerated cellulose (*Spectra/Por RC, MWCO 3500*, Spectrum Laboratories, The Netherlands) and dialyzed against 100 mM EDTA with 0.02% NaN_3 (pH 7.0) at 4 °C, constantly stirring. EDTA solution was daily changed until the aragonite platelets were completely dissolved.
After complete demineralization of the mineral phase, the protein solution was centrifuged at 20000 rpm for 10 min at 4 °C (*Sorvall RC-SB Refrigerated Superspeed Centrifuge*, Sorvall DuPont, Germany). The supernatant was dialyzed extensively against three changes of a buffer solution compatible with the next step.

Extraction of intracrystalline proteins by demineralization of aragonite platelets with acetic acid

Aragonite platelets were dialyzed in dialysis bags of regenerated cellulose (*Spectra/Por, MWCO 3500*, Spectrum Laboratories, The Netherlands). To remove any contaminations and heavy metal ions, the dialysis tubes were boiled for 5 min with 7 mM EDTA and rinsed several times with ultrapure water before use.

Nacre was demineralized with 2.5% acetic acid solution (Sigma Aldrich Chemie GmbH, Germany) at 4 °C, constantly stirring. A solution of fresh 2.5% acetic acid was added every two days until the platelets were completely demineralized.
After complete demineralization of the mineral phase, the protein solution was centrifuged at 20000 rpm for 10 min at 4 °C (*Sorvall RC-SB Refrigerated Superspeed Centrifuge*, Sorvall DuPont, Germany). The supernatant was dialyzed extensively against three changes of a buffer solution compatible with the next purification step.

Ammonium sulfate precipitation of intracrystalline proteins

After demineralization of the aragonite platelets with 100 mM EDTA (pH 7.0), the intracrystalline proteins were dialyzed extensively against 10 mM Hepes (Carl Roth GmbH, Germany) buffer solution (pH 7.0).
Proteins were precipitated with the ammonium sulfate method[15]. Precipitation was performed by adding solid ammonium sulfate, $(NH_4)_2SO_4$, (Sigma Aldrich Chemie GmbH, Germany) to the protein medium to avoid further dilution. The "%-saturation" of ammonium sulfate was increased in steps of 10% (the so called "cuts"). The amount of $(NH_4)_2SO_4$ to add to the protein solution to obtain a desired $(NH_4)_2SO_4$ saturation was calculated according to the table in appendix 6.3 valid for precipitation at 0 °C [Holtzhauer, 1997].
The precipitation was performed as follows

1. Solid $(NH_4)_2SO_4$ was added to the protein solution to reach a saturation of 10%
2. The solution was stirred rapidly to prevent high local concentrations of $(NH_4)_2SO_4$
3. Once the salt was dissolved, the solution was left on ice for 20 min to allow proteins to aggregate
4. The solution was centrifuged at 15000 rpm for 10 min at 4 ºC
5. The supernatant was removed leaving the protein pellets intact
6. A proper amount of $(NH_4)_2SO_4$ was added to the supernatant to increase the saturation of $(NH_4)_2SO_4$ to 20%

[15] It is one of the most common types of precipitation. Ammonium sulfate is the most commonly used salt for precipitation because proteins can retain their activity and native conformation. Each protein precipitates at a characteristic salt concentration [Cooper, 1980].

7. Step 2 - 6 were repeated as above until a saturation of 90% was reached
8. To remove the excess of salt, protein pellets were dialyzed against 1 mM Hepes buffer solution with 0.02% NaN_3 (pH 7.0) at 4 °C

After dialysis protein fractions were concentrated in a speed vac concentrator (*Savant Speed Vac*, Schuett Labortechnik, Germany) for sodium dodecyl sulfate gel electrophoresis (SDS-PAGE). For SDS-PAGE analysis, a minimum of 5 µg proteins must be used in a volume of up to 15 µl [Weiss, 2000]. SDS-PAGE was carried out as described during this section. SDS-PAGE was performed using gels with 12% acrylamide (*NuPage Bis-Tris gels*, Novex, Invitrogen GmbH, Germany). Gels were stained with Coomassie Blue.

Trichloroacetic acid precipitation of intracrystalline proteins[16]

After demineralization of aragonite platelets with 100 mM EDTA (pH 7.0) or with 2.5% acetic acid, intracrystalline proteins were precipitated with trichloroacetic acid TCA as follows

1. A 100% TCA stock solution (corresponding to a concentration of 3 M) was always freshly prepared and not exposed to light for prolonged time
2. 200 µl TCA stock solution were added to 800 µl protein solution
3. The solution was incubated for 10 min at 4 °C and centrifuged at 15000 rpm for 5 min
4. The supernatant was carefully removed leaving the protein pellets intact
5. The pellets were washed with 100 µl cold acetone (-20° C) and centrifuged at 15000 rpm for 5 min
6. Steps 3 - 4 were repeated twice
7. Pellets were dried in a speed vac concentrator (*Savant Speed Vac*, Schuett Labortechnik, Germany) to drive off the acetone

The fractions collected were investigated by SDS-PAGE. After addition of Laemmli´s buffer solution for SDS-PAGE, which contains bromphenol blue, the solution turned yellow due to low pH. The pH was neutralized by slow addition of 1 M NaOH solution

[16] Fractional precipitation can be induced by changing the pH of the protein medium [Lottspeich and Zorbas, 1998]. Trichloroacetic acid (TCA) leads to a decrease in the pH solution and induces an increase of protein hydrophobicity. Aggregation of proteins is induced through hydrophobic interactions [Yvon et al., 1989].

until the colour turned to blue[17]. SDS-PAGE was performed using gels with 12% acrylamide (*NuPage Bis-Tris gels*, Novex, Invitrogen GmbH, Germany). Gels were stained with Coomassie Blue.

Methanol – chloroform precipitation of intracrystalline proteins [18]

The standard methanol-chloroform precipitation protocol [Wessel and Fluegge, 1984] was modified to maximize the amount of precipitated proteins. Due to the presence of methanol, only glassware was used. Any possible organic contamination was removed by cleaning the glassware with a *Piranha solution*. Piranha solution was freshly prepared by mixing 70% sulphuric acid (H_2SO_4) and 30% hydrogen peroxide (H_2O_2). Piranha solution is a strong oxidizer and it hydroxylizes most glass surfaces by addition of OH-groups, the glass surface results to be hydrophilic. To avoid sticking of the proteins on the reagent glass and on the glass pipettes, they were coated with dichlorodimethylsilane ($C_2H_6SiCl_2$) to obtain highly hydrophobic surfaces [Ashurst et al., 2001].

Glass cleaning with Piranha solution

1. Glass tubes were immersed in fresh Piranha solution and sonicated for 30 min
2. Glasses were rinsed several times and sonicated in ultrapure water for 10 min
3. Step 2 was repeated for three times
4. Glass tubes were dried at 150 °C until all the water was completely evaporated and cooled down to room temperature

[17] Bromphenol blue is a colour-sensitive pH indicator. It turns from brilliant yellow (pH $\leq$ 3) to deep purple-blue (pH$\approx$5) [Patel et al., 1973].

[18] Proteins can be precipitated by addition of organic solvents to the protein medium. Organic solvents act by decreasing the *dielectric constant* of the solution, which depresses ionisation of charged amino acid side chains therefore the solubility of the proteins decreases. Methanol-chloroform precipitation [Wessel and Fluegge, 1984] is based on the capacity of chloroform to associate with water molecules by weak hydrogen bonds.

Silanization of glass with dichlorodimethylsilane

Reagent tubes and glass pipettes were exposed to dichlorodimethylsilane (Fluka, Germany) vapours for 1 min and rinsed shortly with chloroform. Reagent tubes were dried with a nitrogen jet.

Methanol-chloroform precipitation

After demineralization of aragonite platelets with 100 mM EDTA (pH 7.0) the intracrystalline proteins were precipitated as follows

1. 4 ml methanol were added to the protein solution
2. 1 ml chloroform was added and the solution was mixed
3. The solution was centrifuged at 7000 rpm for 10 min. Using glass reagent tubes a higher speed could not be used. At higher speed reagents glasses broke
4. After centrifugation the proteins precipitated at the methanol – chloroform interface and formed a white clearly visible layer
5. The supernatant was carefully removed
6. 3 ml of methanol were added
7. The solution was centrifuged at 7000 rpm for 10 min. Pellets were collected at the bottom of the tube and the supernatant was carefully removed
9. Pellets were dried with nitrogen jet

The protein fractions collected were concentrated in a speed vac concentrator and analysed by SDS-PAGE. SDS-PAGE was performed using gels with 12% acrylamide (*NuPage Bis-Tris gels*, Novex, Invitrogen GmbH, Germany). Gels were stained with Coomassie Blue.

MALDI investigation of intracrystalline proteins

Protein fractions precipitated using the methanol-chloroform precipitation and analyzed by SDS-PAGE, were further investigated by MALDI.

After electrophoresis the gel slabs were not dried and protein spots were excised from the gel and digested with trypsin. Proteins were analyzed with an Ultraflex-TOF/TOF system (Bruker Daltonics, Germany) equipped with a N_2-laser.

MALDI measurements were performed by Dr. Anja Resemann (Bruker Daltonics GmbH, Bremen, Germany).

Separation of intracrystalline proteins by ion exchange chromatography

Buffer solutions and proteins solution were filtered (filter with pores of 0.22 µm Ø) to remove particles in the suspension and degassed in a vacuum bell jar (Nalge Company, NY, USA).

Ion exchange chromatography was performed with a Fast Protein Liquid Chromatography (FPLC, *GradiFrac system*, Amersham Pharmacia Biotech, Germany) system using a 5 ml sepharose carboxymethyl fast flow column (*sepharose-CM-FF* column, Amersham Pharmacia Biotech, Germany) and a quaternary ammonium fast flow column (*Q-FF* column, Amersham Pharmacia Biotech, Germany).

CM-FF columns were equilibrated with 20 mM citrate buffer solution with 0.02% NaN_3 (pH 4.8). A linear salt gradient of 0 - 1 M NaCl (1 M NaCl added in the sample buffer solution) was used. Flow rate 5 ml/min. Absorbance was detected at 280 nm.

Q-FF columns were equilibrated with 25 mM TRIS-HCl buffer solution with 0.02% NaN_3 (pH 8.0) respectively. A linear salt gradient of 0 - 1 M NaCl (1 M NaCl added in the sample buffer solution) was used. Flow rate 5 ml/min. Absorbance was detected at 280 nm.

Protein fractions were collected into 1.5 ml polypropylene vials (Eppendorf AG, Germany) and stored at 4 °C. 200 µl of each protein fraction were concentrated to 20 µl in a speed vac concentrator (*Savant Speed Vac*, Schuett Labortechnik, Germany) for SDS-PAGE. SDS-PAGE was performed using gels with a concentration of 12% acrylamide (*NuPage Bis-Tris gels*, Novex, Invitrogen GmbH, Germany). Gels were stained with Coomassie Blue.

Separation of intracrystalline proteins by high performance liquid chromatography (HPLC)

A solution of 0.1% trifluoroacetic acid (TFA) and a solution of acetonitrile with 0.1% (w/v) solution were freshly prepared, filtered sterile (0.22 µm Ø) and degassed in a vacuum bell jar (Nalge Company, NY, USA). All the chemicals used were of HPLC grade (Sigma Aldrich Chemie GmbH, Germany).
After ion exchange chromatography performed with a Q-FF column, with 25 mM citrate buffer solution with 0.02% NaN_3 (pH 4.8) and linear salt gradient of 0 - 1 M NaCl, protein fractions were acidified with TFA, degassed in a vacuum bell jar (Nalge Company, NY, USA) and centrifuged at 14000 rpm for 5 min.
Proteins were investigated by a reverse phase HPLC system (*Waters Delta 600 system*, Waters GmbH, Germany) with a semipreparative C-4 column (*Vydac C-4_214TP*, GraceVydac, California, USA). A linear gradient of acetonitrile with 0.1% TFA (w/v) at a flow rate of 1 ml/min was employed.
Absorbance was measured at two wavelengths 210 nm and 280 nm respectively[19] using a diodearray detector (*Waters 2487 Dual λ Absorbance Detector*, Waters GmbH, Germany, wavelength range: 190 - 650 nm).
200 µl of each protein fraction were concentrated to 20 µl in a speed vac concentrator (*Savant Speed Vac*, Schuett Labortechnik, Germany) for SDS-PAGE. SDS-PAGE was performed using gels with 12% acrylamide (*NuPage Bis-Tris gels*, Novex, Invitrogen GmbH, Germany) or gels with 10 - 20% (*TRIS-Glycine* gels Novex, Invitrogen GmbH, Germany). Gels were stained with Coomassie Blue.

Gel electrophoresis (SDS-PAGE) of intracrystalline proteins

The instruction for SDS-PAGE applied during this thesis are based on the protocol of Laemmli [Laemmli, 1970] and excellently described in the doctoral thesis of Weiss [Weiss, 2000].
Protein fractions were diluted in Laemmli´s buffer solution and 1 M dithiothreitol to an appropriate protein concentration (0.5 – 1 µg/µl). Laemmli´s buffer solution and 1 M

[19] The wavelength of absorbance for peptide bonds is between 190 nm and 230, in this range buffers can also strongly absorb. More specific for proteins is the detection at 280 nm. At 280 nm proteins exhibit a distinct ultraviolet light absorption maximum due primarily to the presence aromatic amino acids as tyrosine and tryptophane [Lottspeich and Zorbas, 1998].

dithiothreitol solution were freshly mixed at a ratio of 9:1 (v/v). Protein samples were afterwards heated for 5 min at 90 °C for and cooled down to room temperature. Gel electrophoresis was performed with a vertical gel system (*XCell SureLock Mini-Cell*, Novex, Invitrogen GmbH, Germany).

Laemmli´s buffer solution[20] (2x concentrated) for 50 ml

130 mM TRIS-HCl (pH 8.6)
20% glycerol
6.6% sodium dodecyl sulfate SDS
0.01% (w/v) bromphenol blue
10% ß-mercaptoethanol

All the chemicals were purchased from Sigma Aldrich Chemie GmbH, Germany.

Gel electrophoresis was performed using two different types of polyacrylamide gels:

1. *NuPage Bis-TRIS* gels with a concentration of 12% acrylamide, 1.0 mm thickness, 15 wells. Molecular weight (MW) range: 2 kDa - 200 kDa (Novex, Invitrogen GmbH, Germany).
2. *TRIS-Glycine* gels with a concentration of 10 - 20% acrylamide, 1.0 mm thickness, 15 wells, MW range: 6 kDa; max resolution 200 kDa (Novex, Invitrogen GmbH, Germany).

The following protein molecular weight markers[21] were employed:

1. *Mark12 Unstained*: 12 proteins in the range of 2.5 - 200 kDa dissolved in TRIS-HCl, glycerol, SDS, phenol red, Coomassie Blue G-250 (Novex, Invitrogen GmbH, Germany).
2. *SeeBlue Prestained Standard*: 9 prestained proteins in the range of 4 - 250 kDa dissolved in TRIS-HCl, formamide, SDS, phenol red (Novex, Invitrogen GmbH, Germany).

[20] Laemmli´s buffer was prepared following the protocol reported in [Laemmli, 1970].
[21] "Protein molecular weight markers" are a mixture of several purified proteins with known molecular weight; they are used to estimate sample molecular weights and to monitor the progress of an electrophoretic run.

Staining of SDS-PAGE gels

Staining with Coomassie Blue

After electrophoresis gel slabs were immersed for 10 minutes in Coomassie Blue gel staining solution. Gels were destained by changing Coomassie Blue gel destaining solution several times.

Coomassie Blue gel staining solution	**Coomassie Blue gel destaining solution**
0.25% Comassie brilliant Blue G-250	75 ml glacial acetic acid
450 ml methanol	50 ml methanol
90 ml glacial acetic acid	875 ml ultrapure water
460 ml ultrapure water	

All the chemicals were purchase from Sigma Aldrich Chemie GmbH, Germany.

Staining with Stains-all[22]

After gel electrophoresis the gels were washed at least 3 times with 50% formamide (Sigma Aldrich Chemie GmbH, Germany) for 20 min. Gels were stained with Stains-all (Sigma Aldrich Chemie GmbH, Germany) solution for 1 hour in total dark and destained with 50% formamide to remove excess of dye.
Stains-all is light unstable and gel bleaches in contact with air. Stains-all stock solution has to be stored in dark and hermetically sealed and can be used only one time.

Stains-all ($C_{30}H_{27}BrN_2S_2$) stock solution	**Stains-all solution gel staining solution**
0.1% Stains-all (w/v) in pure formamide	Stains-all stock solution diluted 1:20 with 50% formamide (v/v)

[22] The protocol is reported in [Holzhauer, 1997].

3.1.9 Extraction and purification of nacre water-soluble proteins

The extraction and characterization of water-soluble proteins is a multi-step process. Nacre of abalone shells was demineralized to collect the proteins. Proteins were separated according to their charge by ion exchange chromatography, to their mass by gels electrophoresis and to their hydrophobic properties by high performance liquid chromatography. Each step is presented in the following sections.

Nacre preparation

Green lip abalone (*Haliotis laevigata*) specimens of 10 - 20 cm in diameter were obtained from Abalone Exports (Laverton North, Victoria, Australia). The outer calcitic layer of the shells was removed by sand blasting (Hommel, Heinrich-Schlick-KG GmbH, Germany) with a working pressure of 7 bar (sandblasting agent: aluminium silicate grains, 0.2 - 0.5 mm Ø, Asilikos GmbH, Germany).
The nacreous parts of the shells were incubated for 2 minutes in a solution of 50% sodium hypochlorite (Sigma Aldrich Chemie GmbH, Germany) and ultrapure water (Millipore GmbH, Germany) to completely remove organic contaminations from the surface.
Sodiumhypochlorite and dissolved organic contaminants were removed by extensive washing with ultrapure water. Nacre was dried at 4° C, crushed into small pieces of 1 cm Ø with a hammer and milled with a ball mill (Fritsch GmbH, Germany) for 10 minutes at 300 rpm.

Extraction of water-soluble proteins by demineralization of nacre with acetic acid

Nacre powder was put into an Erlenmeyer glass flask filled with 12% acetic acid solution at 4° C, constantly stirring. For 100 g nacre 100 ml acetic acid solution were added. Due to the dissolution of calcium carbonate, CO_2 was released and foam developed. The foam, which contained nacre proteins, was collected into a glass bottle and stored at 4° C. Fresh 12% acetic acid solution was added every two days until nacre was completely demineralized.

Each foam fraction and the remaining suspension were centrifuged at 20000 rpm for 10 min at 4° C (*Sorvall RC-SB Refrigerated Superspeed Centrifuge*, Sorvall DuPont, Germany). The supernatant was dialyzed extensively against 20 mM citrate buffer solution with 0.02% NaN_3 (pH 4.8). Dialysis bags (*Spectra/Por RC, MWCO 6 - 8000*, Spectrum Laboratories, The Netherlands) were previously boiled for 5 min in 7 mM EDTA to remove organic contamination and heavy metals.

Separation of water-soluble proteins by ion exchange chromatography

Buffer solutions and protein solutions were filtered (filter with pores of 0.22 µm Ø) to remove particles in the suspension and degassed in a vacuum bell jar (Nalge Company, NY, USA).

Ion exchange chromatography was performed with a Fast Protein Liquid Chromatography system (FPLC, *GradiFrac system*, Amersham Pharmacia Biotech, Germany) using a 5 ml sepharose-carboxymethyl fast flow column (CM-FF column, Amersham Pharmacia Biotech, Germany) buffered with 20 mM citrate buffer solution with 0.02% NaN_3 (pH 4.8). A linear salt gradient of 0 - 1 M NaCl (1 M NaCl was added in the sample buffer solution) was used. Flow rate of 5 ml/min. Absorbance was detected at 280 nm.

Protein fractions were collected into 1.5 ml polypropylene vials (Eppendorf AG, Germany) and stored at 4 °C. 200 µl of each protein fraction were concentrated to 20 µl in a speed vac concentrator (*Savant Speed Vac*, Schuett Labortechnik, Germany) for SDS-PAGE. SDS-PAGE was performed using gels with a concentration of 10 – 20 % acrylamide (*Tris-Glycine gels*, Novex, Invitrogen GmbH, Germany). Gels were stained with Coomassie Blue.

Separation of water-soluble proteins by high performance liquid chromatography (HPLC)

Protein fractions collected after ion exchange chromatography, as above described, were analyzed by HPLC.

0.1% trifluoroacetic acid (TFA) solution and acetonitrile with 0.1% TCA (w/v) solution were freshly prepared, filtered sterile (0.22 µm Ø) and degassed in a vacuum bell jar

(Nalge Company, NY, USA). All the chemicals used were of HPLC grade (Sigma Aldrich Chemie GmbH, Germany).

5 ml of protein solution were filtered sterile (0.22 µm), acidified with TFA, degassed in a vacuum bell jar (Nalge Company, NY, USA) and centrifuged at 14000 rpm for 5 min.

Protein samples were investigated by reversed phase HPLC (*Waters Delta 600 system*, Waters GmbH, Germany) with a semipreparative C-4 column (Vydac C-4_214TP, GraceVydac, California, USA) using a linear gradient of acetonitrile with 0.1% TFA (w/v) at a flow rate of 2 ml/min.

Absorbance was measured at two wavelengths 210 nm and 280 nm respectively[23] using a diodearray detector (*Waters 2487 Dual λ Absorbance Detector*, Waters GmbH, Germany, wavelength range: 190 - 650 nm).

200 µl of each protein fraction were concentrated to 20 µl in a speed vac concentrator (*Savant Speed Vac*, Schuett Labortechnik, Germany) for SDS-PAGE. SDS-PAGE was performed using gels with a concentration of 10 – 20 % acrylamide (*Tris-Glycine gels*, Novex, Invitrogen GmbH, Germany). Gels were stained with Coomassie Blue.

Due to the presence of TFA, which lowers the pH of the solution, some of the samples coloured yellow after addition of Laemmli´s buffer solution. Samples were neutralized by slow addition of 1 M NaOH until the colour turned to blue.

Gel electrophoresis (SDS-PAGE) of water-soluble proteins

Gel electrophoresis was carried out as described in the previous section (3.1.8). Gel slabs were stained with Coomassie Blue.

MALDI investigation of water-soluble proteins

Protein fractions collected after ion exchange chromatography were further investigated by MALDI. A saturated solution of sinapinic acid in 30% acetonitrile with 70% of 0.1% TFA solution was spinned down and mixed 1:1 with the protein sample.

[23] The wavelength of absorbance for peptide bonds is between 190 nm and 230, in this range buffers can also strongly absorb. More specific for proteins is the detection at 280 nm. At 280 nm proteins exhibit a distinct ultraviolet light absorption maximum at 280 nm, due primarily to the presence aromatic amino acids as tyrosine and tryptophane [Lottspeich and Zorbas, 1998].

1 µl of the mixture was deposited on a stainless steel target plate and dried at ambient air.

The crystals formed by cocrystallization of the proteins with the matrix were investigated with a light microscope. Beside the formation of matrix crystals, sodium chloride crystals were found.

To remove NaCl, 30 µl of protein solution were shortly desalted with a porous C-18 microtip (ZIP-TIP, Millipore GmbH, Germany) previously conditioned with 50% acetonitrile and 0.1% TFA. The desalted protein solution was prepared as above. Only protein-matrix crystals were visible.

Proteins were analyzed with an Ultraflex II TOF/TOF system (Bruker Daltonics GmbH, Germany) equipped with a N_2-laser with the kind help of Dr. Anja Resemann (Bruker Daltonics GmbH, Bremen, Germany).

3.2 AFM investigations of influence of nacre proteins on calcium carbonate crystallization

3.2.1 Atomic force microscopy (AFM)

The atomic force microscope (AFM), developed in 1986 by Binnig, Quate and Gerber, is a near-field microscope for the investigation, down to atomic resolution, of surfaces. Non-conducting surfaces can be imaged [Binning et al., 1986]. In particular the ability of AFM to work in fluids makes AFM a valuable instrument to investigate dynamic processes involving biological molecules. Dynamic processes on crystal surfaces, *e.g.* protein-mineral interactions, can be monitored in real time, on the micro- or nanometer scale [Binning et al., 1992; Walters et al., 1997; Blank et al., 2003].

A sharp tip, mounted at the end of a soft cantilever spring, interacts with the scanned sample surface. As the tip travels across the surface the cantilever will deflect following the contours of the surface. The topographic features of a surface are obtained directly measuring the deflection of the cantilever, which bends according to Hooke's law.

The deflection is measured using a laser spot reflected from the backside of the cantilever into a four-quadrant position sensitive photodetector. The difference

between the photodiode signals indicates the position of the laser spot on the detector and thus the angular deflection of the cantilever. By measuring the light intensity on each quadrant and by summing up the corresponding voltages, V_{def} = (A + B) - (C + D), the resulting V_{def} is proportional to the physical detection of the cantilever. The vertical deflection of the cantilever can be monitored with picometer resolution.

The sample can be moved with a piezoceramic actuator, which changes its dimension under applied voltage. The most frequently used driver is a hollow–tube scanner, which can move the tip or the sample in all three mutually perpendicular directions.

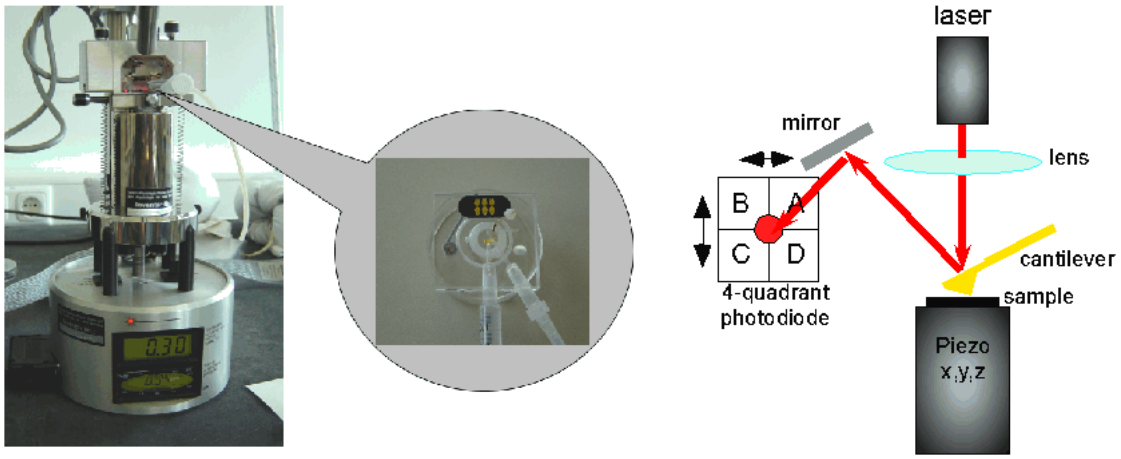

Fig. 3.10. Left. Multimode Nanoscope IIIa and glass fluid cell (inset) [Blank, 2003]. Right. AFM working principle (schematic representation). A sample can be moved in all three mutually perpendicular directions (*x,y,z*) by a piezoelectric tube. While the sample is scanned, a cantilever spring will deflect following the surface contours. The deflection of the cantilever is detected with the help of a laser beam reflected from the backside of the cantilever. The reflected laser beam illuminates a four-quadrant position sensitive photodetector.

Contact mode is one of the most common methods of AFM operation; it provides high spatial resolution and a relatively high speed at which the sample can be scanned. The disadvantage is the relatively high force that is laterally exerted on the sample. The cantilever deflection is mainly due to hard-core repulsion between the electron cloud of the atoms of the sample and the tip. In contact mode cantilever-tip and sample are progressively brought in contact until the electron clouds of the atoms begin to repulse each other electrostatically. The force goes to zero when the distance between the atoms reaches a couple of angstroms, about the length of a

chemical bound. When the total van der Waals force becomes positive (repulsive), the atoms are in contact.

The AFM probes commonly used are cantilevers with integrated tips of silicon nitride (Si_3N_4) or silicon. Cantilevers with different geometry (lengths, thicknesses and shapes) are available for different purposes. Typical elastic spring constants vary in the range of 0.01 - 50 N/m. Cantilevers of small spring constant are most suitable for imaging soft materials, while rigid cantilevers are needed for probing the nanomechanical properties of hard sample surfaces. The tip at the end of the cantilever typically has a pyramidal shape with an apex of 15 nm.

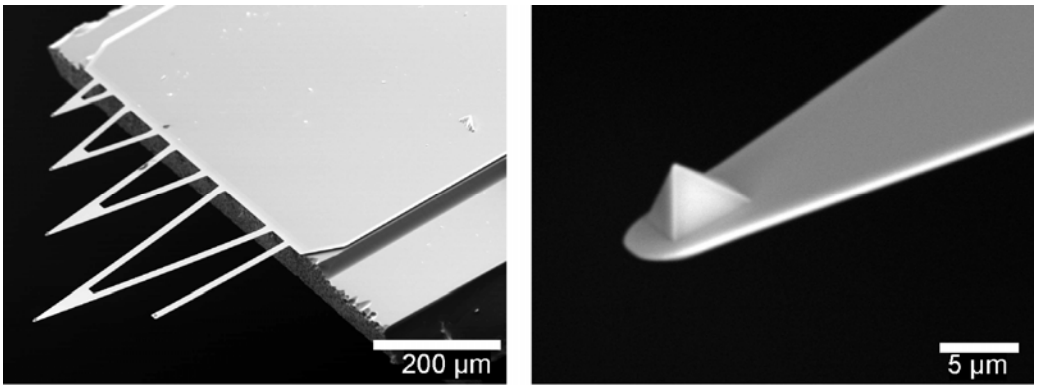

Fig. 3.11. Left. SEM images of a commercial gold-coated silicon nitride (Si_3N_4) cantilever. Right. Magnification of a single cantilever showing a pyramidal tip with an apex of few nanometers. Pictures were gently performed by Fabian Heinemann, Institute of Biophysics, University of Bremen, Germany.

3.2.2 AFM investigations of nacre protein interactions with a calcite surface

The interactions and influences of water-soluble nacre proteins with a calcite substrate were investigated by AFM. AFM is particularly suitable for this kind of investigation because allows the observation *in real* time and operates in fluids. All AFM experiments carried out during this thesis were performed incubating a geological calcite surface (used as substrate) with a supersaturated calcium carbonate solution containing intracrystalline proteins. Calcite was also incubated with perlinhibin dissolved in a calcium chloride and in a supersaturated calcium carbonate solution. Intracrystalline proteins and perlinhibin were investigated separately.

All AFM experiments were performed at ambient conditions using a Nanoscope IIIa scanning probe microscope (Digital Instruments, Santa Barbara, CA, USA) equipped with a piezoelectric scanner (E-scanner maximum scan range of 10 x 10 x 2 µm in the *x*-, *y*- and *z*-directions; J-scanner maximum scan range 100 x 100 x 5 µm) and a glass fluid cell. Surfaces were imaged using commercially available gold-coated Si_3N_4 cantilevers, 200 µm length and spring constant 0.02 N/m (Veeco Instrument GmbH, Germany). Scan rates from 1 to 5 Hz with 512 sampling points per scan line (sample/line) were typically used. For each experiment a freshly cleaved calcite surface was initially in ultrapure water. The aqueous solution in the fluid cell was exchanged during imaging with calcium carbonate solution with nacre proteins. A detailed description of the solution preparation is described in the next sections.
All deflection images were processed with Image SXM software for contrast adjustment and examination of height profile.

Geological calcite preparation

Calcite samples were prepared by cleaving a single large crystal of optical-quality (Kristalldruse, Germany) along the [4 $\underline{4}$ $\underline{1}$] plane. For each experiment new fragments were freshly prepared and handled with tweezers to avoid surface contamination by skin fat. The crystal surface of each calcite fragment was controlled under a light microscope. The crystal showing a relative flat surface was chosen and used as substrate. Calcite was glued with a two-components epoxy glue (Bindulin-Werk, Germany) onto a freshly cleaved mica platelet (Plano W. Plannet GmbH, Germany) with a diameter of 10 mm. Mica, a silicate mineral composed of several atomic layers, was easily cleaved using adhesive tape. This procedure assured that the surface where the calcite was glued was free from contaminations.
The glued crystal was dried in air for at least 10 min and then carefully rinsed with sterile filtered (0.22 µm Ø) ultrapure, degassed water at room temperature. In this way small particles and dust adhering to the crystal surfaces were removed. The sample was positioned on the top of the AFM scanner. The head of the microscope, with the fluid cell and the cantilever, was mounted. All the solutions were manually injected into the fluid cell using a 1 ml dosage syringe (Injekt-F 1ml, Braun, Melsungen AG, Melsungen, Germany).

Cantilever cleaning with UV-light

Gold-coated sharp cantilevers (*MSCT-Sharpened contact microlevers*, Veeco Instrument GmbH, Germany) were cleaned for 15 min using an UV-lamp ("UV pen ray lamp", UVP, San Gabriel, CA, USA) to remove organic contaminants. The atomic oxygen, produced by the decomposition of ozone with UV light, oxidizes organic contaminants to form volatile molecules. Meanwhile the UV light excites the contaminant molecules to make them more reactive with ozone and/or atomic oxygen.

Glass fluid cell cleaning

The glass fluid cell was cleaned with a detergent ("Ultra Joy", Procter & Gamble, Ohio, USA), rinsed with ultrapure water and dried with a nitrogen jet. Before each experiment the fluid cell was irradiated for 5 min with UV-light ("UV pen ray lamp", UVP, San Gabriel, CA, USA).

Supersaturated calcium carbonate solution

Supersaturated $CaCO_3$ solution was prepared following the protocol of Hillner [Hillner, 1992]. 400 ml of 100 mM $NaHCO_3$ were added drop-wise to 1000 ml of 40 mM $CaCl_2$ continuously stirring until the solution became turbid. The pH was adjusted to 8.2 with 10 M NaOH. The solution was sterile filtered through a filter with pores of 0.22 µm and degassed in vacuum bell jar (Nalge Company, NY, USA).

AFM investigations with intracrystalline proteins

Supersaturated $CaCO_3$ solution with intracrystalline proteins

Intracrystalline proteins, stored in 25 mM TRIS-HCl with 0.02% NaN_3 (pH 8.0) at 4° C, were extensively dialyzed against the supersaturated $CaCO_3$ solution (prepared as above described).

The dialysis tube (*Spectra/Por RC, MWCO 3500*, Spectrum Laboratories, The Netherlands) was boiled for 5 min with 7 mM EDTA and rinsed several times with ultrapure water.

The final concentration of 25 µg/ml was determined with a Bradford microassay (see section 3.1.6) using IgG and lysozyme as standard proteins (Sigma Aldrich Chemie GmbH, Germany).
Before AFM investigations the supersaturated $CaCO_3$ solution with intracrystalline proteins was degassed in a vacuum bell jar (Nalge Company, NY, USA), centrifuged at 14000 rpm for 5 min and sterile filtered (filter pores 0.22 µm Ø).

AFM investigations with perlinhibin

Calcium chloride solution with perlinhibin

Freeze dried perlinhibin was dissolved in sterile filtered 7.5 mM $CaCl_2$ (pH 7.0) solution to a final concentration of 20 µg/ml. Before AFM investigations the solution was degassed in a vacuum bell jar (Nalge Company, NY, USA).

Supersaturated calcium carbonate solution with perlinhibin

Perlinhibin, stored in 20 mM citrate buffer solution with 0.02% NaN_3 (pH 4.8) at 4° C, was concentrated in a speed vac concentrator (*Savant Speed Vac*, Schuett Labortechnik, Germany) and dialyzed against the supersaturated $CaCO_3$ solution prepared as above described.
The dialysis tubes (*Spectra/Por RC, MWCO 6 - 8000*, Spectrum Laboratories, The Netherlands) were boiled for 5 min with 7 mM EDTA and rinsed several times with ultrapure water before use.
The final concentration of 20 µg/ml was determined with a Bradford microassay (see section 3.1.6) using IgG and BSA (Sigma Aldrich Chemie GmbH, Germany) as standard proteins.

3.3 Crystallization of calcium carbonate with nacre proteins

3.3.1 Ammonium carbonate vapour diffusion technique

"Ammonium carbonate vapour diffusion" is a widespread and simple technique to precipitate calcium carbonate from solutions and to investigate the influence of additives on the crystallization of calcium carbonate [Addadi et al., 1985; Addadi and Weiner, 1996]. This method is widely used because crystals can be precipitated from a solution in which the additives are present from the beginning.

The decomposition of ammonium carbonate[24] produces carbon dioxide and ammonia that can diffuse into a calcium chloride ($CaCl_2$) solution. Dissolved carbon dioxide (CO_2) will transforms into carbonic acid with a pH dependent distribution of the different protonated states. Ammonia (NH_3) can at the same manner diffuse into the solution causing an increase in the pH and therefore enhancing the amount of carbonate ions (CO_3^{2-}) in solution. When enough CO_3^{2-} is present in the solution, it interacts with the Ca^{2+} inducing $CaCO_3$ to precipitate. The chemical reactions can be summarized as follows

$$(NH_2)CO_{3(s)} \Leftrightarrow 2NH_{3(g)} + CO_{2(g)} \quad \textbf{(3-6)}$$

$$CO_2 + Ca^{2+} + H_2O \Leftrightarrow CaCO_{3(s)} + 2H^+ \quad \textbf{(3-7)}$$

During precipitation the pH value of the solution should drop according to the reaction (2-7) presented in section 2.2.1. Due to the ammonia diffusion into the $CaCl_2$ solution the pH of the solution tends to increase and the pH is not constant during the crystallization.

The crystallization device (fig. 3.9) consists of a sealed chamber in which a powder of ammonium carbonate, put in a glass beaker, can decompose in CO_2 and NH_3. The gases diffuse into crystallization vessels (Nunc disk) containing glass slides immersed into a $CaCl_2$ solution containing the additives to be investigated. The crystallization vessel and the beaker with $(NH_4)_2CO_3$ are covered with pierced aluminium foil to slow down the diffusion of ammonia and to obtain a less drastic pH

[24] Ammonium carbonate decomposes at room temperature.

variation. Crystallization takes place mainly on the glass slide surface in contact with the $CaCl_2$ solution. The morphology of the crystals can be analyzed *e.g.* by scanning electron microscopy.

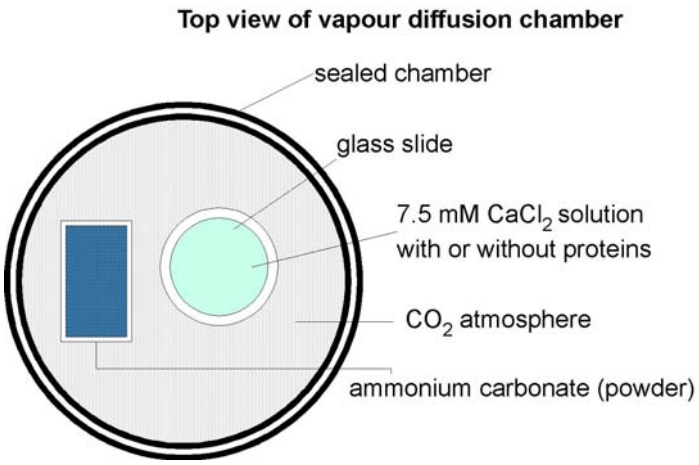

Fig. 3.9. Experimental setup for the vapour diffusion precipitation technique. In a sealed dessicator a saturated carbon dioxide (CO_2) atmosphere is obtained by spontaneous decomposition of solid ammonium carbonate ($(NH_4)_2CO_3$), which decompose in CO_2 and ammonia (NH_3). CO_2 can diffuse into a 7.5 mM calcium chloride ($CaCl_2$) solution (with or without additives) and induces precipitation of calcium carbonate crystals.

Cocrystallization of calcium carbonate with perlucin

The influences of perlucin on calcium carbonate crystal nucleation and growth were investigated with the ammonium carbonate vapour diffusion technique, following the protocol of [Addadi and Weiner, 1996].

To eliminate the presence of organic contaminants on the glass slides, these were cleaned with a freshly prepared Piranha solution.

1. Glass slides (13 mm Ø) were immersed in fresh Piranha solution (30% H_2O_2, 70% H_2SO_4) and sonicated for 30 min
2. Glass slides were rinsed several times with ultrapure water and sonicated in ultrapure water for 10 min
3. Step 2 was repeated for three times
4. Glass slides were dried at 150 °C until all the water was completely evaporated and cooled down at room temperature

Perlucin extracted from the nacre of *H. laevigata*, stored at 4° C in a 20 mM citrate buffer solution with 0.02% NaN_3 (pH 4.8) was dialyzed (dialysis bags *Spectra/Por RC, MWCO 6 - 8000*, Spectrum Laboratories, The Netherlands) against a sterile filtered 7.5 mM $CaCl_2$ (pH 7.0) solution with 0.02% NaN_3 at 4 °C. Dialysis bags were boiled for 5 min with 7 mM EDTA and rinsed several times with ultrapure water before use.

The final protein concentration of 10 µg/ml was determined with a Bradford microassay (Bio-Rad Laboratories GmbH, Germany) using IgG and BSA as standard proteins (Sigma Aldrich Chemie GmbH, Germany).

The glass slides (cleaned with Piranha as above described) were put in Nunc multidishes (Nunc GmbH & Co. KG, Germany) with a well diameter of 15 mm. 1 ml of perlucin dissolved into the $CaCl_2$ solution (prepared as above described) was introduced in each well. The wells were covered with an aluminium foil punctured with a needle. For a negative control measurements only 7.5 mM $CaCl_2$ (pH 7.0) solution was used. The crystallization vessels were put in sealed chamber with powder of ammonium carbonate and the crystals were grown for 5 days at room temperature.

The glass coverslips were gently removed from the crystallization vessel and shortly rinsed with ultrapure water to remove any rest of 7.5 mM $CaCl_2$ (pH 7.0) and avoid secondary crystallization on the crystal surface. The glass slides were dried in an oven at 25 °C.

For scanning electron microscopic (SEM) investigations, the coverslides were glued on SEM stubs and sputter-coated with gold. Sputtering was performed with an *Emitech K550* system (*EM Technologies Ltd., England*) with a current of 10 – 20 mA in a 0.2 mbar argon atmosphere.

The crystals were investigated at kV using a Camscan Series 2 SEM (Cambridge Instruments, England).

Cocrystallization of calcium carbonate with perlinhibin

Perlinhibin, stored in 20 mM citrate buffer solution (pH 4.8) was dialyzed against a 7.5 mM $CaCl_2$ solution (pH 7.0, adjusted with 1 M NaOH) at 4 °C. Dialysis bags (*Spectra/Por Membrane MWCO: 6 - 8000 vol/length 0.32 ml/cm*) were boiled for 5 min with 7 mM EDTA and rinsed several times with ultrapure water before use.

Wells were filled with $CaCl_2$ solution with perlinhibin (as described above). As control, some wells were filled with 800 µl 7.5 mM $CaCl_2$ (pH 7.0).
Crystallization and SEM investigation were performed as above described.

Cocrystallization of calcium carbonate with non-nacreous proteins (immunoglobulin, bovine serum albumin and albumin)

Negative control experiments were carried out in the same way with non-nacreous proteins as immunoglobulin (IgG), bovine serum albumin (BSA) and albumin from chicken. Lyophilized proteins were added directly to 7.5 mM $CaCl_2$ (pH 7.0) and mixed until they were completely dissolved. The final protein concentration was 10 µg/ml.
Crystallization and SEM investigation were performed as above described.

Cocrystallization of calcium carbonate with buffer substances

Several buffer substances were also tested to minimize the pH variation. 2 mM TRIS buffer salt (pH 7.0) and with 2 mM citrate buffer salt (pH 4.8) were added to 7.5 mM $CaCl_2$ (pH 7.0) separately. Crystallization and SEM investigation were performed as above described.

3.3.2 Calcium carbonate precipitation assay

The effect of nacre intracrystalline proteins on calcium carbonate precipitation was monitored observing the pH behaviour in a supersaturated calcium carbonate solution following the protocol of Wheeler [Wheeler et al., 1981].

Precipitation of calcium carbonate without proteins

A supersaturated calcium carbonate solution was prepared by pouring 60 ml of 20 mM $CaCl_2$ into 60 ml of 20 mM $NaHCO_3$ (pH 8.4) in a reagent glass. The pH of the $CaCl_2$ solution was before each experiment adjusted with 0.05 mM NaOH to pH 8. After mixing the two solutions the reagent glass was covered with aluminium foil to

prevent excessive diffusion of CO_2 in the atmosphere. The pH was monitored with a pH meter (*Sartorius PP-20*, Sartorius AG, Germany). All experiments were carried out at room temperature.

Precipitation of calcium carbonate with intracrystalline proteins

Intracrystalline proteins extracted as describe in section 3.1.8 and stored in 25 mM TRIS-HCl with 0.02% NaN_3 (pH 8.0) at 4 °C, were dialyzed (dialysis tube *Spectra/Por RC, MWCO 3500*, Spectrum Laboratories, The Netherlands) against 20 mM $NaHCO_3$ (pH 8.4) at 4 °C.
The final protein concentration was determined with a Bradford microassay (Bio-Rad Laboratories GmbH, Germany) using lysozyme as standard protein (Sigma Aldrich Chemie GmbH, Germany). The $NaHCO_3$ solution with proteins was mixed with 20 mM $NaHCO_3$ to reach a final volume of 60 ml. 20 mM $CaCl_2$ solution were added to 60 ml of $NaHCO_3$ solution with proteins. After mixing the two solutions the reagent glass was covered with aluminium foil to prevent excessive diffusion of CO_2 in the atmosphere. The pH was monitored with a pH meter (*Sartorius PP-20*, Sartorius AG, Germany). All experiments were carried out at room temperature.

3.3.3 Staining method for differentiating calcium carbonate polymorphs

The calcium carbonate polymorphs, calcite and aragonite can be distinguished by a staining method [Friedman, 1959]. Feigl´s test is commonly used to distinguish aragonite from other carbonates. Feigl´s solution stains aragonite surface black whereas calcite remains unstained.

Differential staining for calcium carbonate polymorphs

Feigl´s solution was prepared according the protocol presented in [Arnoldi, 2001] by addition of 7.2 g $MnSO_4 \cdot H_2O$ in 100 ml H_2O. The solution was heated while constantly stirring. 1 g Ag_2SO_4 was added. The solution was stirred constantly until it started to boil. The solution was filtered with a paper filter and 1 drop of 1 M NaOH

was added. After 90 min the solution was filtered again and stored in a closed dark bottle.
Calcium carbonate crystals (geological calcite, geological aragonite, calcite incubated with nacre proteins) and nacre were incubated for 5 min with some drops of Feigl´s solution. Changes in colours of the mineral surfaces were monitored.

3.4 XRD investigation of calcite incubated with perlinhibin

3.4.1 X-ray diffraction (XRD)

X-ray diffraction (XRD) is a non-destructive technique for characterizing crystalline materials. It provides information on phases, crystal orientations (texture) and other structural parameters. X-ray diffraction peaks are produced by constructive interference of X-ray photons scattered from each set of lattice planes at specific angles. The spacing in the crystal lattice can be determined using the Bragg's law [Lottspeich and Zorbas, 1998].
For diffraction applications, only short wavelength X-rays (hard X-rays) in the range of a few angstroms to 0.1 Å (1 keV - 120 keV) are used, because their wavelength is comparable to the size of atoms. During the interaction of X-ray photons with electrons surrounding the atoms in the sample, some photons from the incident beam are elastically scattered. The elastically scattered X-rays are only considered in diffraction experiments because they carry information about the electron distribution in materials.
Diffracted waves from different atoms interfere with each other and the resultant intensity distribution is strongly modulated by this interaction. If the atoms are arranged in a periodic fashion, as in crystals, the diffracted waves will consist of sharp interference maxima (peaks) with the same symmetry as in the distribution of atoms. Measuring the diffraction pattern the distribution of atoms in a material can be elucidated.
The peaks in an X-ray diffraction pattern are directly related to the atomic distances. For a given set of lattice plane with an inter-plane distance of d, the condition for a diffraction (peak) to occur can be simply written according to the *Bragg's law*

$$n\lambda = 2d\sin\theta$$

where n is an integer, λ is the wavelength of X-rays, d is the spacing between the planes in the atomic lattice, and θ is the angle between the incident ray and the scattering planes [Lottspeich and Zorbas, 1998]. XRD investigation of calcite incubated with a supersaturated calcium carbonate solution with perlinhibin.

Geological calcite cleaved along the [4 4̲ 1̲] plane was incubated for 20 hours with perlinhibin dissolved in a supersaturated calcium carbonate solution (as described at pag. 59). The sample previously investigated by AFM and after investigation dried in air at room temperature. The sample was investigated by XRD in Bragg Brentano geometry.
Measurements were gently performed by Fabienne Bosselmann, University of Duisburg-Essen, Germany.

3.5 Small angle neutron scattering investigations of nacre aragonite platelets

3.5.1 Small angle neutron scattering (SANS)

Small angle neutron scattering (SANS) is a technique in which neutrons are elastically or inelastically scattered by the atomic nuclei of a sample. The resulting scattering pattern provides information about the size, shape and orientation of some component of the sample achieving a resolution of a few angstroms[25].
In a SANS experiment, a beam of collimated radiation is directed at a sample, illuminating a small volume, V ($V=At_s$, where A is the cross-sectional area of the beam and t_s is the path length of the sample). A detector element of dimensions $dxdy$ positioned at a distance L_{sd} from the sample at scattering angle θ, records the flux of radiation scattered into a solid angle element, $\Delta\Omega$ ($\Delta\Omega=dxdy/L_{sd}^2$). The flux, $I(\lambda,\theta)$ is expressed as

[25] The theoretical introduction of SANS is adapted from [King, 1999].

$$I(\lambda,\theta) = I_0(\lambda)\Delta\Omega\eta(\lambda)TV\frac{\partial\sigma}{\partial\Omega}(Q) \quad \textbf{(3-8)}$$

where I_0 is the incident flux, η is the detector efficiency or response; T is the sample transmission and $(\partial\sigma/\partial\Omega)(Q)$ is the *microscopic differential cross-section function*.

The differential cross-section contains all the information on shape, size and interactions of the scattering bodies in the sample. The differential cross-section is given by

$$\frac{\partial\sigma}{\partial\Omega}(Q) = N_p V_p^2 (\Delta\delta)^2 P(Q)S(Q) + B_{inc} \quad \textbf{(3-9)}$$

where N_p is the number of the scattering bodies, V_p is the volume of one scattering body, $(\Delta\delta)^2$ is the square of the difference in *neutron scattering length density* or *contrast*, $P(Q)$ is the *form* or *shape factor function*, $S(Q)$ is the *interparticle structure factor*, Q is the modulus of the *scattering vector* and B_{inc} is the (isotropic) incoherent background signal. The microscopic differential cross-section $(\partial\sigma/\partial\Omega)(Q)$ has dimensions of [length]$^{-1}$.

The microscopic differential cross-section is typically replaced by the product of $N_p \cdot(\partial\sigma/\partial\Omega)(Q)$, termed as *macroscopic differential cross-section* $(\partial\Sigma/\partial\Omega)(Q)$.

The scattering vector ($\boldsymbol{Q}$), the modulus of the resultant between the incident wavevector, $\boldsymbol{k_i}$, and scattered wavevector, $\boldsymbol{k_f}$, is given by

$$Q = \left|\vec{Q}\right| = \left|k_f - k_i\right| = \frac{4\pi}{\lambda}\sin\left(\frac{\theta}{2}\right) \quad \textbf{(3-10)}$$

Q has dimensions of [L]$^{-1}$. The scattering vector is also defined as the *momentum transfer*, because the product hQ, where h is the Planck's constant, is equal to the change in the momentum of the neutron during scattering.

The three most important parameters for SANS are the contrast term, the form factor and the structure factor.

The *contrast term* $(\Delta\delta)^2 = (\delta p - \delta m)^2$ is the difference in length density δ, between the part of the sample of interest (δp) and the surrounding medium (δm). If $(\Delta\delta)^2$ is zero

the scattering bodies are said to be at *contrast match*. The contrast matching technique is used to simplify the scattering patterns from a multicomponent system.
Contrast match technique is based on the substitution of H with D, which present a different scattering length. The scattering lengths b of deuterium and hydrogen are very different, opposite in sign (b_D= 6.671 fm and b_H= - 3.742 fm respectively) and neutrons are scattered much more strongly from D than from H. Modulating the ratio H/D in a buffer, the scattering signal from different components of the sample can be "matched out" and the contrast of the different components is matched by the background scattering.
The *form factor* $P(Q)$ is a function that describes how the microscopic cross section $(\partial\sigma/\partial\Omega)(Q)$ is modulated by interference effects between the radiation scattered by different parts of the same scattering body. It depends on the shape of the scattering body. The general form of $P(Q)$ is given by Van de Hulst's equation

$$P(Q) = \frac{1}{V_p^2}\left|\int_0^{V_p} \exp[if(Q\alpha)]dV_p\right| \qquad \textbf{(3-11)}$$

where α is shape parameter that might represent a length or a radius of gyration.
The *interparticle structure factor* $S(Q)$ is a function that describes how $(\partial\sigma/\partial\Omega)(Q)$ is modulated by interference effects between radiation scattered by different scattering bodies, it is given by (3-12) and it is dependent on the degree of local order in the sample

$$S(Q) = 1 + \frac{4\pi N_p}{QV}\int_0^{\infty} [g(r)-1]r\sin(Qr)dr \qquad \textbf{(3-12)}$$

3.5.2 SANS investigations of nacre aragonite platelets

Small angle neutron scattering was performed to investigate the distribution of the organic matrix within single nacre aragonite platelets (from the nacre of *H. laevigata*), the size of the molecules and more in general the structure of single aragonite platelets. SANS investigation was performed at the diffractometer KWS1 at the

FRJ2-reactor of the “Forschungszentrum Jülich”, kindly performed by Dr. Dieter Schwahn and Dr. Vitaliy Pipich (“Forschungszentrum Jülich”, Jülich, Germany).

Green lip abalone (*Haliotis laevigata*) specimens of 10 - 20 cm in diameter were obtained from Abalone Exports (Laverton North, Victoria, Australia). The outer calcitic layer of the shells was removed by sand blasting (Hommel, Heinrich-Schlick-KG GmbH, Germany) with a working pressure of 7 bar (sandblasting agent: aluminium silicate grains, 0.2 - 0.5 mm Ø, Asilikos GmbH, Germany).

Nacre was incubated for 2 minutes in a solution of 50% sodium hypochlorite (Sigma Aldrich Chemie GmbH, Germany) and ultrapure water (Millipore GmbH, Germany) to remove any organic contaminants from the surface.

Nacre was extensively washed with ultrapure water and dried at 4 °C. For the extraction of aragonite platelets 100 g of nacre, obtained from *H. laevigata* shells as above described, were crushed in small pieces with a hammer (approx. 0.5 – 1 cm Ø). Nacre was immersed into a 3% sodium hypochlorite (NaOCl) solution (Merck GmbH, Germany) constantly stirring at 4 °C. The supernatant was daily removed and fresh 3% NaOCl solution was added. This procedure was repeated until all the nacre was dissolved. NaOCl was removed by extensively washing with 10 mM TRIS with 0.02% NaN_3 (pH 8.5). The aragonite platelets were dried in an incubator at 25 °C.

Nacre aragonite platelets were heated up to 350 °C, 430 °C and 500 °C respectively. The temperature was increased with a constant rate of 10 K/min. The final temperature was kept constant for 10 min and the samples were let cool down at room temperature.

Quartz cells for SANS investigation were filled with nacre aragonite platelets before and after temperature treatment. The cells were further filled with a D_2O/H_2O solution for “contrasts match”.

Scattering experiments were performed within a momentum transfer range of $0.002 < Q\ (Å^{-1}) < 0.2$. Neutron wavelength was 7 Å. The detector to sample distances and the corresponding collimation distances were fixed at 2, 4, 8 and 20 m.

The scattering data were corrected for background, efficiency of the single detector cells, then radially averaged and calibrated in absolute units by a Plexiglas secondary standard.

Native nacre and geological aragonite were also investigated.

SANS investigations of nacre

Green lip abalone (*Haliotis laevigata*) specimens of 10 - 20 cm in diameter were obtained from Abalone Exports (Laverton North, Victoria, Australia). The outer calcitic layer of the shells was removed by sand blasting (Hommel, Heinrich-Schlick-KG GmbH, Germany) with a working pressure of 7 bar (sandblasting agent: aluminium silicate grains, 0.2 - 0.5 mm Ø, Asilikos GmbH, Germany).
Nacre was incubated for 2 minutes in a solution of 50% sodium hypochlorite (Sigma Aldrich Chemie GmbH, Germany) and ultrapure water (Millipore GmbH, Germany) to remove any organic contaminants from the surface.
Nacre was extensively washed with ultrapure water and dried at 4 °C. Approximately 50 g of nacre were crushed into small pieces of 1 cm in diameter with a hammer and milled with a ball mill (Fritsch GmbH, Germany) for 10 minutes at 300 rpm. Nacre grains with different size were obtained (2 mm as maximal diameter).
Nacre was not heated but investigated in its native state. In section 4.1.2 the term *native nacre* is used for this reason.
Quartz cells for SANS investigation were filled with native nacre and further filled with a D_2O/H_2O solution for “contrasts match”.
Scattering experiments were performed within a momentum transfer range of $0.002 < Q\ (Å^{-1}) < 0.2$. Neutron wavelength was 7 Å. The detector to sample distances and the corresponding collimation distances were fixed at 2, 4, 8 and 20 m.
The scattering data were corrected for background, efficiency of the single detector cells, then radially averaged and calibrated in absolute units by a Plexiglas secondary standard.

SANS investigations of geological aragonite

Geological aragonite was used for comparison and reference. Aragonite crystals (Steinzeit, Bremen, Germany) were crushed with a hammer and pulverized with a ball mill (Fritsch GmbH, Germany) for 10 minutes at 300 rpm. After milling aragonite showed homogenous powder consistence.
Geological aragonite was heated up to 350 °C, 430 °C and 500 °C respectively. The temperature was increased with a constant rate of 10 K/min. The final temperature

was kept constant for 10 min and the samples were let cool down at room temperature.

Quartz cells for SANS investigation were filled with geological aragonite powder before and after temperature treatment respectively. The cells were further filled with a D_2O/H_2O solution for “contrast match”.

Scattering experiments were performed within a momentum transfer range of $0.002 < Q\ (Å^{-1}) < 0.2$. Neutron wavelength was 7 Å. The detector to sample distances and the corresponding collimation distances were fixed at 2, 4, 8 and 20 m.

The scattering data were corrected for background, efficiency of the single detector cells, then radially averaged and calibrated in absolute units by a Plexiglas secondary standard.

3.6 Interactions of poly-γ-methyl-L-glutamate with calcium carbonate

3.6.1 Poly-γ-methyl-L-glutamate

Several studies on natural biomaterials showed that acidic proteins associated with invertebrates biominerals typically present a β-sheet conformation and are often rich in glutamic acid [Weiner et al., 1983; Aizemberg, 1996]. Proteins in a β-sheet conformation have charged side chains spaced at regular intervals. If the side chains are negatively charged, it can be assumed that they can interact with calcium ions, therefore forming nucleation centres for crystals growth. A schematic representation of such a polymer is given in fig. 3.10. The negative side chains can be obtained for example using glutamate molecules. A commercial available polymer presenting these characteristics is poly-γ-methyl-L-glutamate, a hydrophobic ester derivative of poly-L-glutamate.

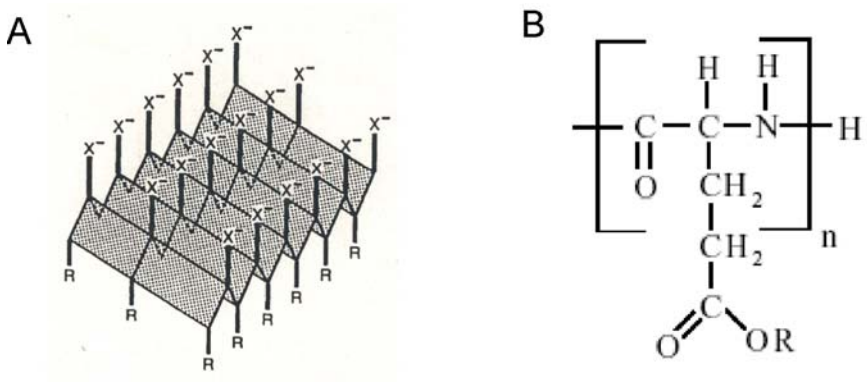

Fig. 3.10. A. Schematic representation of a generic protein adopting a β-sheet conformation. The anionic side-chains (x^-), spaced at regular intervals one side of the β-sheet, may interact with calcium ions and acting as nucleating centres. The anionic side chain can be obtained with glutamate molecules. B. Structural formula of poly-L-glutamate.

PMG is a homopolymer[26] that may adopt either α-helical or β-sheet conformation, depending on the conditions [Baier et al., 1970]. For example the transition from α-helix conformation to β-sheet conformation can be easily induced by temperature variation or by dissolving PMG in specific solvents [Gillgren et al., 2002]. This ability in conformational changes makes PMG a suitable molecule to simulate *in vitro* protein self-assembling and misfolding.

3.6.2 Precipitation of calcium carbonate with poly-γ-methyl-L-glutamate

Poly-γ-methyl-L-glutamate as purchased (Sigma Aldrich Chemie GmbH, Germany) was always stored at –20° C. The mean molecular weight stated by the manufacturer was 10000 – 50000 Da, which corresponds to an average degree of polymerization approximately comprised between 70 and 330.

Precipitation was performed in glass reagent tubes. The tubes were carefully cleaned with a freshly prepared Piranha solution to remove any possible organic contamination. Glassware was cleaned as previously described (see section 3.1.8).

A supersaturated $CaCO_3$ (pH 8.2) solution was prepared following the protocol of Hillner [Hillner, 1992] as previously described (see section 3.2).

[26]Typically homopolymers of L-amino acids are used as simple models for native hydrophobic and amphiphilic proteins and polypeptides.

Poly-γ-methyl-L-glutamate as purchased was put in the cleaned glass reagent tubes and dissolved in chloroform (Sigma Aldrich Chemie GmbH, Germany) to a concentration of 1 mg/ml and extensively mixed with a vortex. To enhance the solubility of poly-γ-methyl-L-glutamate, methanol (Sigma Aldrich Chemie GmbH, Germany) was added to the chloroform solution in a concentration of 1/10 (v/v). The solution was further mixed and sonicated (*Bandelin Sonoplus HD 70, model UW 70*, Bandelin electronic, Germany) for one hour, until all the poly-γ-methyl-L-glutamate was completely dissolved. The solution was cured in an incubator at 70°C until completely evaporated. The inner surface of the tubes was further dried with a nitrogen jet to remove any rest of solution.

The supersaturated calcium carbonate solution (pH 8.2) was introduced into the tubes were poly-γ-methyl-L-glutamate was dissolved to obtain a concentration of 0.1 mg/ml. The supersaturated $CaCO_3$ solution with poly-γ-methyl-L-glutamate was extensively mixed and sonicated for 30 min.
The solution was let swelling for 5 days at room temperature and centrifuged at 7000 rpm (*Sorvall RC-SB Refrigerated Superspeed Centrifuge*, Sorvall DuPont, Germany) for 10min. The precipitate was removed, put on a clean glass slide (13 mm Ø), dried in an incubator at 25° C and investigated by scanning electron microscopy (SEM). The coverslides were glued on SEM stubs and sputter-coated with gold. Sputtering was performed with a current of 10 – 20 mA in a 0.2 mbar argon atmosphere (*Emitech K550* system, EM Technologies Ltd., England).
The crystals were investigated at 20 kV using a Camscan Series 2 SEM (Cambridge Instruments, England).

3.6.3 Cocrystallization of calcium carbonate with poly-γ-methyl-L-glutamate

Calcium carbonate crystals in the presence of poly-γ-methyl-L-glutamate were precipitated by the ammonium carbonate vapour diffusion technique.
To eliminate the presence of organic contamination on the glass slides (13 mm Ø) these were cleaned with a freshly prepared Piranha solution as previously described (3.3.1). Poly-γ-methyl-L-glutamate was dissolved in a chloroform-methanol solution

as before described (3.6.1). The solution was evaporated and of sterile filtered calcium chloride solution (7.5 mM) was added to a concentration of 0.1 mg/ml. The $CaCl_2$ solution with poly-γ-methyl-L-glutamate was extensively mixed and sonicated for 30 min.

The cleaned glass slides were put on the bottom of a Nunc multidish (Nunc GmbH & Co. KG, Germany) with a well diameter of 15 mm, 1 ml of $CaCl_2$ with poly-γ-methyl-L-glutamate - $CaCl_2$ solution was introduced into each well. The wells were covered with aluminium foil punctured with a needle. The crystallization vessels were put in sealed chamber where a saturated atmosphere of CO_2 was previously created by the decomposition of solid ammonium carbonate (Sigma Aldrich Chemie GmbH, Germany). The vessels were let in the incubator for five days at room temperature and then gently rinsed with ultrapure water and dried in an incubator at 25° C.

The crystals obtained were investigated by scanning electron microscopy (SEM). The coverslides were glued on SEM stubs and sputter-coated with gold. Sputtering was performed with a current of 10 – 20 mA in a 0.2 mbar argon atmosphere (*Emitech K550* system, EM Technologies Ltd., England).

The crystals were investigated at 20 kV using a Camscan Series 2 SEM (Cambridge Instruments, England).

4 Results and discussion

4.1 Characterization of nacre aragonite platelets

4.1.1 Extraction of aragonite platelets from *H. laevigata* nacre

Nacre from the shells of *H. laevigata* was used to collect single aragonite platelets as described in 3.1.8.

Nacre was crushed with a hammer and pieces with variable sizes (from fine powder to 2 cm in size) were obtained. The interlamellar organic matrix was removed with sodium hypochlorite. Scanning electron microscopy (SEM) investigation showed (fig. 4.1, A-B) that mostly intact aragonite platelets with a size of 5 – 10 µm were obtained. Aragonite platelet fragments were also visible.

SEM investigations of the platelets rinsed with an alkaline buffer solution (pH 8.5) showed that most of the platelet fragments were removed (fig. 4.1, C-D).

Nacre ground with a ball mill appeared as a fine powder, with more homogenous grain size. The maximal grain size corresponded to 2 mm in diameter. The organic matrix was removed as described above. SEM investigations showed that a higher amount of platelet fragments were obtained (fig. 4.1, C-D). The platelets fragments were not completely removed by extensive rinsing with an alkaline buffer solution (fig. 4.1, E-F).

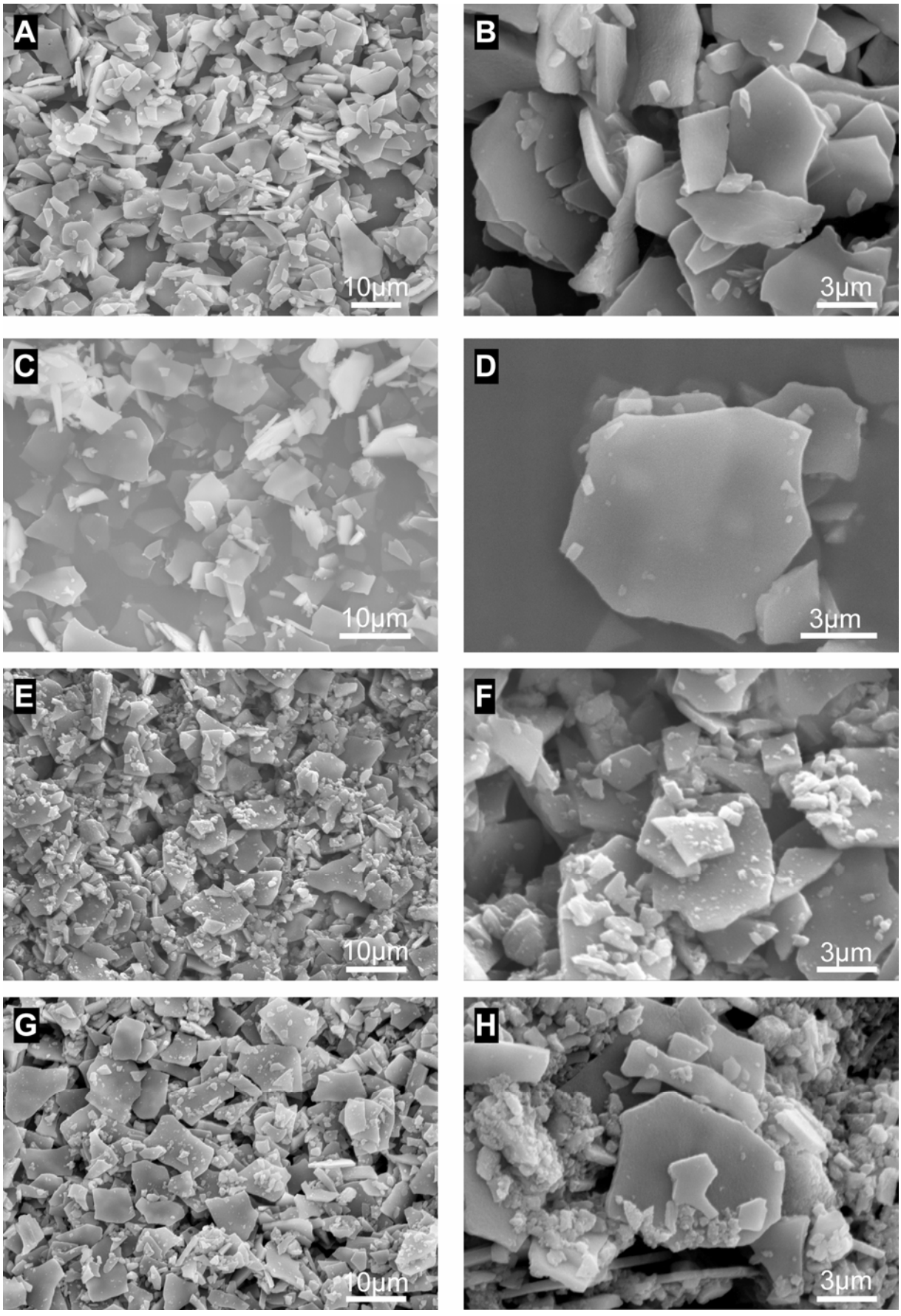
A
10μm
B
3μm
C
10μm
D
3μm
E
10μm
F
3μm
G
10μm
H
3μm

Fig. 4.1. (Previous page) SEM images of purified aragonite platelets from the nacre of *H. laevigata*. A. Aragonite platelets obtained by crushing nacre with a hammer. The interlamellar organic matrix was removed with a 3% sodium hypochlorite solution. Mostly intact aragonite platelets were obtained. Some aragonite fragments indicated that some platelets got broken during the preparation. B. Magnification of A, single aragonite platelets with a diameter of 5 – 10 µm are visible. C. Aragonite platelets obtained by crushing nacre with a hammer, the interlamellar organic matrix was removed with a 3% NaOCl solution. The platelets were rinsed with a 10 mM TRIS buffer solution with 0.02% NaN_3 (pH 8.5). Most of the broken platelets were removed. D. Image of a single aragonite platelet.
E-F. Aragonite platelets obtained by milling nacre with a ball mill, the interlamellar organic matrix was removed with a 3% NaOCl solution. A high amount of fragments is visible. G-H. Aragonite platelets, obtained as in described in E, were rinsed with a 10 mM TRIS buffer solution with 0.02% NaN_3 (pH 8.5). Platelets fragments were not completely removed.
Nacre crushed with a hammer showed larger and mostly intact aragonite platelets whilst after ball milling the platelets are mostly reduced to fragments. It is clearly visible that by washing with an alkaline buffer solution (pH 8.5) the mineral phase is not demineralized and the amount of small fragments (broken platelets) is slightly reduced.

Parallel investigations SEM investigations showed that aragonite platelets, crushed with a hammer, treated with NaOCl and rinsed with ultrapure water (not with an alkaline solution) presented a marked surface roughness (fig. 4.2, A-B).
Thermally induced changes in phase, structure of the aragonite platelets were investigated. Aragonite platelets were heated up to 350° C at 10K/min imaged by SEM (fig. 4.2, C-D). SEM investigations showed the formation of pores (with a diameter of 50 - 100 nm) on the platelet surface. Pore formation was addresses to the pyrolysis of organic matrix inside the platelets. The development of pores took place at about 350 °C together with the phase transformation of aragonite into calcite (data are not shown, personal correspondence with Dr. Regina Knitter Forschungszentrum Karlsruhe GmbH, Karlsruhe, Germany).
Further investigation indicated that the amount of organic material in the platelets is about 1.5% (weight). (Data not shown, personal correspondence with Dr. Regina Knitter Forschungszentrum Karlsruhe GmbH, Karlsruhe, Germany).

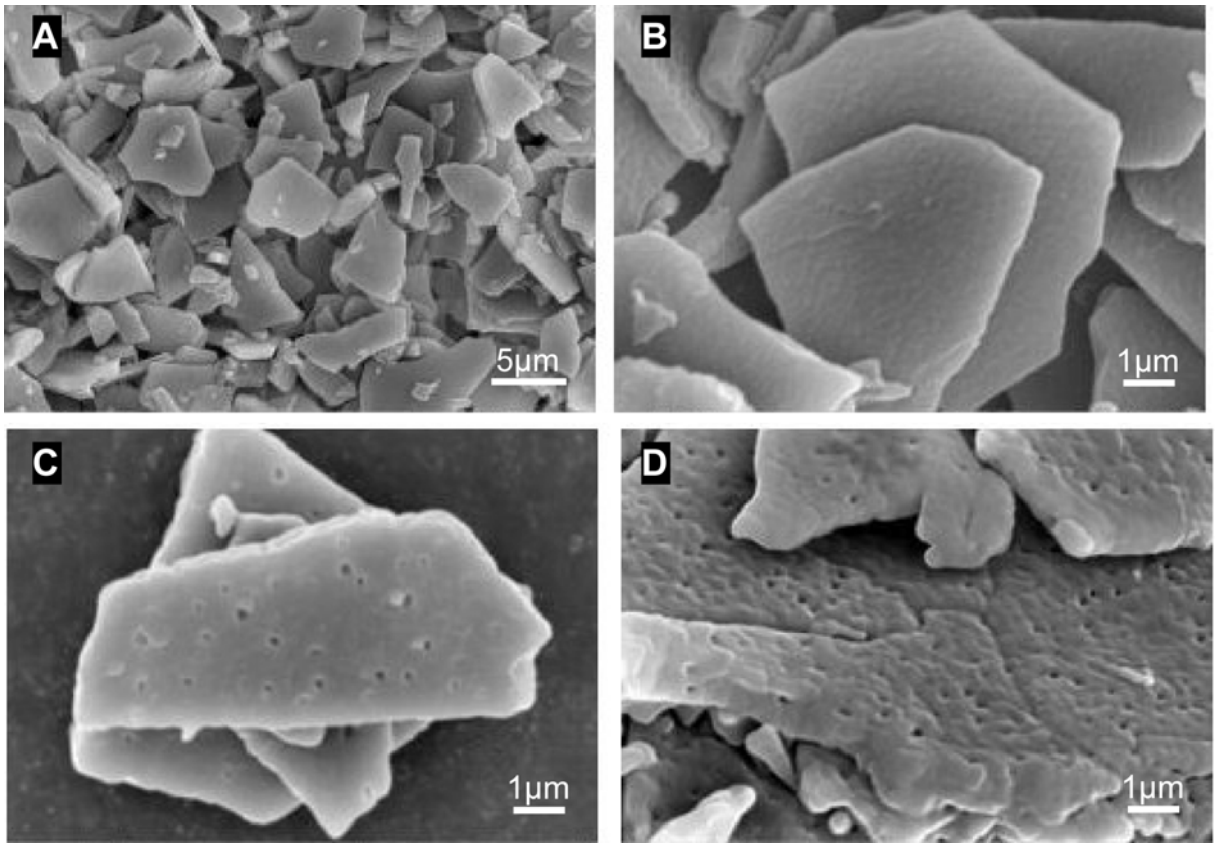

Fig. 4.2. A. SEM image of the aragonite platelets before heat treatment. Aragonite platelets were extracted from nacre of *H. laevigata* by crushing it with a hammer. The intercrystalline organic material was removed with a solution of 3% sodium hypochlorite (NaOCl). The platelets were extensively washed with ultrapure water. The surface of the platelets presented a higher roughness compared with platelets washed with TRIS buffer solution (pH 8.5) (fig. 4.1, C-D). The roughness of the platelet surface is an indication that predissolution of the mineral phase already took place during the extraction of aragonite platelets from nacre. B. Magnification of A. C-D. Aragonite platelets after heat treatment (350° C). Pores on the platelet surface formed, maybe due to rearrangement and agglomeration of the mineral phase and pyrolysis of the organic phase included in the platelets. The content of organic material was estimated to be 1.5% (weight). The development of pores took place at 350° C, together with the polymorph transition from aragonite to calcite (calorimetric measurements were kindly performed by Dr. Regina Knitter, Forschungszentrum Karlsruhe GmbH, Karlsruhe, Germany). D. Magnification of C.

Discussion

SEM investigation showed that aragonite platelets obtained by crushing nacre with a hammer were more intact and uniform in size. They maintained a diameter of 5 - 10 µm, which corresponds to the diameter of aragonite platelets in native nacre (fig. 4.1, A-B). Several fragments (broken platelets) were also produced but they were mostly removed with buffer solutions (fig. 4.1, C-D). By ball milling most of the platelets were reduced into many micro-fragments with non-homogeneous size (fig. 4.1, E-F) and could not be entirely removed with buffer solutions (fig. 4.1, G-H). Crushing nacre with a hammer was the best way to obtain mostly intact aragonite platelets.

The surface of the platelets washed with ultrapure water presented a marked roughness, not detected in the platelets washed with an alkaline solution. The roughness of the surface suggested that dissolution of the mineral phase took place during the platelets extraction. Therefore for extraction of the intracrystalline proteins only buffers solutions were employed. Predissolution of the mineral phase may induce a loss of proteins, which can be affected and maybe denaturated.

Hole formation accompanying the polymorph transformation was a clear evidence for the presence of organic molecules enclosed into the aragonite platelets. The pores observed formed during rearrangement and agglomeration of the mineral after the pyrolysis of the organics.

The content of organic material (1.5% weight) was in accordance with previous preliminary DSC investigations of native *H. laevigata* nacre, which revealed an approximate content of organic material of 3.2% weight [Knitter at al., 2006].

Polymorph transition from aragonite into calcite at high temperatures was observed. In the case of aragonite platelets the polymorph transformation took place at 350 °C. Previous calorimetric investigation of native nacre showed that the polymorph transition takes place around 435 °C [Knitter et al. 2006]. This discrepancy is not completely understood. It might be that the lower transition temperature is due to the possibility of the purified platelets to expand.

4.1.2 SANS investigations of nacre aragonite platelets

The structure and distribution of proteins in single aragonite platelets extracted from *H. laevigata* were investigated by small angle neutron scattering (SANS). Furthermore thermally induced changes in phase, structure and composition of the nacre aragonite platelets and nacre were investigated. The thermal investigation was carried out at 350° C, 430° C and 500° C.

Aragonite platelets were prepared as described in section 3.5.2.

Native nacre was also investigated only at room temperature. Geological aragonite was used as reference.

The coherent scattering length densities (δ) of nacre proteins ($\delta_{PROTEIN}$), water ($\delta_{H2O/D2O}$) and geological aragonite ($\delta_{ARAGONITE}$) were obtained by varying the H_2O/D_2O ratio of the aqueous solution (fig. 4.3). By increasing the content of D_2O, water showed the most evident change of δ compared with proteins and geological aragonite. The δ variation of the proteins ($\delta_{PROTEIN}$) on the surface of the nacre aragonite platelets (fig. 4.3, green line) was due to a partial exchange of H/D at the outer surface of the proteins. For the proteins at the surface a scattering length density of $\delta_{PROTEIN}$= 1.65 x 10^{10} cm^{-2} was assumed.

The matching condition value (Φ), at which aragonite particles become invisible by neutrons, was Φ = 0.82. Φ was calculated from the intersection of $\delta_{H2O/D2O}$ (fig. 4.3, blue line) and $\delta_{ARAGONITE}$ (fig. 4.3, orange line).

Fig. 4.3 (Next page) SANS scattering length density (δ) variation as a function of the H_2O/D_2O ratio. The scattering length density variation of H_2O/D_2O, geological aragonite and proteins, measured at room temperature, are reported. The scattering length density of D_2O/H_2O mixture (blue line) plotted as a function of the D_2O content. The "free" proteins represent the proteins at the surface of the nacre aragonite platelets and therefore in contact the with the H_2O/D_2O solution. The "incorporated" proteins represent the proteins inside each nacre aragonite platelet, not in contact with the H_2O/D_2O solution. For the proteins a scattering length density of 1.65 x 10^{10} cm^{-2} was considered.

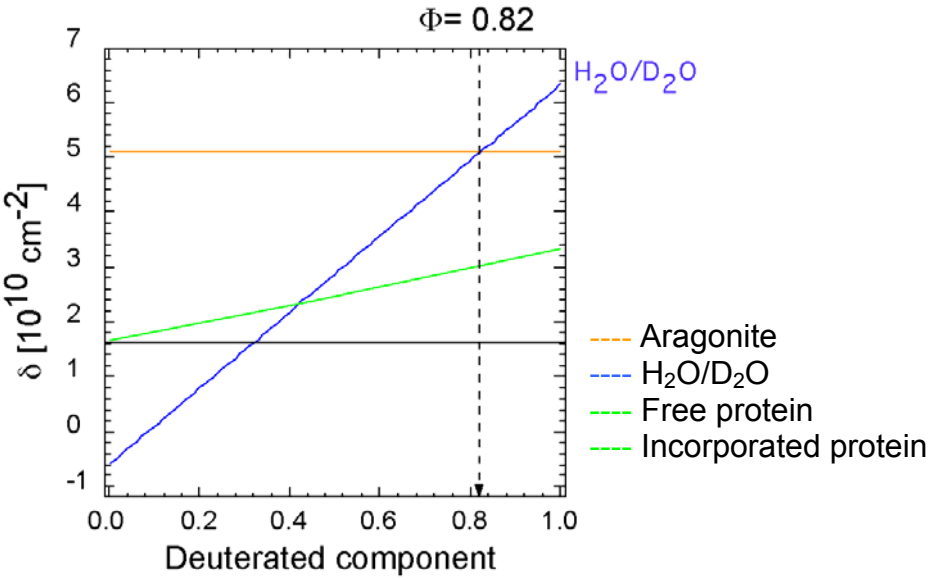

SANS analysis of nacre aragonite platelets, native nacre and geological aragonite without temperature treatment

The scattering cross sections, the variation of the macroscopic cross section $(\partial\Sigma/\partial\Omega)(Q)$ as a function of the momentum transfer Q ($Å^{-1}$), for geological aragonite, aragonite platelets and nacre were calculated before heat treatment (fig. 4.4, A-C). Geological aragonite showed a Q-dependent scattering profile (fig. 4.4, A, green asterisks) indicating inhomogeneous occlusions in the sample. With high probability these occlusions are related to the presence of impurities or crystalline defects. The exact nature of these impurities is unknown.

Fig. 4.4. (Next page) A. Scattering cross sections of geological aragonite (green asterisks), nacre aragonite platelets (red circles), native nacre (black circles) and D_2O/H_2O (blue triangles) measured at room temperature. The Q-dependent scattering profile of geological aragonite indicated the presence of inhomogeneous occlusions, maybe impurities, in the sample. B. Scattering cross section of nacre aragonite platelets. The scattering profile showed a Q^{-4} behaviour deriving from large three-dimensional occlusions. The surface of the occlusions was calculated by fitting the data with the Porod scaling law with a scaling prefactor P_4= 1.15 x 10^{-8} $cm^{-1}Å^{-1}$. These inclusions are supposed to be intracrystalline proteins. The calculated protein radius was R_g= (39.1 ± 0.1) Å. A protein amount of 4% (volume) in the platelets was estimated. C. Scattering cross section of native nacre. The total amount of proteins corresponded to 6.6% of the total volume. Proteins radius was estimated about R_g= (36.5± 0.1) Å. Additional scattering signal from occlusions with a radius of 316 Å was observed. These occlusions might be protein aggregates.

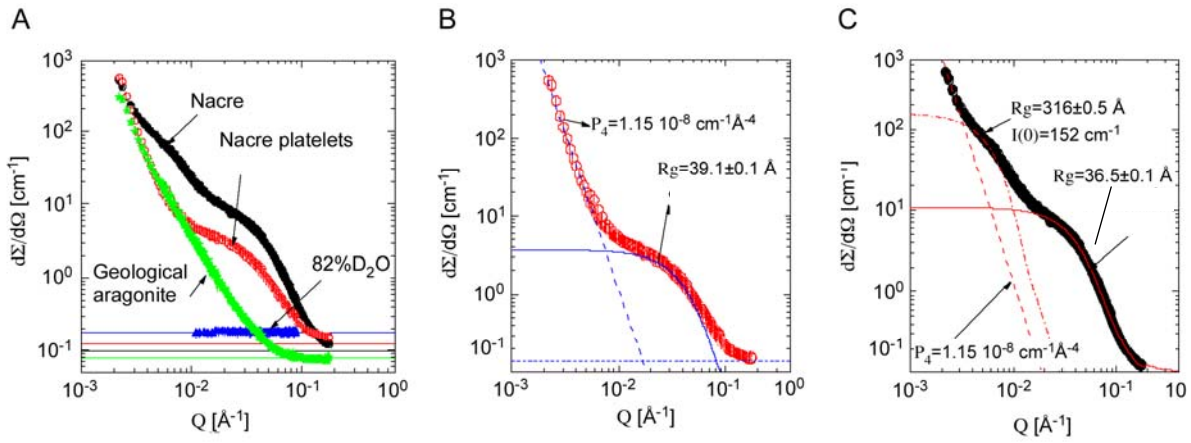

The scattering profile of nacre aragonite platelets (fig. 4.4, B) contained a scattering signal of individual proteins inside platelets and an additional scattering signal of plate-like structures. To measure the surface area of scattering domains data were fitted using the Porod scaling law[27] $I(Q)\sim P_4Q^{-4}$ (fig. 4.4, B, dashed line) with a scaling prefactor P_4= 1.15 x 10^{-8} $cm^{-1}Å^{-1}$ proportional to the total surface of the scattering structures and scattering contrast. Assuming a spherical shape for the proteins, the form factor of the sphere was defined as $P(Q,R)=sin(QR)/QR$, where R is the protein radius. The same scaling prefactor P_4 for mineral particles was used for nacre aragonite platelets and nacre. The Q^{-4}–behaviour of the scattering profiles suggested the presence of three-dimensional inclusions, as intracrystalline proteins, in nacre aragonite platelets.

The scattering of individual intracrystalline protein was fitted using the spherical form factor. The averaged radius of protein inside the mineral (intracrystalline proteins), calculated considering polydispersity[28] was R_g= (39.1 ± 0.1) Å with a variance σ= (17 ± 3) Å. Considering a scattering length density of $\delta_{PROTEIN}$=1.65 x 10^{10} cm^{-2}, a total volume fraction of $\Phi_{PROTEIN\ IN\ PLATELET}$= 4% was obtained.

For native nacre (fig. 4.4, C) the average radius of the proteins resulted of R_g= 36.5 ± 0.1 Å with a variance of σ= 18 ± 3 Å, for a total amount of $\Phi_{PROTEIN}$ = 6.6% (volume). The proteins found in the aragonite platelets and native nacre presented the same size and the distribution. The amount of organic material found in native nacre is evidently higher (65 %) than the one found in purified aragonite platelets.

[27] Several SANS scaling laws and factors are listed in [King, 1999; Hammouda, 1995].
[28] In case of polydispersity the scattering signal is convoluted with distribution function, described by Gaussian distribution function with variance σ and averaged radius *R*.

Nacre platelets and native nacre showed additional scattering within the low Q-range from particles with a radius of R_g=316 Å. These relative big inclusions may indicate the presence of protein aggregates.

SANS analysis nacre aragonite platelets and geological aragonite with temperature treatment

Nacre aragonite platelets and geological aragonite were investigated after temperature treatment. Both samples were heated at 350° C, 430° C and 500° C respectively (fig. 4.5).

The scattering profile of geological aragonite (fig. 4.5, A) presented no significant variations by temperature increment. Only an increase in scattering intensity was observed in the sample heated up to 500° C. After 1 hour all the geological aragonite transformed calcite. This result confirmed previous investigations [Knitter et al., 2006].

The scattering profiles of nacre aragonite platelets heated up to 350° C, 430° C and 500° C showed a different behaviour (fig. 4.5, B). After treatment at 350°C the scattering from the protein monomers disappeared and a strong increase of the scattering signal was observed (fig. 4.5, B red circles). The increase of the scattering intensity was related to the formation of additional scattering centres, as cavities, in the mineral phase. At 430° C a coarsening mechanism, maybe related to the transformation of aragonite to calcite, was observed. The same was observed when the sample was heated up to 500° C.

Fig. 4.5. (Next page) A. Scattering cross section of geological aragonite at different temperatures. The only strong variation observed was an increase in scattering intensity for the sample heated at 500° C. B. Scattering cross sections of nacre aragonite platelets at different temperatures. The scattering signal from the protein monomers disappeared after temperature treatment at 350° C. At temperature higher than 430° C a strong increase of the scattering signal was observed as well as a coarsening mechanism. This is maybe related to the phase transformation of aragonite to calcite.

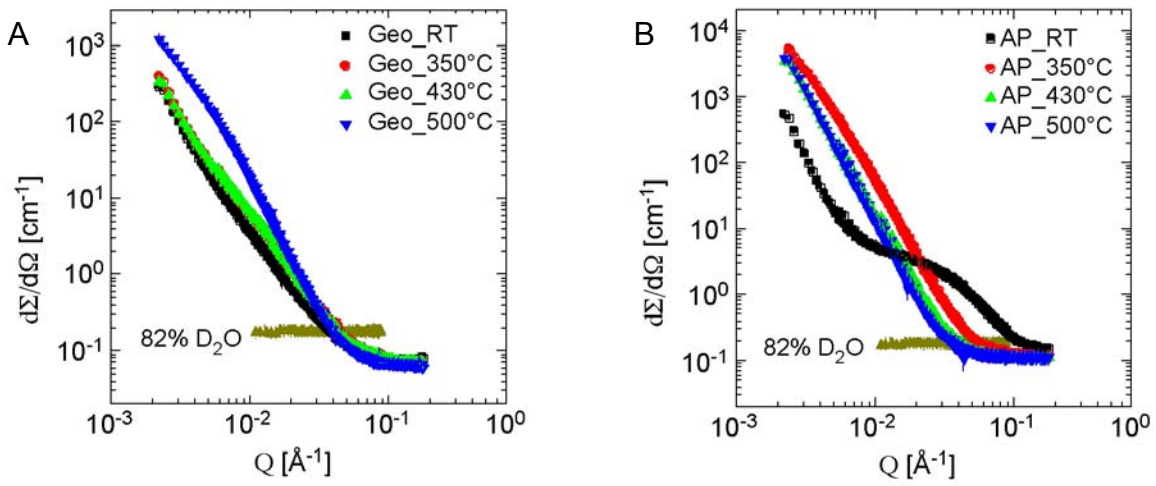

Formation of plate-like structures in the geological aragonite (heated at 500° C) was observed. The plates presented a thickness of 415 Å and a relative scattering length density of 4.75 x 10^{10} cm^{-2}. The plates might be calcite as suggested by comparison with the scattering length density of calcite reported in literature (4.69 x 10^{10} cm^{-2}).
A similar scattering was also observed in nacre aragonite platelets after temperature treatment at 350° C (fig. 4.6). The plate-like inclusions presented a thickness of 610 Å.

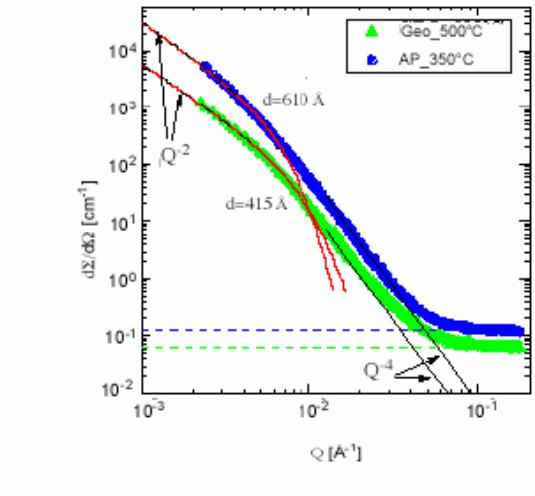

Fig. 4.6. SANS scattering profiles geological aragonite at 500° C and nacre aragonite platelets at 350° C. Plats of a thickness of 415 Å were individuated in the geological aragonite. The newly formed plates were supposed to be calcite deduced by comparison of their scattering length density (4.75 x 10^{10} cm^{-2}) with that of calcite (4.69 x 10^{10} cm^{-2}). Aragonite after heat treatment transformed completely in calcite. Formation of plate-like structure during heat treatment was observed also in the aragonite platelets. The plates showed a size of 610 Å and their formation took place at 350°C.

Discussion

The presence of intracrystalline proteins within single nacre platelets was clearly demonstrated by SANS investigation. The radius of the intracrystalline proteins was estimated around 40 Å. The amount of organic material in single platelets (4.2% volume) seemed too high if compared with the total amount of organic material found in native nacre (6.6%).

Large three-dimensional occlusions with a radius of R_g=316 Å were found in the nacre aragonite platelets and native nacre. These occlusions might be aggregated proteins or other organic substructures that are removed or destroyed during heat treatment.

After heat treatment at 350° C the organic matrix in the platelets disappeared as already shown by previous calorimetric investigation [Knitter et al., 2006]. Aragonite platelets after temperature treatment at 350°C showed the same scattering behaviour of geological aragonite treated at 500 °C. This suggested that in the nacre platelets the aragonite-calcite polymorph transition might take place at a lower temperature compared with geological minerals. In geological aragonite the transformation in calcite takes place at 400 °C.

An interestingly plate-like substructure in heat-treated aragonite platelet was detected. Single sub-platelets showed a thickness of 610 Å. Plates-like structure formed also in geological aragonite and presented a different thickness (415 Å).

After heat treatment an increasing of the scattering centres was observed and could be related to the polymorph transition from aragonite to calcite. The scattering centres, which present the shape of cavities, could be related to the pores observed during previous thermal investigation as presented in the previous section and also in [Knitter et al., 2006].

4.2 Intracrystalline proteins extraction and purification

4.2.1 Nacre demineralization

The intracrystalline proteins were obtained by demineralization of nacre platelets. Nacre was prepared as described in section (3.1.8) by removing the calcite layer by sandblasting and crushing nacre with a hammer. The intercrystalline organic matrix was removed by soaking nacre in 3% sodium hypochlorite (NaOCl) solution and washing with 10 mM TRIS buffer solution (pH 8.5).

Aragonite platelets were dissolved using a chelating agent (100 mM EDTA solution with 0.02% NaN_3, pH 7.0) or 2.5% acetic acid solution, both carried out in dialysis membranes of regenerated cellulose. Dialysis tubes with a pore diameter of 6000 - 8000 and 3500 Da (indicated as molecular weight cut off, MWCO) were used.

Demineralization with acetic acid resulted to be two times faster than EDTA demineralization. After complete dissolution of the mineral phase flake-like particles, visible with eyes, were always found in the supernatant, independently from the demineralization procedure used. These flakes might be of proteinaceous nature and/or chitin remnants. After demineralization the protein concentrations were estimated with a Bradford microassay. The concentrations obtained are presented in table 4.1.

Dialysis tube MWCO [Da]	Demineralization with EDTA	Demineralization with acetic acid
6000 - 8000	5 - 7 µg/ml	< 1µg/ml
3500	10 - 12 µg/ml	2 µg/ml

Table 4.1. Intracrystalline protein concentration after demineralization of aragonite platelets. Aragonite platelets were dissolved using with 100 mM EDTA or 2.5% acetic acid respectively. Demineralization was carried out in dialysis tubes of regenerated cellulose with a MWCO of 6000 - 8000 or 3500 Da. Protein concentration was estimated with the Bradford microassay using lysozyme and IgG as standard proteins.

4.2.2 Precipitation of intracrystalline proteins

After demineralization of the aragonite platelets, intracrystalline proteins were concentrated by precipitation. Precipitation was performed with the ammonium sulfate method, by trichloroacetic acid precipitation and by the methanol-chloroform technique.

Ammonium sulfate precipitation

Ammonium sulfate precipitation was carried out adding solid salt, instead of a saturated solution, to the protein medium to avoid further dilution. Precipitation was performed as described in section (3.1.8). Proteins precipitated at different salt concentrations were collected and dialyzed against a salt-free buffer solution at neutral pH to remove the excess of salt. Protein fractions were investigated by sodium dodecyl sulfate gel electrophoresis (SDS-PAGE) with Coomassie Blue staining. No protein bands were detected in the gels, maybe proteins diffused out of the gel or did not precipitate.

Trichloroacetic acid precipitation

Intracrystalline proteins obtained after demineralization of aragonite platelets with acetic acid and EDTA were precipitated with trichloroacetic acid. Proteins collected by EDTA demineralization of aragonite platelets were obtained in two distinct preparations started at two different times (here indicated as *preparation-I* and *preparation-II*) and investigated simultaneously. *Preparation-I* indicates that the proteins were stored at 4° C for three weeks. *Preparation-II* indicates that the proteins were immediately investigated after demineralization.
Precipitates and supernatants were collected for SDS-PAGE. A chaotropic salt (urea) was used to allow a better diffusion of the proteins through the gel. The gel obtained (fig. 4.7) showed several protein bands. The concentration of the proteins obtained by EDTA demineralization (fig. 4.7, lanes 4 - 12) was visibly higher than the ones obtained with acetic acid (fig. 4.7, lanes 1 - 3) because the bands in the gel were more intensively stained. The proteins dissolved in 6 M urea showed a higher mobility than the same proteins dissolved in 3 M urea. Some proteins could not enter

the gel (fig. 4.7, lanes 4 and 10 grey arrows).

The proteins visualized showed a molecular weight between ~3.5 and ~31 kDa (fig. 4.7, lanes 4 and 12) as deduced by comparison with the molecular weight standards. Proteins of *preparation-II* showed a higher concentration than the ones collected with *preparation-I*. Bands with an approximate molecular weight of 15 kDa (fig. 4.7, lanes 1 – 2, black arrow), 6 kDa (fig. 4.7, lanes 6 – 7, white arrow) and between 3 and 6 kDa (fig. 4.7, lanes 11 – 12, red arrow) were observed.

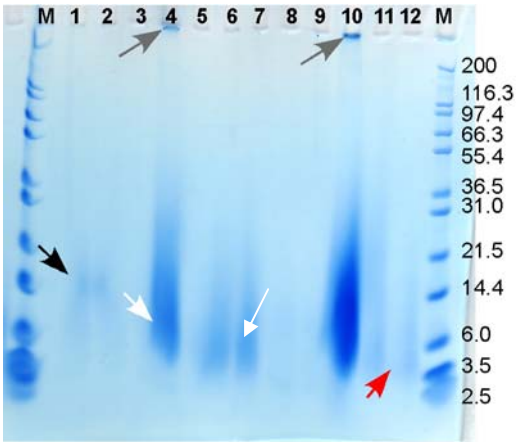

Fig. 4.7. SDS-PAGE (NuPAGE Bis-TRIS, 12% acrylamide) of intracrystalline proteins precipitated with trichloroacetic acid. To achieve a better diffusion of the proteins through the gel a saturated solution of urea was added at different concentrations to the protein solution. Lanes 1-3. Demineralization with 2.5% acetic acid. Lane 1. Pellets dissolved in 3 M urea. Lane 2. Supernatant with 3 M urea. Lane 3. Supernatant with 6 M urea. A protein band with a weight of approximately 15 kDa was visible (black arrow).

Lanes 4 – 9. Demineralization with 100 mM EDTA (*preparation-I*). Lane 4. Pellets dissolved in 3 M urea. Lane 5. Supernatant with 3 M urea. Lane 6. Pellets dissolved in 6 M urea. Lane 7. Supernatant with 6 M urea. Lane 8. Supernatant without urea. Lane 9. Pellets not dissolved in urea.

Lanes 10 – 12. Demineralization with 100 mM EDTA (*preparation-II*). Lane 10. Pellets dissolved in 3 M urea. Lane 11. Supernatant with 3 M urea. Lane 12. Supernatant with 3 M urea. Proteins with a weight of ~6 kDa (white arrow) and between 3 and 6 kDa (red arrow) were visible. Lane M. Molecular weight standards with masses in kDa indicated on the right.

In the supernatant collected after trichloroacetic acid precipitation (*preparation-I*), the formation of macroscopic, transparent crystals (approximately 1 mm wide, 5 mm length) with a needle-like shape was observed. The crystals were analyzed by X-ray diffraction. The scattering pattern (fig. 4.8) presented a dominant peak at $2\theta = 26.7°$, other minor peaks were found at 12.7°, 16.3° and 24.2°. Data base search did not

match with any mineral, *e.g* calcium carbonate minerals. This suggested the hypothesis that the crystals could be a protein/mineral crystal.

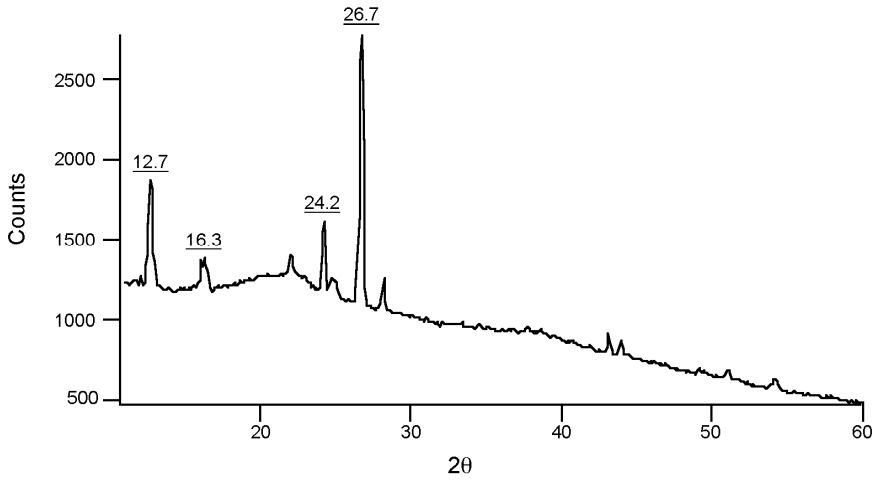

Fig. 4.8. X-ray diffraction pattern of the crystals obtained after TCA-precipitation. The main peaks with relative angles (2θ) are highlighted in the graph. Data base search did not match with any mineral.

Methanol-chloroform precipitation

Intracrystalline proteins were further precipitated with methanol-chloroform precipitation as described in section 3.1.8.

Proteins were obtained by demineralization of aragonite platelets by EDTA and the protein medium was mixed with methanol and chloroform. Visible protein precipitation was observed already after adding chloroform to the methanol-protein solution (fig. 4.9, A, black arrow). The proteins formed whitish droplets that spontaneously precipitated. Proteins were collected by centrifugation and typically formed a white film at the methanol-chloroform interface. The proteinaceous film stuck to the reagent glass and some of the precipitated proteins could not be collected.

To collect most of the proteins reagent tubes and the pipettes were silanized with dichlorodimethylsilane. This enhanced the amount of proteins collected after precipitation.

Proteins collected after precipitation were investigated by SDS-PAGE and stained with Coomassie Blue (fig. 4.9, B). The fraction collected with modified hydrophobic

glass presented a higher concentration (fig. 4.9, B lane 2). Two main protein bands were detected, one corresponding to a molecular weight of approximately 6 kDa (fig. 4.9, B lane 1 – 2, red arrows) and a less visible one around 25 kDa (fig. 4.9, B lane 1, black arrow). Again proteins did not appear in sharp bands but diffused. Some of the proteins collected did not enter the gel (fig. 4.9, B lane1 – 2, grey arrows).

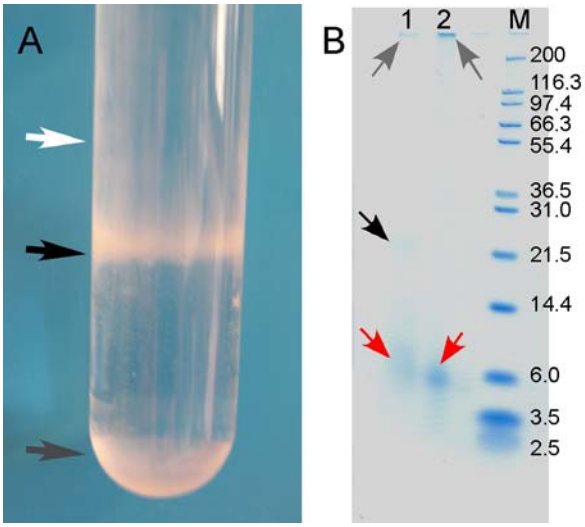

Fig. 4.9. Precipitation of intracrystalline nacre proteins by the methanol – chloroform precipitation. A. Proteins were precipitated in a reagent glass and formed a visible band (black arrow). The upper phase contains methanol (white arrow). The bottom contains chloroform (grey arrow). B. SDS-PAGE (Tris-Glycine, 10-20% acrylamide gradient gel) stained with Coomassie Blue. Lane 1. Proteins precipitated in a not silanized reagent glass. Lane 2. Proteins precipitated in a silanized reagent glass. The proteins presented a higher concentration. Glassware was silanized with dichlorodimethylsilane, to obtain a hydrophobic surface and to easily recollect most of the precipitated proteins. Part of the proteins could not enter the gel as indicated by the grey arrows. Lane M. Molecular weight standards with masses in kDa reported on the right.

Further precipitations of proteins by the methanol-chloroform method with silanized reagent glasses were performed. Precipitated proteins were visualized with Coomassie Blue after SDS-PAGE (fig. 4.10). Urea, a chaotropic salt, was added to the sample to increase protein diffusion though the gel (fig. 4.10, lane 2).

Proteins with a molecular weight between ~3.5 and ~25 kDa stained quite intensively. Two main distinct bands were found around 6 and 14 kDa (fig. 4.10, lane 2). The same bands are found in lane 1 (fig. 4.10) but the separation was not so marked. A second protein with a molecular weight of ~25 kDa was present in both lanes (fig. 4.10, black arrows). Proteins or peptides with a molecular weight lower

than 6 kDa were visible (fig. 4.10, red arrows). Without addition of urea most of proteins could not enter the gel (fig. 4.10, lane 1, grey arrow).

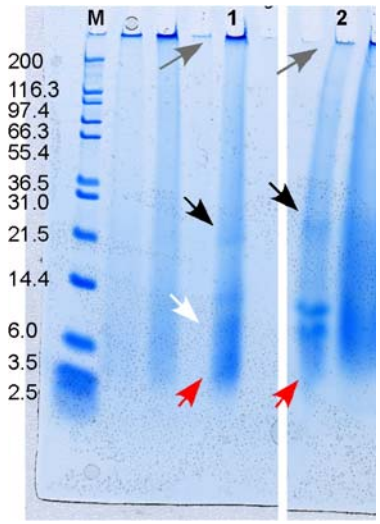

Fig. 4.10. SDS-PAGE (NuPAGE Bis-TRIS, 12% acrylamide) of the proteins collected with the methanol-chloroform precipitation. To achieve a better diffusion of the proteins through the gel a saturated solution of urea was added at different concentrations to the protein solution. Lane 1. Proteins obtained after precipitation without addition of urea. Lane 2. Proteins obtained after precipitation with addition of 6 M urea. A protein with a molecular weight of 25 kDa was present in both lanes (black arrows). Proteins or peptides with a molecular weight lower than 6 kDa (red arrows) were also visible. Lane M. Molecular weight standards with relative masses in kDa indicated on the left.

The proteins visualized by SDS-PAGE were analyzed by mass spectroscopy. Mass spectroscopy was performed with the kind help of Dr. Anja Resemann (Bruker Daltonics GmbH, Bremen, Germany). Peptides detected after *in-gel digestion* were used for data base search (Swissprot and NCBR data bases). No matches were found.

De-novo-sequencing was performed using the resulting sequences for BLAST database search. But again no matches were obtained. A large number of peptides showed a neutral loss of 64 Dalton, which could be the result of a labile modification of amino acid residue (data not shown, personal communications with Dr. Anja Resemann, Bruker Daltonics GmbH, Bremen, Germany).

4.2.3 Intracrystalline proteins characterization by gel electrophoresis and differential staining

To obtain more information about the nature of the intracrystalline proteins, they were further investigated by SDS-PAGE and stained at the same time with two different staining methods, Coomassie Blue and Stains-all. Protein samples were loaded twice on the gel (in two different lanes), after electrophoresis the gel slab was split in two parts, one half was stained with Stains-all and the other half was stained with Coomassie Blue. Most of the protein bands stained blue with both stains (fig. 4.11).

The gel stained with Stains-all, characterized by a light purple background colour, showed intensively stained proteins. Proteins with an approximate molecular weight of 6 - 14 kDa and 25 kDa (fig. 4.11, black arrow) were visible, the bands corresponding to 6 kDa and to 14 kDa seemed to overlap (fig. 4.11, white arrow). Proteins with a molecular weight between 3.5 and 6 kDa were detectable and presented a purple colour. The gel needed to be investigated immediately after staining because of its light instability. Pink-purple stained bands faded within 5 min and blue-stained bands faded within 2 hours.

In the gel stained with Coomassie Blue, the protein bands stained less intensively. Proteins with an apparent molecular weight between 6 - 14 kDa and 25 kDa were visible. The same proteins were already detected in previous investigations. Diffused bands between 3.5 and 6 kDa appeared again (fig. 4.11, red arrow). They were less visible than the ones in the gel stained with Stains-all. Some of the proteins could not enter the gel (fig. 4.11, grey arrow). This was not observed in the gel stained with Stains-all.

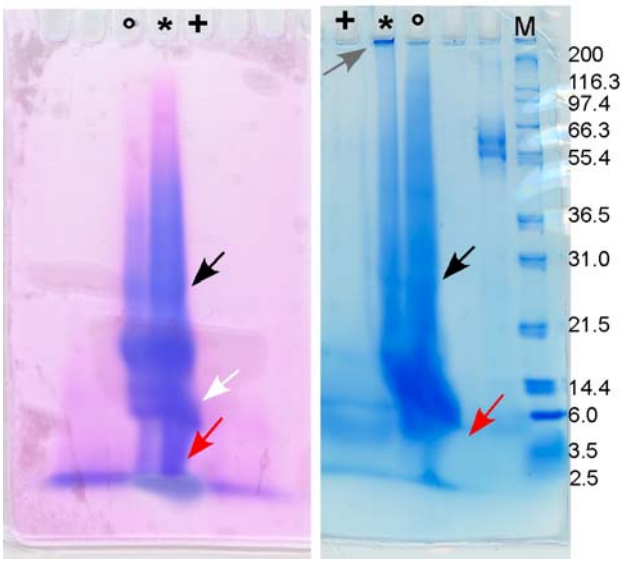

Fig. 4.11. Differential staining after SDS-PAGE (10 - 20% TRIS-glycine). The gel was split in two parts, stained separately with Stains-all (left) and Coomassie Blue (right). Proteins from the same sample were loaded twice on the gel and indicated as °, * and +. To achieve a better diffusion of the proteins through the gel a saturated solution of urea was added at different concentrations to the protein solution. Lane °. Proteins with 6 M urea. Lane *. Proteins with 3 M urea. Lane +. Pure protein solution (without urea). Proteins stained with Stains-all stained more intensively than with Coomassie Blue. Proteins with an approximate molecular weight of 3.5 – 6 kDa (red arrow), 6 - 14 kDa (white arrow) and 25 kDa (black arrow) were detected. When urea was added in a low concentration some of the proteins could not enter the gel (grey arrow). Lane M. Molecular weight standards with relative masses in kDa indicated on the right.

4.2.4 Intracrystalline proteins separation by ion exchange chromatography

Ion exchange chromatography was used as a further non-denaturing purification step to separate the proteins according to their charges.

Proteins extracted by demineralization of aragonite platelets by EDTA were fractionated by ion exchange chromatography on a weak cation-exchanger. The chromatogram (fig. 4.12) was characterized by the absence of protein peaks, indicating that no proteins bound to the exchanger. Only the absorption of buffer solution used for chromatography (blue line) was observed.

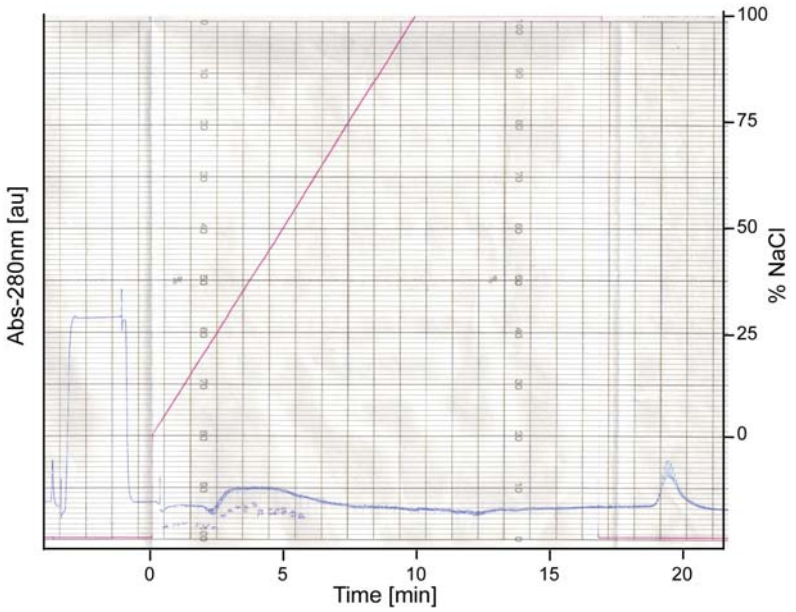

Fig. 4.12. Chromatogram of intracrystalline protein purification. Ion exchange chromatography was performed with a weak cation exchanger (sepharose carboxymethyl CM-FF) at pH 4.8 and elution gradient with 0 – 1 M NaCl in the sample buffer solution (20 mM citrate buffer solution, pH 4.8). The blue line represents the absorbance (in arbitrary units) detected at 280 nm. The red line represents the salt gradient applied during elution, 100% correspond to a concentration of 1 M NaCl. Only the absorption of buffer solutions used for chromatography was detected. The absence of peaks suggested that the intracrystalline proteins did not bind to the cation exchanger.

Separation of intracrystalline proteins was successful with an anion exchanger. A typical chromatogram (fig. 4.13) was characterized by an initial minor peak (fraction 1) always followed by a second major peak (fractions 2-14), which contained most of the proteins according to SDS-PAGE analysis (fig. 4.14).

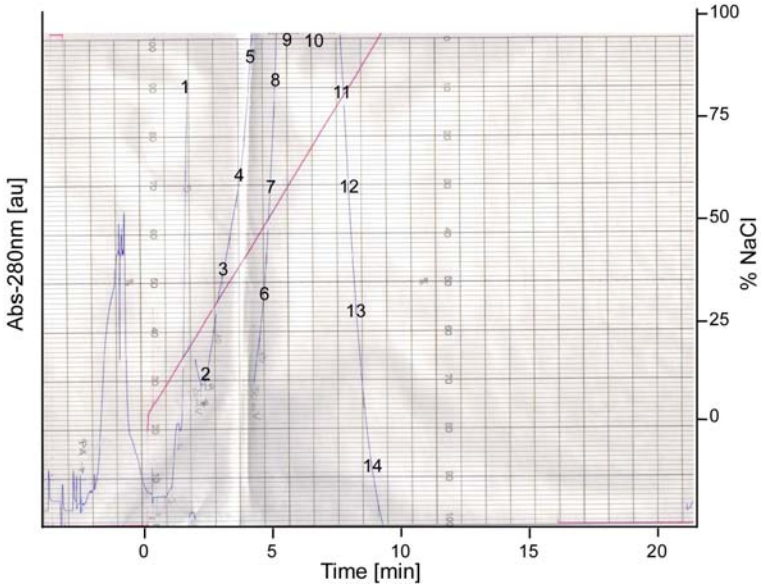

Protein fractions collected after ion exchange chromatography were investigated by SDS-PAGE and stained with Coomassie Blue (fig. 4.14). Proteins appeared, as previously observed, mainly diffused and not in sharp clear bands. Bands corresponding to proteins with a molecular weight of 6, 14 and 25 kDa were visible (fig. 4.14, yellow, green and red arrow respectively). As the salt concentration increased some of the proteins did not enter the gel (fig. 4.14, lanes 8 - 14, white arrow).

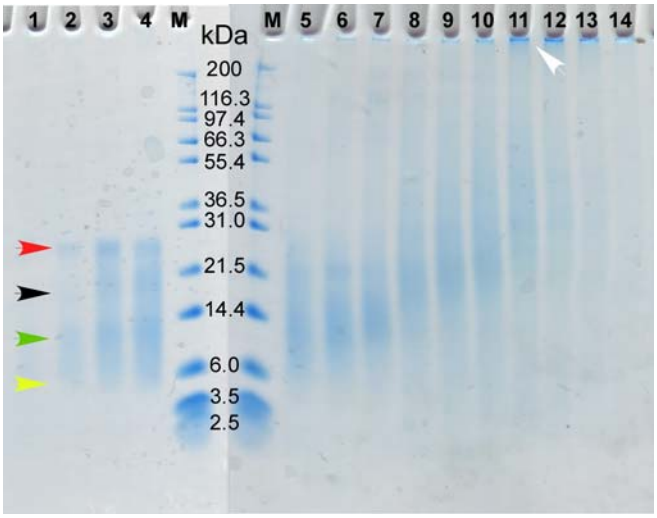

Fig. 4.14. SDS-PAGE (NuPAGE Bis-TRIS, 12% acrylamide) of the ion chromatography purification step using a quaternary ammonium anion exchanger (Q-FF) with 25 mM TRIS-HCl buffer solution (pH 8) with a linear 0 – 1 M NaCl gradient. Lane 1. Light visible 6 kDa protein. Lane 2. Several proteins with a molecular weight of ~6 kDa (yellow arrow), ~14 kDa (green arrow) and 25 kDa (red arrow) were visible. A protein of approximately 20 kDa was lightly visible (black arrow). Lane M. Molecular weight standards with masses in kDa are reported in the middle.

4.2.5 Intracrystalline proteins separation by HPLC

High performance liquid chromatography was used to achieve a further purification and separation of the proteins (fig. 4.15, A and B). The elution profile of the proteins fractionated on a C-4 column (3 - 70% linear acetonitrile gradient; 2 ml/min flow) showed a single broad peak between 20% and 52% acetonitrile content. The proteins eluted under this peak were visualized by SDS-PAGE (fig. 4. 17).

To achieve a better separation several HPLC runs were tested modifying the gradient elution and flow rate. The chromatograms were always characterized by the presence of a bright peak and not single sharp peaks (data not shown).

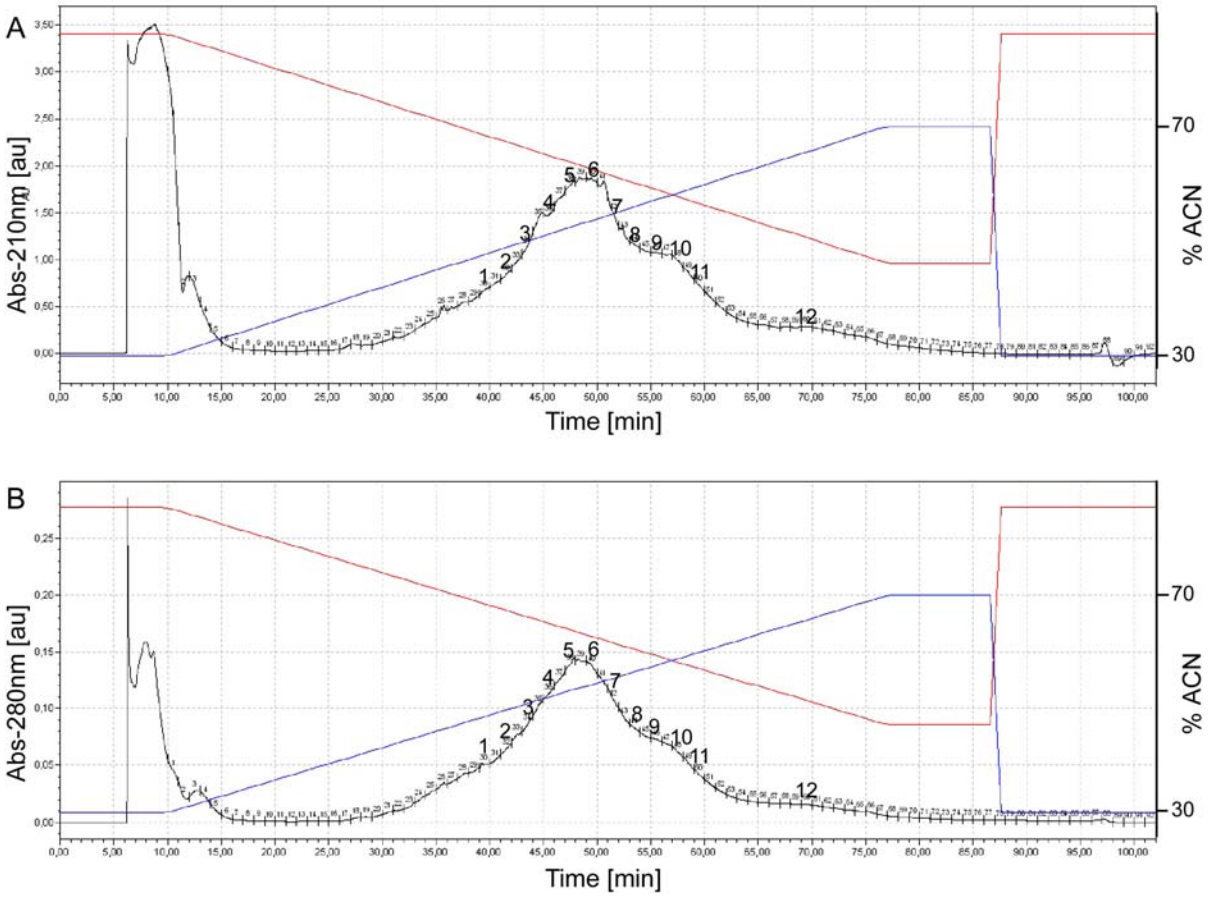

Fig. 4.15. Typical high performance liquid chormatography (HPLC) chromatograms of intracrystalline proteins. HPLC was performed using a semipreparative C-4 column. Acetonitrile gradient 3 - 70% (blue line), TFA concentration (red line), flow rate 2 ml/min. Absorption was detected at 210 nm (A) and at 280 nm (B). The numbers (1 - 12) correspond to protein fractions collected. A broad peak was detected. According to SDS-PAGE analysis (fig. 4.16) most of the proteins were eluted at 37 - 40% acetonitrile (fraction 5 - 8) and contained proteins with a molecular weight between 6 and 10 kDa (fig. 4.16, lane 6 and 7).

SDS-PAGE of the protein fractions (fig. 4.16) collected after HPLC analysis showed that most of the proteins were eluted at 37 - 40% acetonitrile (fraction 5 - 8) and contained proteins with a molecular weight between 6 and 10 kDa (fig. 4.16, lane 6 and 7). The proteins presented a light difference in molecular weight. The proteins with a molecular weight of 6 kDa were clearly visible whilst the band corresponding to 25 kDa (black arrows) was faded and not well resolved.

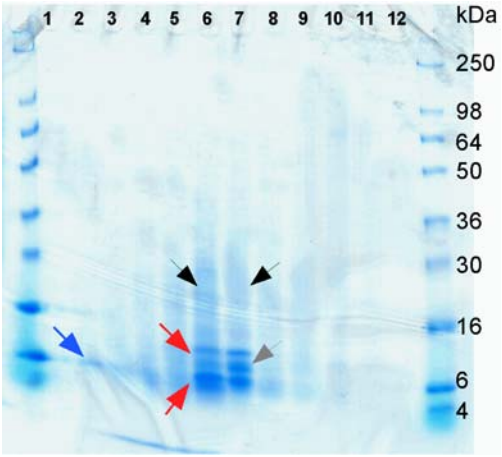

Fig. 4.16. SDS-PAGE (NuPAGE Bis-TRIS, 12% acrylamide) of HPLC purification step with a semipreparative C-4 column. Lane 1. Protein fraction contains a 6 kDa and ~14 kDa proteins; Lane 2. A 6 kDa protein is visible (blue arrow). Lane 6 – 7. Proteins with a molecular weight between 6 kDa and 10 kDa were visible. Bands corresponding to 25 kDa were also visible (black arrows). Lane 8 – 12. Proteins appeared widespread through the gel, and no single bands were visible. Lane M. Molecular weight standards with masses in kDa indicated on the right.

4.2.6 Discussion

The biochemical characterization of the intracrystalline proteins was a very challenging and fundamental step for the investigation of nacre intracrystalline proteins. Numerous technical problems related to the nature of the proteins were encountered and hindered the investigation. The consolidated biochemical analysis used for the purification of the other nacre proteins, as perlucin and perlinhibin, resulted to be inappropriate for the intracrystalline proteins, therefore it was necessary to develop new strategies.

By demineralization of aragonite platelets with EDTA a higher amount of proteins was obtained compared with that of acetic acid demineralization. The amount of

proteins obtainable with EDTA was approximately five times higher.

Demineralization of nacre with acetic acid led to a low amount of proteins. Maybe intracrystalline proteins are sensitive and at the low pH of acetic acid solutions (pH < 2.2) they might undergo hydrolysis.

The higher amount of proteins obtained by EDTA demineralization was maybe a consequence of the conditions at which demineralization was carried out (pH neutral). Under these conditions denaturation of the proteins may be hindered.

The flakes found after complete demineralization of the mineral phase could presumably be protein aggregates, denaturated proteins, chitin or protein-chitin complexes. Chitin remnants could be still present between some platelets and can released only after demineralization. The nature of these flakes is still under investigation.

Three main intracrystalline proteins with an approximate molecular weight of 6, 15 and 25 kDa were detected. Other proteins with a size between 3.5 and 6 kDa were detected and typically appeared as diffused bands in electrophoresis gel slabs. The nature of these small proteins is not well characterized, they could be peptides or protein fragments formed after unknown degradation processes.

Precipitation with ammonium sulfate revealed to be not suitable to precipitate intracrystalline proteins. This is maybe due to the incapability, in some cases, of ammonium sulfate to bind to Ca^{2+}-binding proteins [Lottspeich and Zorbas, 1998], or proteins diffused out of the gel during electrophoresis, as reported in [Gotliv et al., 2003].

After gel electrophoresis of proteins precipitated with trichloroacetic acid, proteins did not appeared as bands but diffused and smeared. It was observed that the time between protein extraction and analysis was a determining factor influencing the protein concentration. This may indicate that intracrystalline proteins might easily degrade after their extraction from the mineral phase, although during the investigations constant storing conditions were carefully maintained and monitored.

Interesting was the spontaneous formation of crystals after precipitation with trichloroacetic acid. XRD analysis did not led to recognition of any known mineral and left several questions open. The crystals could not be a calcium carbonate polymorph, formed after recrystallization of the dissolved mineral; neither the crystal was calcium acetate that could eventually be formed by the presence of calcium ions

and acetic acid in the solution. One possibility is that the crystals are protein-mineral crystals. Unfortunately no clear results are available.

Methanol-chloroform precipitation revealed to be the best method to precipitate proteins and to get mostly clear data about their molecular weight. Gel electrophoresis clearly showed the existence of three proteins with an approximate molecular weight of 6, 14 and 25 kDa. Unfortunately more precise information about their molecular weight by mass spectroscopy could not be obtained.

MALDI analysis and data base search did not lead to identification of known proteins. A large number of the peptides obtained showed a weight loss of 64 Dalton, which could be the result of a labile modification of amino acid residues. The difficulties during mass spectroscopy investigation seems to be related to an unknown modification of the protein, maybe induced during protein extraction with organic solvent (personal communication with Dr. Anja Resemann and Dr. Markus Meyer, Bruker Daltonics GmbH, Bremen, Germany).

During the whole investigation an unusual behaviour of the proteins was observed during electrophoresis. Electrophoresis gels typically presented a poor resolution of the protein bands after staining and the band appeared mostly diffused and smeared. The same phenomenon, also reported in [Gotliv et. al., 2003], could be related to a high charge density of the proteins. Eventually intracrystalline proteins have a high tendency to form agglomerates that cannot easily enter the gel. Furthermore intracrystalline proteins may bind poorly with sodium dodecyl sulfate, an anion detergent used to defold the tertiary structure of proteins. Complete defolding of the proteins is maybe not achieved and proteins could remain partially aggregated. This was suggested by the fact that some of the protein did enter the gels. The same phenomenon was also reported in [Dauphin and Cuif, 1997, Gotliv et al., 2003].

The weak binding of sodium dodecyl sulfate to proteins and their anomalous migration in gels is a phenomenon often detected with highly anionic proteins. This is supposed to depend on the protein charge densities [Dauphin and Cuif, 1997]. The same behaviour is also shown by Glu-rich recombinant proteins [McGrath et al., 1992].

Sometimes no bands at were visible after SDS-PAGE and Coomassie staining, suggesting that intracrystaline proteins show a tendency to diffuse from the gel, this is typical for proteins presenting an acidic nature. Coomassie Blue stain bound poorly

to the intracrystalline proteins suggesting that they could leak of nonacidic segments or aromatic residues [Gotliv et al., 2003].

Differential staining also indicated that the intracrystalline proteins should have an acidic nature and present calcium-binding sites. The possible presence of sialo- and phosphoproteins cannot be neglected as suggested in [Kevin et al., 1983, Goldberg et al., 1997]. Analogous results were also observed with other acid nacre proteins [Fu et al., 2005].

The results obtained by chromatographic separation (ion exchange chromatography and HPLC) were in accordance with the data obtained after precipitation techniques. Gel electrophoresis of the protein fractions collected after chromatography showed the presence of proteins with approximate molecular weights of 6 kDa, 14 kDa and 25 kDa respectively. In particular ion exchange chromatography could be performed using an anion exchanger indicating that a physiological pH-value of most of the intracrystalline proteins presented a dominant negative charge. A cation exchanger, revealed to be inadequate for separation of intracrystalline proteins.

All these observations lead to a first conclusion that the intracrystalline proteins are a novel group of proteins detected in nacre of the *H. laevigata*. Intracrystalline proteins maybe characterized by a high density charge, high tendency to form agglomerates and an overall acidic nature, furthermore they seemed to be sensitive and degrade easily.

4.3 Interaction of intracrystalline proteins with calcium carbonate

4.3.1 Investigations by atomic force microscopy

The influence of the intracrystalline proteins on the growth of calcium carbonate minerals were investigated by atomic force microscopy, incubating a geological calcite surface with a mixture of proteins dissolved in a supersaturated calcium carbonate solution.

The proteins were extracted by demineralization of nacre platelets using EDTA, as described in section 3.1.8, and dialyzed against a supersaturated calcium carbonate solution (pH 8.2). Protein concentration of 10 µg/ml was estimated with the Bradford microassay using lysozyme and IgG as standard proteins.

AFM investigations were carried out at room temperature, in contact mode using a J-scanner and Si_4N_3 cantilever. A scan rate of 3 Hz with 512 lines per image was used.

A freshly cleaved calcite surface ([4 $\underline{4}$ $\underline{1}$] cleavage plane), imaged in ultrapure water showed several layers of 0.3 - 0.4 nm height, corresponding to single atomic layers which started to dissolve rapidly (fig. 4.17, A-C; 1 min interval between two frames). During imaging the aqueous solution in the fluid cell was replaced with a supersaturated calcium carbonate solution with intracrystalline proteins (10 µg/ml).

Once the ultrapure water in the fluid cell was replaced by the supersaturated $CaCO_3$ solution with intracrystalline proteins, a drastic and rapid alteration of the surface morphology was observed. Proteins interacted with the mineral step edges (fig. 4.17, D red arrow) retarding their growth while nucleation and growth of new layers with a round shape was observed (fig. 4.17, D white arrows). The crystal surface presented after 30 minutes (fig. 4.17, G) a grain-like structure with a homogeneous distribution. Some deep holes formed (fig. 4.17, green arrows) suggesting that inhibition of mineral growth took place where protein adhered. The main features of the initial calcite surface were clearly visible indicating that intracrystalline proteins could inhibit

the growth of new mineral at the point of adhesion. After 8 hours incubation the surface was littered with small crystals grains.

Fig. 4.17. (Next page) AFM images of geological calcite ([4 $\underline{4}$ $\underline{1}$] cleavage plane) before and after incubation with intracrystalline proteins. A-C. Calcite surface imaged in ultrapure water. Dissolution of a single atomic layer took place (white arrows). Height scale (black to white 2 nm). D-I. The same calcite surface incubated with a supersaturated calcium carbonate solution (pH 8.2) with intracrystalline proteins. Proteins adhered to calcite step edges (red arrows) inhibiting their growth. At the same time nucleation of new mineral layers, presenting a round shape, took place (white arrows). Due to the strong inhibition effect of the proteins some holes formed and the orientation of the step edges of the calcite crystal was clearly recognizable (green arrows). K. Magnification of the highlighted area in J. The grains presented squared structures with a size between 100 and 200 nm and 20 nm height. Height scale (black to white 80 nm). L. The calcite surface after 8 hours incubation with the supersaturated $CaCO_3$ solution and intracrystalline proteins. The surface appeared littered with crystals grains.

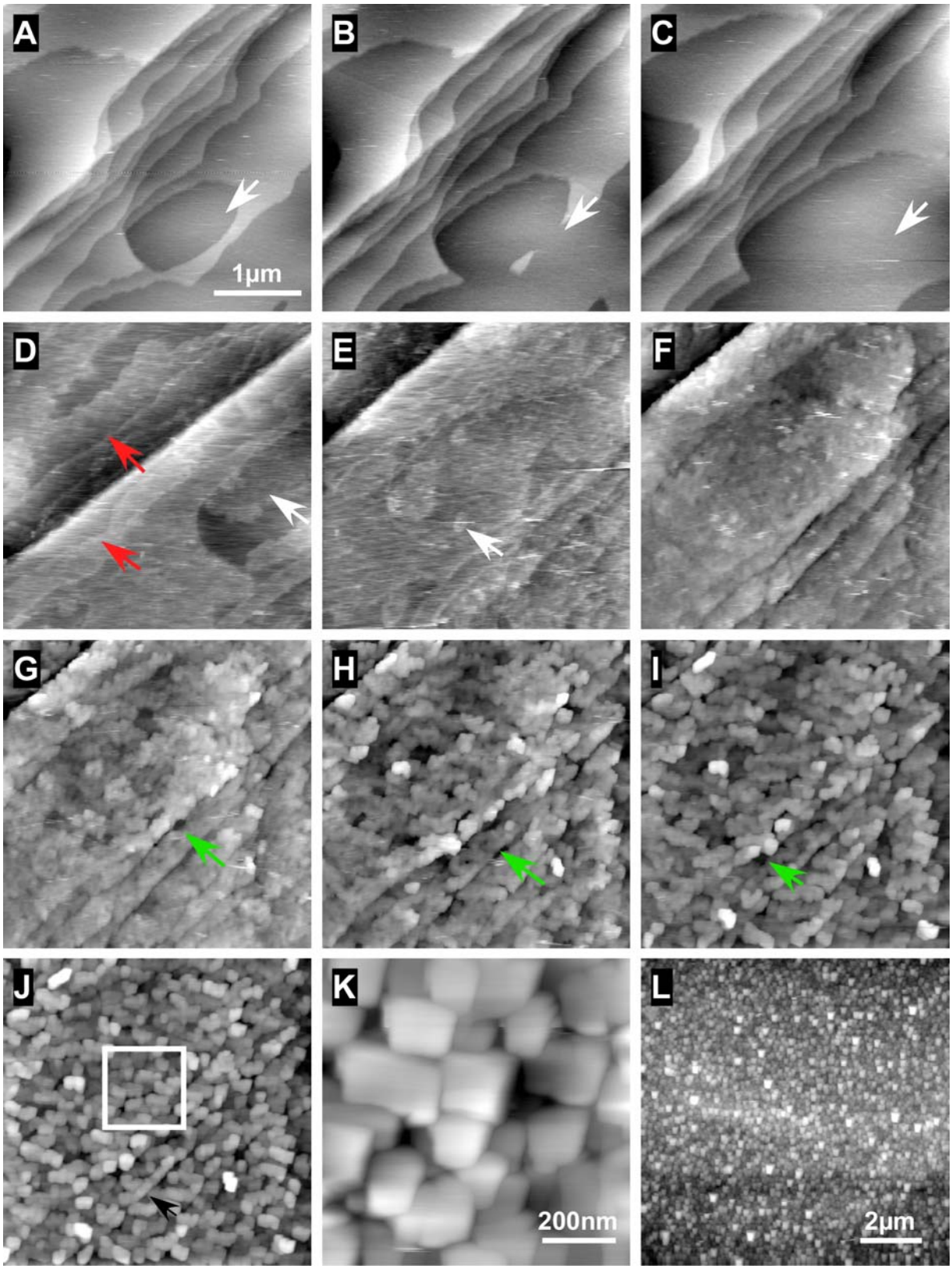
A
1µm
B
C
D
E
F
G
H
I
J
K
200nm
L
2µm

To better understand the interactions of the intracrystalline proteins with the mineral surface the proteins concentration was diminished to 5 µg/ml. AFM investigations were carried out as described before (scanning rate 5 Hz with 512 lines/sample).
A freshly cleaved calcite surface, initially imaged in ultrapure water, presented a flat surface characterized by steep atomic layers with a height of 0.3 - 0.4 nm. The apex angle of one layer was estimated about 60°. The atomic layers started rapidly to dissolve layer-by-layer (fig. 4.18, A). A light curvature of the step edges was visible due to dissolution of calcite layers while scanning. By exchanging the solution in the fluid cell perturbations were induced (fig. 4.18, B, horizontal stripes). As the supersaturated calcium carbonate solution with intracrystallline proteins was introduced in the fluid cell, a fast and evident surface modification took place (fig. 4.18, B). In the lower part of the image the mineral surface not affected by the proteins was still visible. In the upper part intracrystalline proteins were already bound to the mineral step edges. Proteins adhered to the step edges (fig. 4.18, B, white arrows) inhibiting the growth of mineral at the point of their attachment and retarding their growth in the plane direction. At the point where the proteins attached and increments of 1 - 2 nm were observed (see fig. 4.19). This suggested that the intracrystalline proteins might present a weight comprised between 10 and 20 kDa.
After 2 minutes of incubation the calcite surface became littered with proteins that induced the formation of new mineral structures with a needle-like shape (fig. 4.18, C and D) that presented a strong orientation in the vertical direction. The orientation was maybe induced by scanning. After 10 minutes the surface presented a grain-like morphology similar to that previously observed (fig. 4.17).

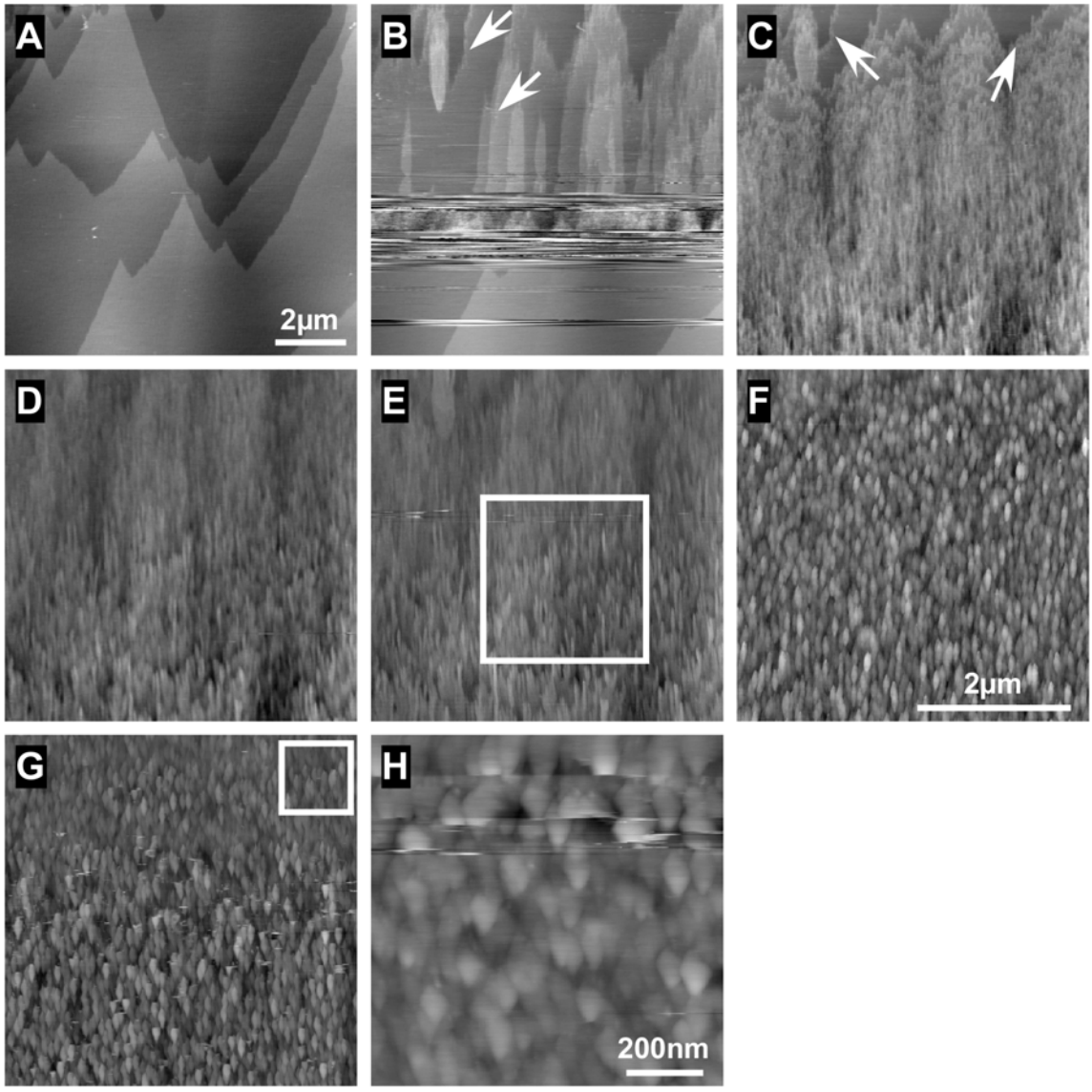

Fig. 4.18. AFM images of a freshly cleaved geological calcite surface ([4 4 1] cleavage plane) in ultrapure water (A) and incubated with a supersaturated calcium carbonate solution with intracrystalline proteins (B - H). The protein concentration, estimated with Bradford assay, was 5 µg/ml. A. Calcite surface imaged in ultrapure water presented a flat surface with steps of 0.3 - 0.4 nm and steep edges. Light distortions of the step edges were visible due to dissolution of calcite layers during scanning. Height scale (black to white 4.3 nm). B. During imaging the aqueous solution in the fluid cell was replaced with a supersaturated $CaCO_3$ solution with intracrystalline proteins. Exchanging the solution perturbations in the fluid cell were induced (horizontal stripes). In the lower part of the image the mineral surface not affected by the proteins was still visible. In the upper part intracrystalline proteins were already bound to the mineral step edges, causing an increment in their height. C. The effect of the protein became more evident and steps edges increased by 1 - 2 nm. The rapid growth of new layers took place. The calcite surface appeared covered with needle-like structures (2 nm height). F. Magnification of the surface highlighted in E. Height scale (black to white 15 nm). H. Magnification of the surface highlighted in G.

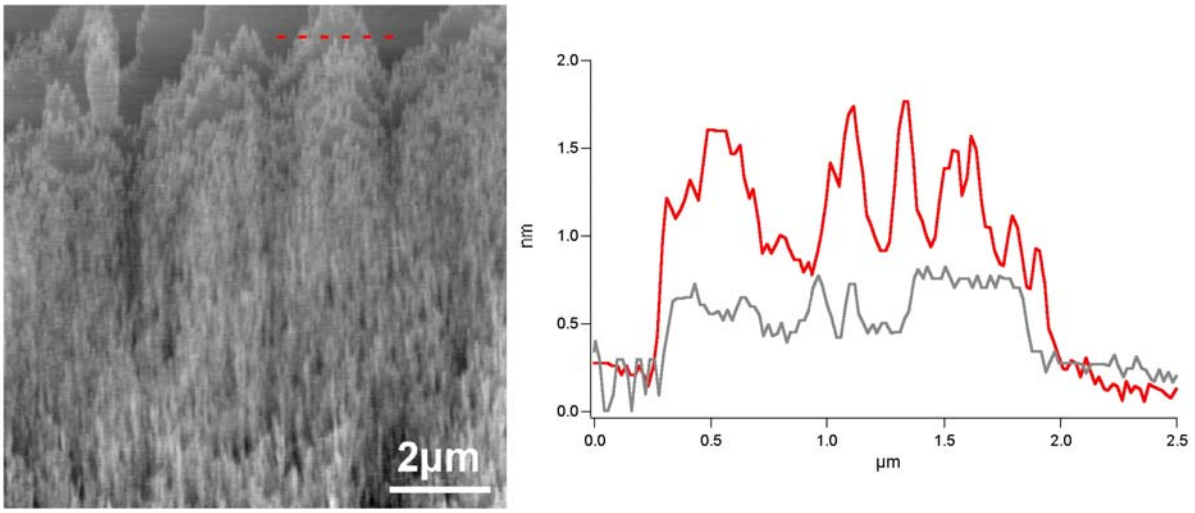

Fig. 4.19. Height profile of (fig. 4.18, C). Grey line: profile of the crystal before protein incubation. Red line: profile of the surface after protein incubation (30 seconds). After incubation with a supersaturated $CaCO_3$ solution with intracrystalline proteins (5 µg/ml) needle-like structure were observed. The spikes presented a height of 1 - 2 nm suggesting that the intracrystalline proteins might have a molecular weight comprised between 10 and 20 kDa.

After 10 hours of incubation with the calcium carbonate solution with intracrystalline proteins, the solution on the fluid cell was replaced with ultrapure water to remove excess of calcium carbonate and proteins. The calcite surface was further imaged (fig. 4.20). The main features of the initial calcite surface were still recognizable. The orientation of the mineral layers and the apex angle of layers (fig. 4.20, A-C-D white lines) were maintained. The whole surface was covered with grain-like structures with homogeneous distribution.

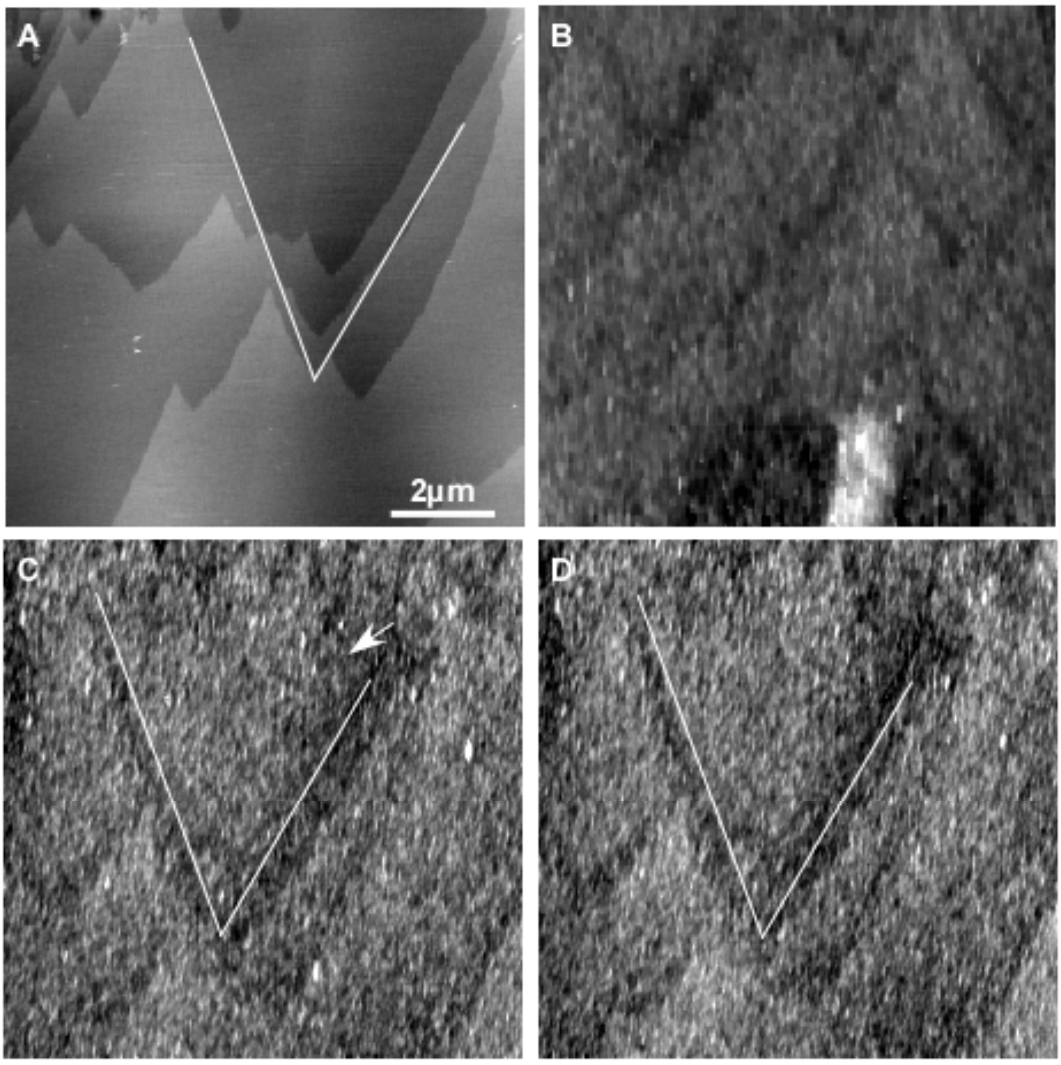

Fig. 4.20. Interaction of intracrystalline proteins with a geological calcium carbonate surface. A. The calcite surface imaged in ultrapure water before incubation with the supersaturated calcium carbonate solution with intracrystalline proteins (5 µg/ml). B-D. The surface after incubation with the calcium carbonate solution with intracrystalline proteins was imaged again in ultrapure water. The surface lightly dissolved revealing the orientation and structure of the underlying calcite substrate. The white lines show the characteristic structure of the calcite surface with an apex angle of nearly 60°. 5 minutes between two images.

4.3.2 Detection of aragonite

To investigate whether a possible polymorph transition on the calcite surface was induced by the intracrystalline proteins, the Feigl´s test was used. The geological calcite crystal incubated with a supersaturated calcium carbonate solution with intracrystalline proteins (5 µg/ml), previously investigated by AFM, was dried at room temperature and incubated with some drops of Feigl´s solution. After 5 min the

crystal showed a dark-brown colour, suggesting that aragonite formation was induced. After 30 minutes the intensity of the colour increased. For a negative control pure geological calcite, and calcite incubated with a supersaturated calcium carbonate solution with lysozyme (5 µg/ml) or with albumin (5 µg/ml) were incubated at the same way with the Feigl´s solution. The crystal remained unstained. The results are summarized in Table 4.2.

Sample	5 minutes incubation with Feigl´s solution	30 minutes incubation with Feigl´s solution
geological calcite without protein	-	-
geological calcite + intracrystalline proteins (5 µg/ml)	+	++
geological calcite + lysozyme (5 µg/ml)	-	-
geological calcite + albumin (5 µg/ml)	-	-

Table 4.2. Feigl´s test for detection of aragonite. A negative reaction (–) indicates that no aragonite formed on the calcite surface; a positive reaction (+) indicates that formation of aragonite took place. The intensity of the colour increased with the incubation time (++).

4.3.3 Function of intracrystalline proteins in terms of calcium carbonate precipitation

The effect of the intracrystalline proteins on the rate of calcium carbonate precipitation was determined by recording the change of pH in a supersaturated calcium carbonate solution during precipitation. In fig. 4.21 investigations with and without proteins are shown. The initial pH-value was initially adjusted to pH 8.7, where calcium carbonate precipitates spontaneously at room temperature.

When precipitation was performed without proteins (fig. 4.21, grey curve) the pH-value suddenly dropped after addition of $CaCl_2$ solution to the $NaHCO_3$ solution. The pH decrease did not indicate a nucleation of crystals but probable formation of complexes between the ionic species. The pH slightly increased and stayed stable for nearly 5 min, until nucleation and precipitation occurred with pH decline and turbidity of the solution.

When the intracrystalline proteins were present in the solution (fig. 4.21, red curve) with a concentration of 1.25 µg/ml, the same fast pH drop was observed but it recovered immediately and slightly increased during the whole investigation time. No pH decline or solution turbidity was observed, suggesting that the proteins had an inhibitory effect. The upward pH drift was addressable to the loss of carbon dioxide to the atmosphere and not to the presence of proteins. The same result was obtained with a mixture of the water-soluble matrix of bivalve nacre as reported in [Wheeler et al., 1981].

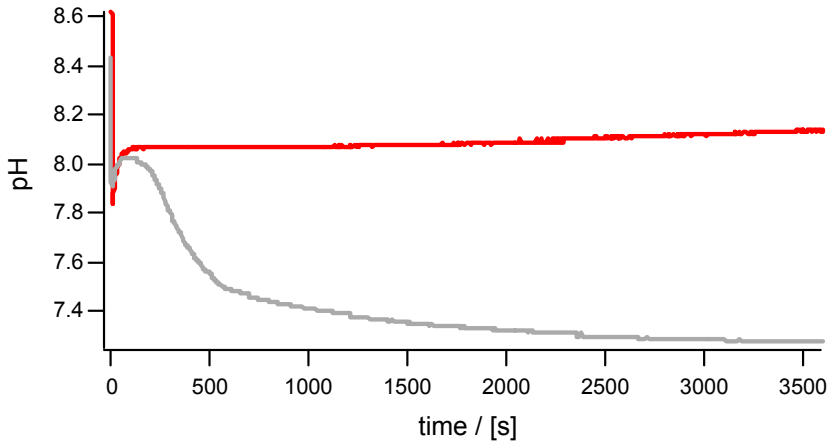

Fig. 4.23. Recording of $CaCO_3$ precipitation in a supersaturated solution. In absence of proteins (grey curve) the pH-value after an initial drop remained constant for approximately 5 min and regularly decreased, while nucleation and precipitation occurred. When proteins were present in the solution (1.25 µg/ml), after an initial drop, the pH recovered and slightly increased. During the all investigation the solution became not turbid. The inhibitory effect of intracrystalline proteins on calcium carbonate precipitation was clearly visible.

4.3.4 Discussion

Crystal growth studies with the intracrystalline proteins indicated that this group of proteins acts mainly as inhibitor of calcium carbonate crystallization. Intracrystalline proteins seem to bind strongly to certain step-edges of a calcite surface, inhibiting the crystal growth at the point of adhesion. A surface of geological calcite incubated with the intracrystalline proteins typically presents a uniform grain-like structure that could suggest that the proteins can initially build a template that can modulate the crystal orientation and the crystal morphology. The grains observed on the surface could be

microcrystals containing proteins. The mechanism of interaction of the intracrystalline proteins with the crystal surface is not clear, it seems that they initially inhibit growth and afterwards they can react with the free calcium ions in the solution and induce crystal formation and become occluded into the crystal itself. The inhibitory effect maybe depends on the presence of multiple anionic binding sites on the protein surface. The binding sites might interact with the nucleation site or surface of the forming crystal in a way that can prevent further growth of the mineral by rising the free energy for the activation of crystal formation or decreasing the mineral solubility. For the protein-crystal association the proteins must have a higher affinity for the crystal than for the free calcium ions, as the binding sites of the proteins would be normally saturated with calcium ions from solution.

The inhibitory effect of the intracrystalline proteins was also observed on the precipitation of calcium carbonate from saturated solutions. Proteins, due to their negative charge may bind to free calcium ions in solutions and the protein-calcium complexes may be involved in the initiation of crystal nucleation. It can also not be excluded that the proteins may inhibit and regulate crystal growth possibly by binding to the growing centres of the mineral.

Furthermore the intracrystalline proteins, inducing growth of aragonite polymorph on a calcite surface, can be involved in polymorph selection regulating in the shell formation the transition from calcite to aragonite.

In vitro studies of the intracrystalline proteins carried out until here had furnished a first overview about the main molecular characteristics and properties and their interactions with calcium carbonate crystals. More precise information about their molecular structure and chemical properties are necessary for a better understanding of their role in the shell formation. Anyway the discovery of the intracrystalline proteins can be related to the ubiquitous detection of acidic proteins within various calcareous biominerals, which has led to the prevalent speculation that these macromolecules, through interaction with positively charged calcium ions in solution or at the mineral surface, are most influential during the mineral formation [Gotliv et al., 2006].

4.4 Perlucin purification and influence of perlucin on calcium carbonate crystallization

4.4.1 Perlucin extraction and purification

Perlucin purification by ion exchange chromatography

Nacre from specimens of *H. laevigata* was used to collect the crude protein material. Nacre was ground to a fine powder with a ball mill and demineralized with 12% acetic acid. When nacre started to dissolve, foam was produced due to carbon dioxide formation. Foam fractions, which contain nacre proteins, were collected and separately investigated by ion exchange chromatography. Ion exchange chromatography was carried out with a sepharose carboxymethyl column equilibrated with citrate buffer, pH 4.8 and an elution gradient of 0 – 1 M NaCl. The chromatogram showed a characteristic double elution peak. The second elution peak (black arrow) contained perlucin according to SDS-PAGE analysis (fig. 4.26) and Edman degradation.

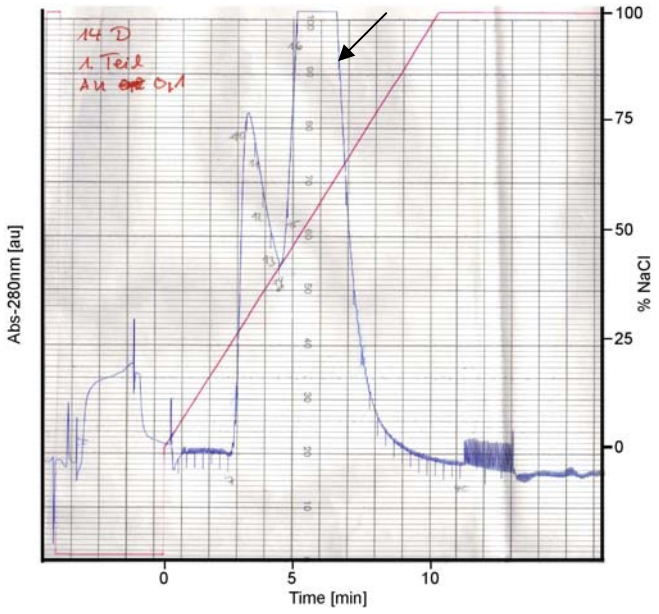

Fig. 4.25. (Previous page) Typical chromatogram of perlucin purification by ion exchange chromatography. Purification was performed using a sepharose carboxymethyl (CM-FF) column, 20 mM citrate buffer, pH 4.8, and a linear elution gradient of 0 – 1 M NaCl. Absorbance, detected at 280 nm (blue line), is plotted as a function of the salt concentration (red line). The salt concentration was linearly increased, 100% NaCl correspond to 1 M NaCl. The second elution peak (black arrow) contained perlucin according to SDS-PAGE analysis (fig. 4.26) and Edman degradation.

Protein fractions collected after ion exchange chromatography were investigated by SDS-PAGE and stained with Coomassie Blue. SDS-PAGE (fig. 4.26) showed that mostly pure perlucin was extracted. Perlucin often appears as a double band.

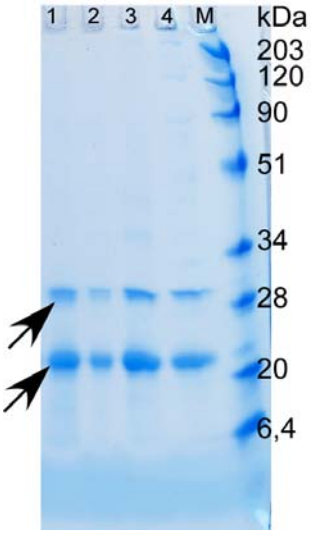

Fig. 4.26. SDS-PAGE (Tris-Glycine, 10-20% acrylamide gradient gel) stained with Coomassie Blue of perlucin fractions collected after ion exchange chromatography. Lane 1-4 corresponded to mostly pure perlucin. Perlucin appeared as a double band (black arrows). Lane M. Molecular weight standard with relative masses in kDa indicated on the right.

Perlucin characterization by MALDI

Protein fractions, collected after ion exchange chromatography, were analyzed by SDS-PAGE and mass spectroscopy (MALDI). SDS-PAGE showed that several proteins fractions (fig. 4.27, lane 1-3) contained an intensely stained protein with a molecular weight of approximately 20 kDa. This protein was supposed to correspond to perlucin (fig. 4.27, black arrow). Other water-soluble nacre proteins were also present in the sample in a lower concentration. The molecular weight of these proteins was approximately 6 kDa (fig. 4.27, red arrow).

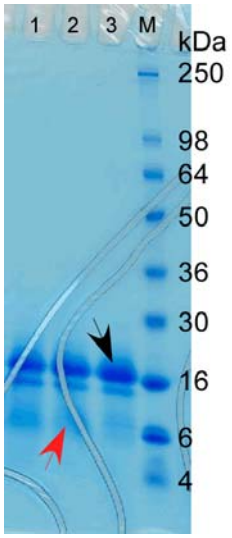

Fig. 4.27. SDS-PAGE (Tris-Glycine, 10-20% acrylamide gradient gel) stained with Coomassie Blue of the ion exchange chromatography purification step for perlucin purification. Lane 1-3. Protein fractions containing perlucin in a high concentration (black arrow). Other proteins with an approximate molecular weight of 6 kDa (red arrow) were present in a lower concentration. The protein fraction containing the highest percentage of perlucin (lane 3) was used for MALDI analysis. Lane M. Molecular weight standards with relative masses in kDa indicated on the right.

Protein fractions were analyzed by MALDI in a sinapinic acid matrix. The linear mode spectrum of the sample (fig. 4.28) showed the presence of different proteins in the sample as already detected by SDS-PAGE. Protein fragment masses were comprised between 4.5 kDa and 18 kDa. A base peak was found at 9329 Da with the relative double charged ion at 4663 Da. A peak, maybe generated from other proteins present in the sample, was located at 16246 Da with its double charged ion at 8127 Da. Further peaks were found at 17282 Da and at 18253 Da.

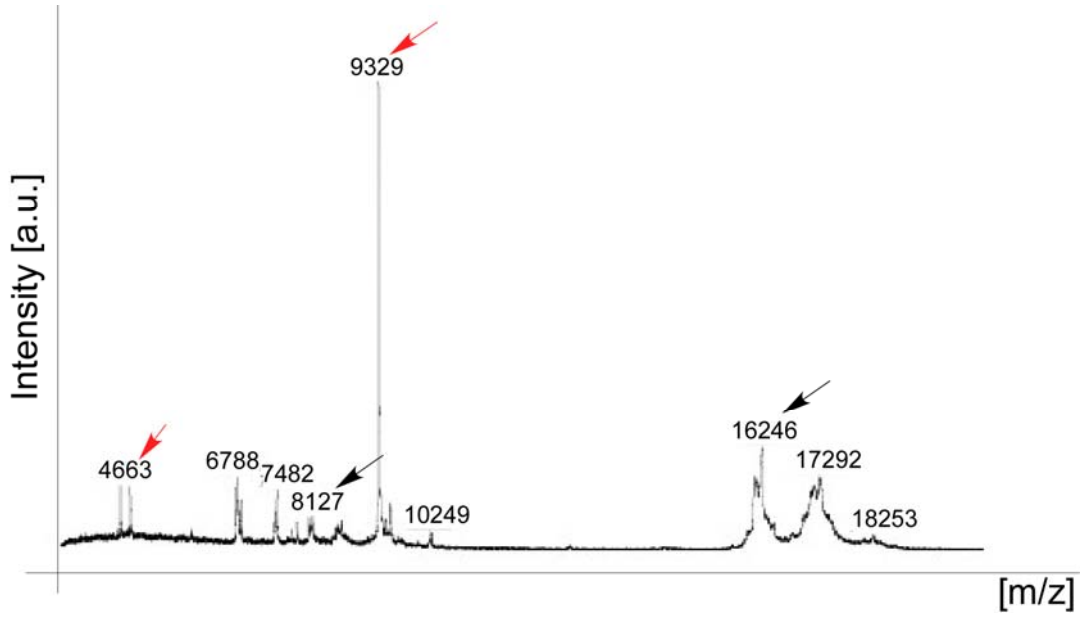

Fig. 4.28. (Previous page) MALDI-TOF-MS spectrum of intact nacre proteins. Absolute intensity in arbitrary units is plotted against the mass-to-charge ratio (*m/z*). The masses for each component are reported on the graph. Protein fractions, collected after ion exchange chromatography, were desalted with a C-18 ZIP-tip. A base peak was found at 9329 Da, the relative double charged ion at 4663 Da (red arrows). Further analysis (sequence tag data search) revealed that these two peaks corresponded to perlucin fragments. Other peaks were found at 16246 Da, 8127 Da, 17282 Da and at 18253 Da corresponded to other proteins. MALDI measurements were performed with the kind help of Dr. Anja Resemann, at the laboratories of Bruker Daltonics (Bruker Daltonics GmbH, Bremen, Germany).

In-Source-Decay analysis of fragments generated, led to the identification of two-sequence tags (fig. 4.29). The first identified sequence consisted of tryptophan-tyrosine and phenylalanine (represented by one letter code as Y-W-F). The second tag consisted of eight amino acids, threonine-leucine-arginine-serine-serine-phenylalanine-alanine and glutamic acid.

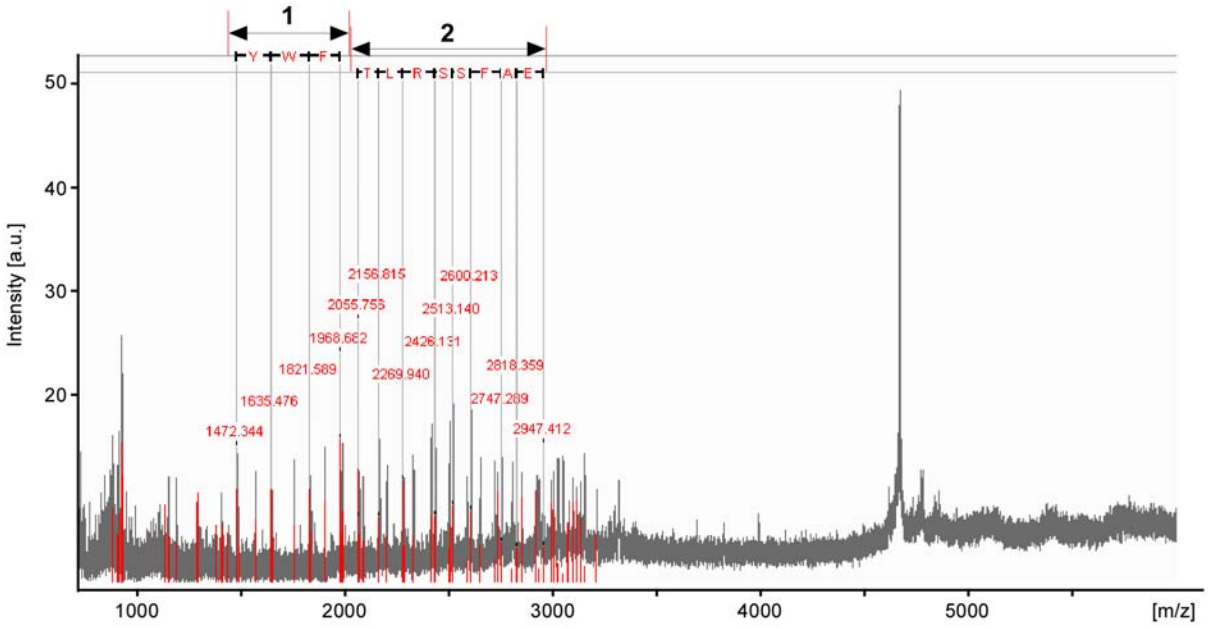

Fig. 4.29. *In-Source-D*ecay analysis and relative sequence tags. Analysis of the two fragments generated (indicated as *1* and *2*) showed that the fragments consisted of three and eight amino acids respectively. Single amino acids are represented by the one letter code. The first sequence consists of tryptophan - tyrosine - phenylalanine (Y-W-F); the second partial sequence consists of threonine – leucine – arginine – serine – serine – phenylalanine - alanine - glutamic acid (T-L-R-S-S-F-A-E).

The two partial internal sequences were used for “tag sequence search“. Database search showed that the two fragments corresponded to perlucin.

Discussion

The purification and extraction of water-soluble proteins from milled nacre led to the extraction of perlucin with a high degree of purity. The influence of ball milling on the proteins is still unknown, possibly the heat produced due to mechanical friction during milling, may destabilize most of the proteins but not perlucin, which could be more temperature resistant.
The possibility to obtain perlucin, or more in general nacre proteins, with a high degree of purity just modifying the preparation of nacre has several positive consequences. Only proteins of interest can be purified avoiding or diminishing the need for further separation methods. Often the heterogeneity of the proteins fractions hinders the analysis. If more information about the nature and the properties of single proteins can be achieved, a wider and deeper knowledge about nacre itself can be gained.

4.4.2 Cocrystallization of perlucin with calcium carbonate

The influence of perlucin on calcium carbonate crystallization from an aqueous solution was investigated with the ammonium carbonate vapour diffusion technique. In parallel control experiments were performed using buffer salts and non-nacreous proteins to better discern and understand the effect of perlucin on calcium carbonate growth.

Crystallization of calcium carbonate by vapour diffusion technique

The ammonium carbonate vapour diffusion technique is based on the diffusion of carbon dioxide in a calcium chloride solution. CO_2 is obtained by spontaneous decomposition of solid ammonium carbonate. Beside the release of CO_2, ammonia is also produced and therefore can diffuse in the $CaCl_2$ solution as well. Diffusion of ammonia led to an increase of the pH.

The pH value of the $CaCl_2$ solution during the crystal formation was monitored. Crystallization was performed as described in section 3.3.

An initial pH value of 8.1 was monitored and started to rise quite fast after a few seconds from the beginning of the experiment. After 20 minutes the pH reached a value of 8.6 and of pH 9.8 after one hour. Afterwards the pH value remained constant at 9.8 for the rest of the experiment. This result shown in fig. 4.30 was in accordance with literature data [Becker et al., 2003].

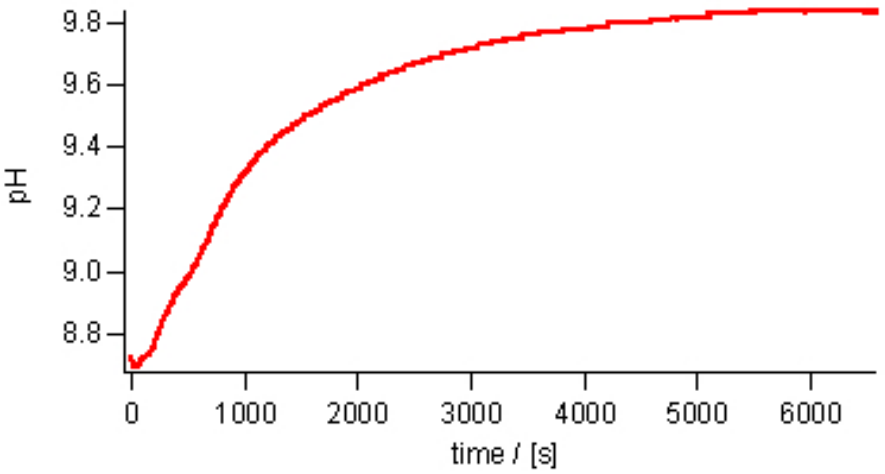

Fig. 4.30. Recording of pH variation during crystallization of calcium carbonate with the ammonium carbonate vapour diffusion technique. A rapid pH increase in pH-value was observed already at the beginning of the experiment. The initial pH (8.1) reached a value of 8.6 after 20 min and a value of 9.8 after 1 hour that remained stable for the rest of the experiment.

To circumvent the rise in pH, buffer salts were added to the $CaCl_2$. Separately the influence of non-nacreous proteins (immunoglobuline (IgG), bovine serum albumin (BSA) and albumin) was investigated.

Crystallization was performed as described in section 3.3. All the experiments were carried out at room temperature. Crystals were investigated by scanning electron microscopy.

Crystals grown in pure $CaCl_2$ solution developed a rhombohedral habit, typical for calcite, and presented a size of 20 µm (fig. 4.31, A-C). In presence of additives modified calcite crystals were nucleated. Larger crystals, with an approximate size of 100 µm, precipitated using a $CaCl_2$ solution with citrate buffer (fig. 4.31, D). Some crystal faces were unaffected whilst other showed several steps, densely packed and characterized by round edges. In presence of TRIS buffer salt crystals with different

sizes (~20 - 150 µm) precipitated (fig. 4.31, E). The rhombohedral calcite structure was still recognizable, some faces showed rounded features and typically polycrystallites were present. The same effect was observed when IgG was added to the calcium chloride solution. When BSA and albumin were added to the calcium chloride solution mainly polycrystallites nucleated (fig. 4.31, H and I respectively). The polycrystallites were formed by several subcrystals characterized by a rhombohedric shape.

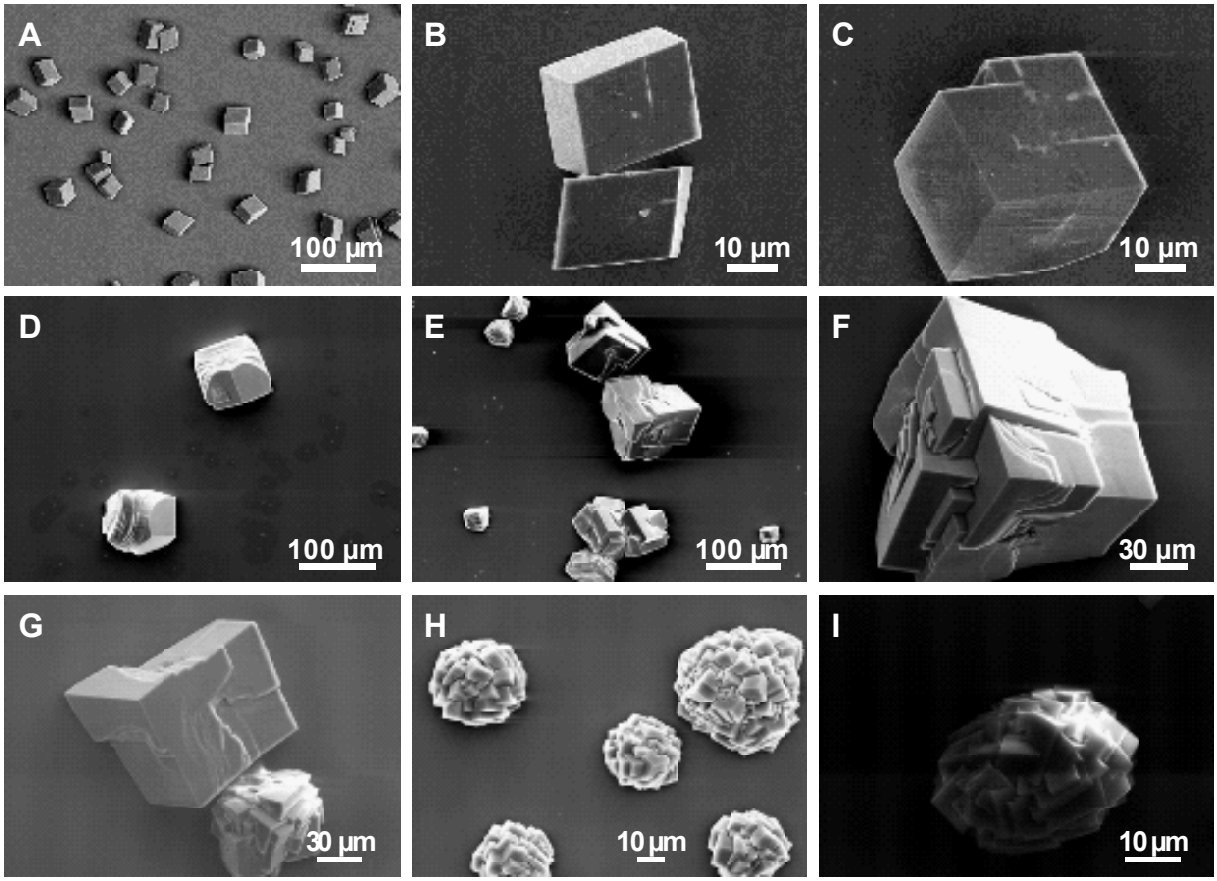

Fig. 4.31. SEM images of crystals grown with the ammonium carbonate vapour diffusion technique. A-C. Calcite crystal precipitated from a 7.5 mM $CaCl_2$ solution. The marked rhombohedral shape indicates that only calcite has formed. D. Crystals grown from a $CaCl_2$ solution with 2 mM citrate buffer. Only some faces were affected showing a rounded shape and corrugated appearance. E-F. Crystals precipitated from a $CaCl_2$ solution with 2 mM TRIS buffer. G-I. Crystals precipitated with non-nacreous proteins (IgG, BSA and albumin) added to the $CaCl_2$ solution. The final protein concentration was of 0.2 mg/ml. G. IgG induced the precipitation of relative large crystals and polycrystallites. H. In presence of BSA polycrystallites typically formed. I. Also in presence of albumin polycrystallites formed.

Cocrystallization of calcium carbonate with perlucin

The cocrystallization of perlucin with calcium carbonate was investigated with the ammonium carbonate method. Perlucin fractions collected after ion exchange chromatography (stored in citrate buffer pH 4.8), were dialyzed against 7.5 mM $CaCl_2$ solution, and crystallized at different concentrations (10 to 100 µg/ml) in a closed dessicator for five days at room temperature. The nucleated crystals were investigated by scanning electron microscopy (fig. 4.32). In parallel negative control investigations without additives were carried out.

In absence of perlucin or in presence of perlucin in low concentration (10 µg/ml) only the nucleation of calcite crystals took place (data not shown). The crystals presented the typical rhombohedric shape as previously observed (fig. 4.31, A). When perlucin was added to the calcium chloride solution in a concentration of 30 µg/ml, fewer crystals were formed. They presented a cubic shape rather than rhombohedral with a size of 10-30 µm (fig. 4.32, A). On each crystal surface the nucleation of new layers with parallel edges was visible (fig. 4.32, B and C, white arrows). The edges of confluent layers appeared slightly smoothed out (fig. 4.32, C, black arrow). The layered morphology became more marked as the concentration of perlucin in the solution increased. At a concentration of perlucin of 100 µg/ml, fewer and smaller crystals formed and several polycrystallites were visible (fig. 4.32, D). Crystals with a diameter of approximately 10 µm showed a denser staged and compact structure. The height of each layer was estimated less than 500 nm. Each new nucleated layer grew parallel to the underlying layer, with mostly straight edges. The surface of the layer appeared slightly rough (fig. 4.32, E and H, black arrows).

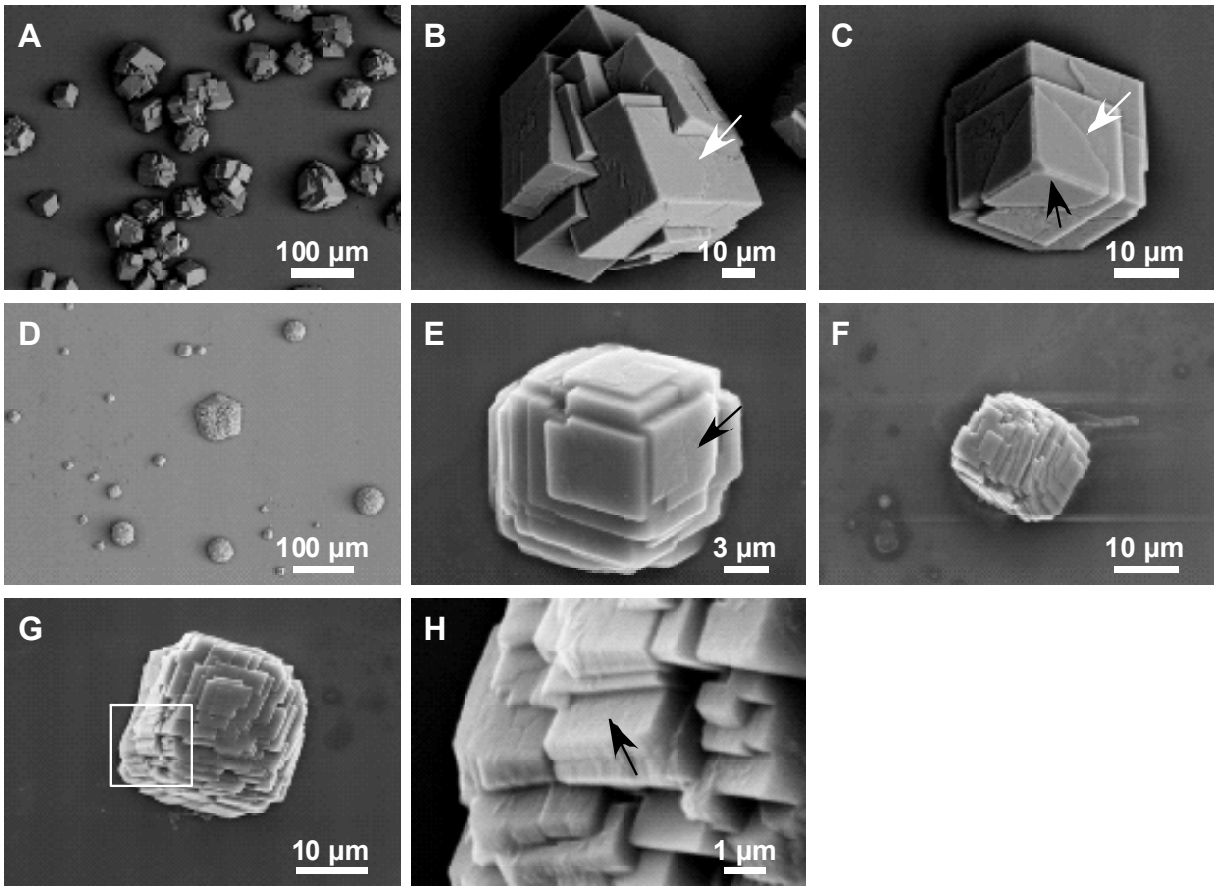

Fig. 4.32. SEM images of calcium carbonate crystals obtained with ammonium carbonate vapour diffusion method in presence of perlucin. A-C. Perlucin in a concentration of 30 µg/ml induced the formation of polycrystallites, which were characterized by a cubic form rather than a rhombohedral form. New mineral layers are nucleated on the crystal faces. The edges between confluent layers appeared parallel to underlying layer and slightly smoothed out. D-H. At a higher concentration (100 µg/ml) less and smaller crystals were formed with a denser layered structure. H. Magnification of the region highlighted in G. The slight roughness of the layer is visible.

Discussion

The ammonium carbonate vapour diffusion technique resulted to be a fast and straightforward technique to obtain initial information about the interaction and the influence of perlucin on the nucleation of calcium carbonate crystals. The presence of additives in the solution, before any crystallization process can take place, makes this method suitable for the investigation of nucleation processes. Unfortunately the initial rise of the pH value can influence the charge distribution on the protein surface and therefore modifies the interaction between the proteins and the ions in solution. Proteins are charged molecules with titrable positive and negative charges that can

modify according to the pH medium. A change in the protein charges can induce a loss in protein specific binding capability and protein function. To overcome this problem the calcium chloride solution was buffered with different buffer substances, but they strongly influenced the crystal morphology. Therefore buffer salts were not used to not effect and alter the function of the protein.

The results obtained using the vapour diffusion technique were in accordance with previous AFM investigation [Blank et al., 2003], which showed that perlucin in a supersaturated calcium carbonate solution nucleated new mineral layers onto a calcite surface. These layers presented a typical height of about 0.5 nm and rounded edges (see fig. 2.14). The formation of new mineral layers was observed with the vapour diffusion technique and demonstrated clearly that perlucin is strongly involved in the nucleation of the mineral crystals. The fact that two different techniques, based on different principles and performed at different conditions, led to the same conclusion is particular important, because the role and function of the perlucin can be more clearly defined. Furthermore the characteristic interaction of perlucin with calcium carbonate nucleation demonstrated once more the active and specific role of nacre proteins in calcium carbonate crystal formation. The influence of perlucin cannot be attributed to a general effect of proteins on calcium carbonate crystals, because non-nacreous proteins affected the crystal growth differently.

Because *in vitro* perlucin induced the nucleation of the most thermodynamically stable polymorph, this suggested that perlucin seems not to be involved in the formation of aragonite. The influence, *in vivo,* of perlucin of polymorph transition otherwise cannot be excluded.

4.5 Influence of perlinhibin on calcium carbonate crystallization

4.5.1 Cocrystallization of calcium carbonate with perlinhibin

The role of perlinhibin on the nucleation and growth of calcium carbonate crystals was investigated with the ammonium carbonate vapour diffusion technique. Perlinhibin fractions collected after ion exchange chromatography (performed with a sepharose CM-FF column, 20 mM citrate buffer solution (pH 4.8) and linear NaCl gradient) were dialyzed against a 7.5 mM $CaCl_2$ solution (pH 7.5) to a final concentration of 20 µg/ml. Crystallization was performed as described in section 3.3. The crystals were investigated by scanning electron microscopy (fig. 4.34). Crystals and polycrystallites of different sizes (approximately from 10 to 100 µm) formed and were characterized by a rhombohedric-cubic shape. This morphology, similar to that of calcite crystals, suggested that mainly the most thermodynamically stable calcium carbonate polymorph nucleated. Some crystal faces appeared highly corrugated and the nucleation of new layers with an irregular contour took place on the pre-existing mineral layers (fig. 4.34, C – E, black arrows). Some crystal faces were not affected. The newly nucleated layers presented a parallel orientation respect to the layers beneath. The presence of deep holes in the crystal faces (fig. 4.34, F, red arrows), suggested that inhibition of crystal growth took place at the protein-binding site. The presence of deep holes on some crystal faces suggested that the growth of new crystal layers was only possible around the protein-binding sites (fig. 4.34, F).

The step edges of the crystals appeared smoothed out (fig. 4.34, C – D, white arrows) as already observed during crystallization of calcium carbonate with perlucin. Negative control measurements without additives were carried out in parallel. Only calcite precipitated (data not shown).

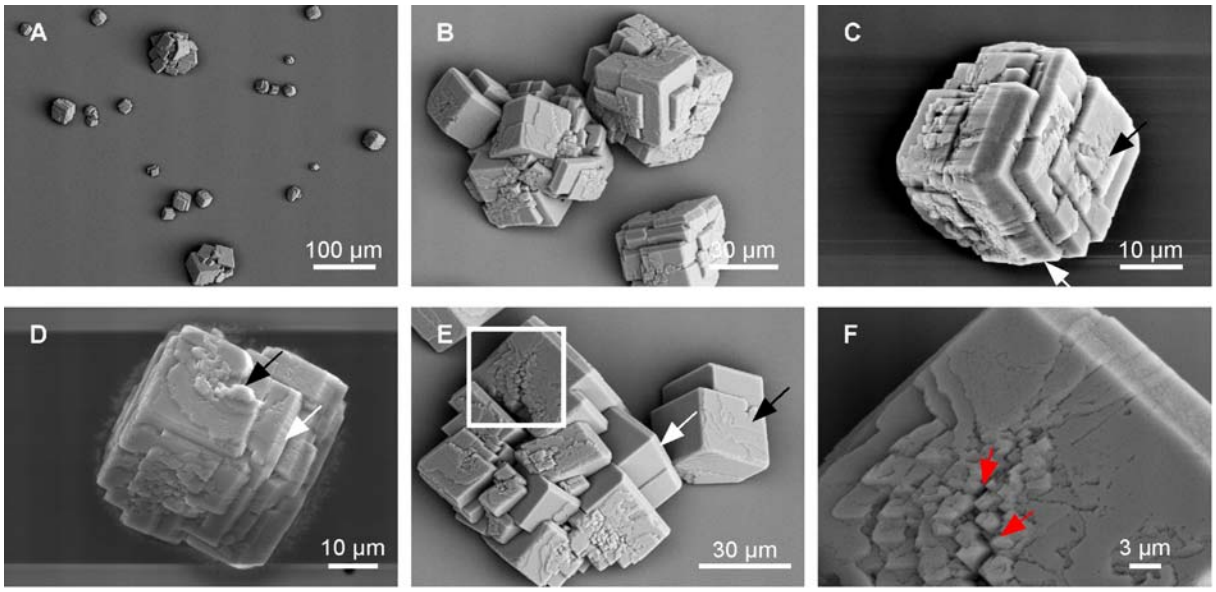

Fig. 4.34. SEM images of crystals grown with the ammonium carbonate vapour diffusion technique in the presence of perlinhibin (20 µg/ml). A. Single crystals and polycrystallites with different sizes precipitated. The crystals presented a rhombohedric habit typical of calcite. B. Polycrystallites presented a random oritentation. Some crystal faces presented an uneven surface. C – D. Single crystals with a cubic shape precipitated. The uneven surface of some faces was attributed to the effect of perlinhibin. The newly nucleated layers presented a curved profile. The formation of new layers on the pre-existing ones took place, the mineral layers grew mostly parallel respect to the crystal faces (black arrows). Some crystal edges appeared smoothed out (white arrows). E. Polycrystallites. Some faces presented an uneven corrugate surface while other faces were unaffected. Perlinhibin seem to interact specifically with certain crystal planes. F. Magnification of the area highlighted in E. The formation of deep holes (red arrows) suggested that perlinhibin suppressed the growth of calcium carbonate mineral at the protein-binding site. Growth of mineral layers around the protein-binding site caused the formation of deep holes.

4.5.2 AFM investigations of the influence of perlinhibin on calcium carbonate crystallization

AFM investigations with perlinhibin dissolved in a calcium chloride solution

The interactions of perlinhibin with calcium carbonate crystals were investigated by atomic force microscopy. A freshly cleaved calcite surface was incubated with perlinhibin, dissolved in a calcium chloride solution, to investigate the interaction of

perlinhibin with the calcite surface. Freeze dried perlinhibin was dissolved in a 7.5 mM $CaCl_2$ solution (pH 7.5) to a final concentration of 20 µg/ml.

AFM investigations were carried out at room temperature, in contact mode using a J-scanner and Si_4N_3 cantilever, scan rate of 6 Hz with 512 lines/sample.

A freshly cleaved calcite surface was initially imaged in ultrapure water for several minutes (fig. 4.35, A). The calcite surface presented the characteristic rhombohedral defects with a depth of 0.4 nm, which corresponded to singular atomic layers. The spontaneous dissolution of calcium carbonate layers took place (data not shown). After 20 minutes the aqueous solution in the fluid cell was exchanged against the calcium chloride solution with perlinhibin. Flushing-in induced perturbations in the fluid cell and a progressive sample drift along the upper-right direction (fig. 4.35, B - C). Visible modification of the calcite surface took place mostly at the mineral steps edges where perlinhibin bound (fig. 4.35, B - C black arrows). Steps edges became progressively frayed a presented a curved contour. Single perlinhibin molecules bound progressively to the crystal edges (single molecules are visible as white small dots at the crystal step layers). The inhibiting effect seems to occur by adsorption and pinning at step edges to kinetically impede step flow during layer dissolution. The surfaces of the mineral layers remained unmodified.

During all the investigation an enhancements of the step edges in the vertical direction was observed, due a progressive binding of the proteins at calcium carbonate mineral edges (fig. 4.36). After 25 minutes no visible variations of the surface morphology were detected (fig. 4.35, F - I, red and white arrows) indicating that perlinhibin suppressed any kind of process taking place on the calcite surface.

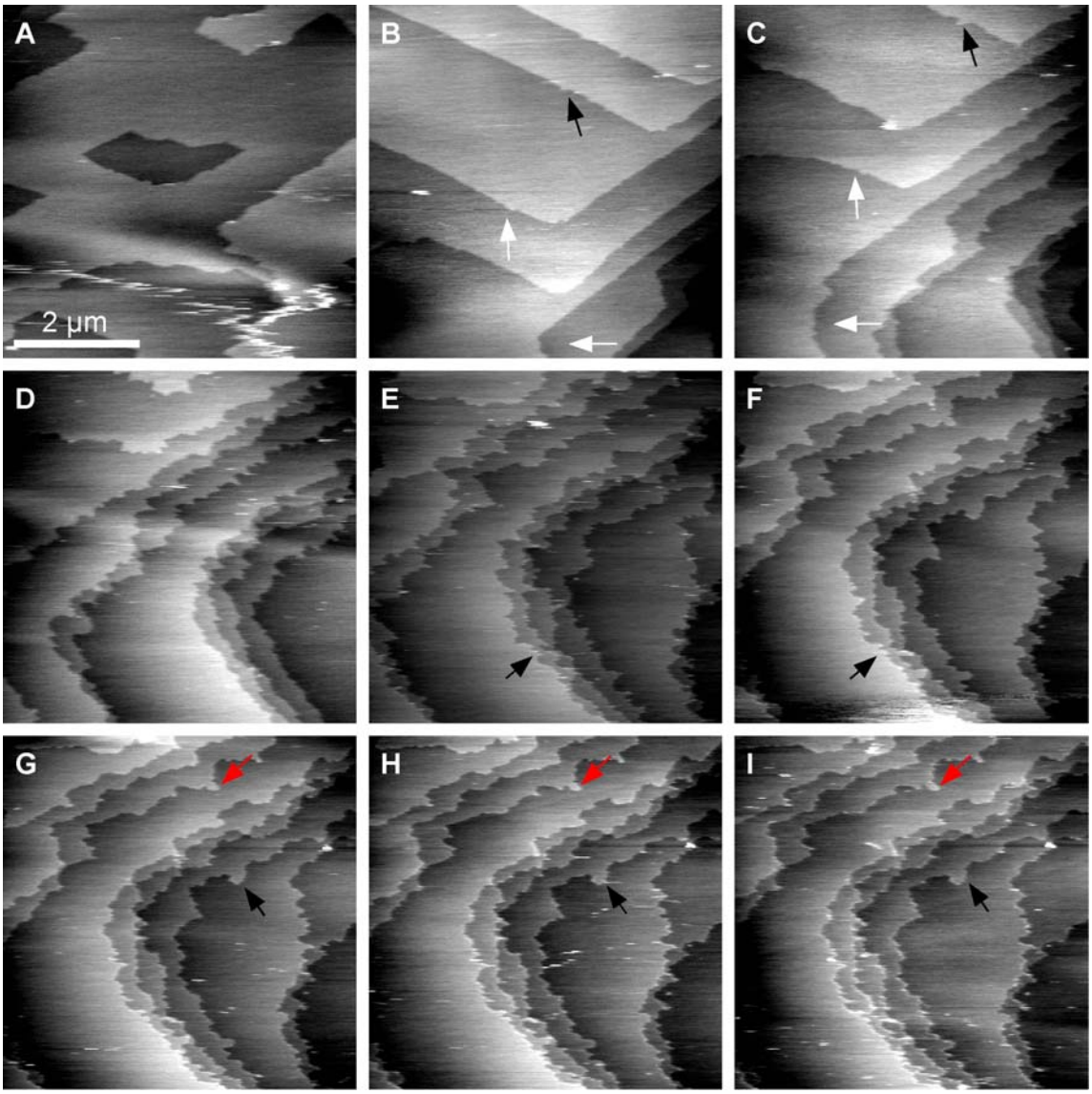

Fig. 4.35. AFM measurements of the interaction of perlinhibin with a geological calcite surface ([4 $\underline{4}$ $\underline{1}$] cleavage plane). A. Calcite surface imaged in ultrapure water. The calcite surface was initially characterized by rhombohedral voids with a depth of 0.4 nm, which corresponds to atomic monomolecular layers. Spontaneous dissolution layer-by-layer of the calcite surface was observed. (Data not shown). B-I. Consecutive images of a freshly cleaved calcite surface incubated with a 7.5 mM $CaCl_2$ solution containing perlinhibin (20 µg/ml). After exchanging the solution in the fluid cell perturbations, a progressive sample drift along the upper-right direction was visible. B-E. Perlinhibin caused a visible modification of the calcite edges (white arrows), while the crystal layers remained unmodified. Perlinhibin molecules bound specifically to calcite steps (black arrows) retarding and afterwards completely suppressing the dissolution of the calcite layers. Mineral dissolution only took place where perlinhibin was not bound. The inhibiting effect seems to occur by adsorption and pinning at step edges to kinetically impede step flow during layer dissolution.

After 20 min the surface remained unmodified due to the inhibitory effect of perlinhibin. The white and red arrows (F-I) point to some surface features, which evidently did not modify with time. Scan rate 6 Hz, 512 lines/sample, 3 min between two images.

By measuring the height of the ridges at the point, where perlinhibin molecules were bound (fig. 4.36), an enhancement of 0.4 – 0.5 nm was estimated.

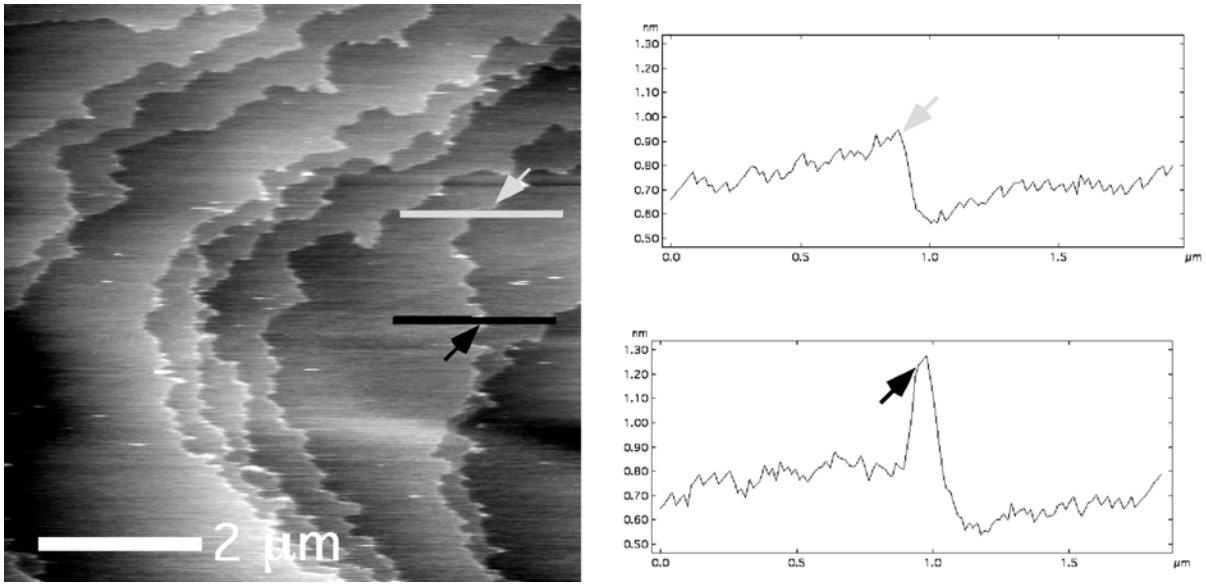

Fig. 4.36. Left. AFM image of calcite surface incubated with perlinhibin dissolved in a calcium chloride solution (as shown in fig. 4.35, I). Perlinhibin molecules bound to step edges of the monomolecular layers. The drawn black line indicates a site where perlinhibin is bound to the calcite edges. The grey line is place at a site where proteins did not bind. The relative plot profiles are shown on the right. Right. Profile plot of the calcite surface without bound proteins (above) and with proteins (bottom). Where perlinhibin was bound, a step enhancement of 0.4 – 0.5 nm was observed.

AFM investigations with perlinhibin dissolved in a supersaturated calcium carbonate solution

Further AFM investigations were carried out incubating a freshly cleaved calcite surface with perlinhibin dissolved in a supersaturated calcium carbonate solution (pH 8.2), to investigate the influence of perlinhibin on crystal growth. Perlinhibin, purified by ion exchange chromatography, was dialyzed against a supersaturated calcium carbonate solution (pH 8.2) as described in section 3.2. The final protein concentration was 20 µg/ml. AFM investigations was carried out at room temperature (scan rate of 3 Hz with 512 sample/lines).

The surface of calcite crystal, cleaved along the [4 $\underline{4}$ $\underline{1}$] plane, was initially imaged in ultrapure water. Calcite presented a flat surface characterized by flat plane with a curved profile maybe due to a not perfect cleavage or crystal defects (fig. 4.37, A).

During imaging the aqueous solution in the fluid cell was exchanged against a supersaturated $CaCO_3$ solution with perlinhibin (20 µg/ml). After 2 minutes incubation the surface appeared littered with white points, corresponding to perlinhibin molecules. An initial growth of the monomolecular layers on the top of the surface was visible (fig. 4.37, B, white arrows). After 1 hour of incubation (fig. 4.37, C) the growing monomolecular layers became confluent forming a mostly flat homogenous surface. Hole formation (black arrows) was visible which was the direct consequence of perlinhibin adhesion to calcite steps. Perlinhibin seemed to inhibit the growth at adhesion point. Growth of new layers was only possible where perlinhibin was not bound. The same surface imaged after 5 hours (fig. 4.37, D), 10 hours (fig. 4.37, E) and 20 hours (fig. 4.37, F). During this long time interval, the formation of new layers and deepening of the holes, due to the growth of mineral layers surrounding the protein-binding site, were observed.

Fig. 4.37. (Next page) AFM images of a freshly cleaved calcite surface incubated with perlinhibin (20 µg/ml) dissolved in a supersaturate calcium carbonate solution (pH 8.2) at room temperature. A. Calcite surface imaged in ultrapure water. Dissolution of mineral layers took spontaneously place. The round profile of some steps was possibly caused by cleavage of the crystal or crystal defects. B. The same surface of A imaged after 2 min of incubation with supersaturated $CaCO_3$ with perlinhibin. Formation of new monomolecular layers was visible (white arrows). C. The same surface imaged after 1 hour. Growing layers became confluent forming a mostly flat homogenous layer. Hole formation (black arrows) was visible and causes by the adhesion of perlinhibin to calcite steps. Perlinhibin inhibited the mineral growth at certain spots at the edge of the calcite layers. Mineral growth was only possible where perlinhibin was not bound. D. The same surface imaged after 5 hours, after 10 hours (E) and after 20 hours (F). Formation of new mineral layers took place.

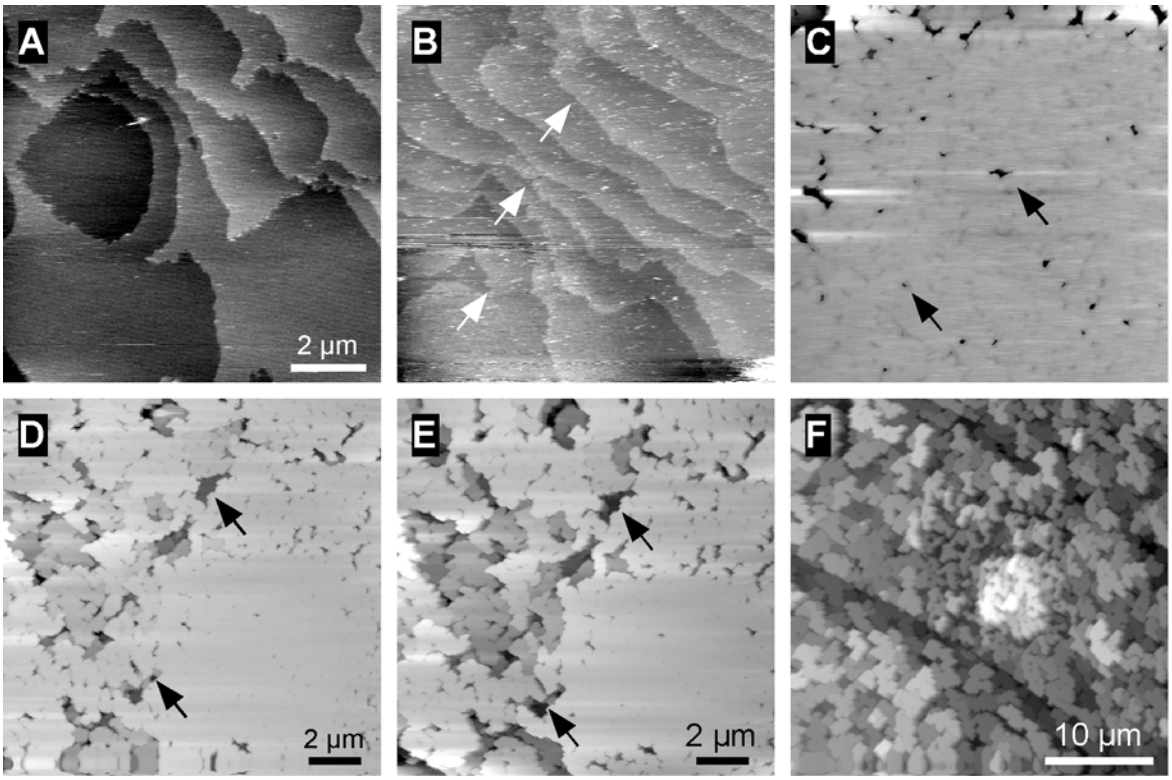

XRD investigation of calcite incubated with a supersaturated calcium carbonate solution with perlihinibin

The calcite surface, previously investigated by AFM (see previous section) and incubated for 20 hours with a supersaturated calcium carbonate solution (pH 8.2) with perlinhibin (20 µg/ml), was investigated by X-ray diffraction. The X-ray diffraction pattern (fig. 4.38) showed several peaks corresponding to calcite, aragonite and mica. A peak corresponding to aragonite suggested that perlinhibin induced *in vitro* the polymorph transition at ambient conditions. The formation of aragonite can be only addressable to the effects of perlinhibin. Some peaks corresponded to mica. Mica, a silicate mineral, was used as sample holder used for AFM investigations.

Fig. 4.38. (Next page) XRD diffraction pattern of geological calcite incubated for 20 hours with a supersaturated $CaCO_3$ solution with perlinhibin (20 µg/ml). The presence of the aragonite peak indicated that perlinhibin induced the formation of aragonite on the calcite substrate. The formation of aragonite can be only addressable to the effects of perlinhibin. The peaks corresponding to mica, a silicate, were induced from the substrate were the calcite crystal was glued for AFM investigations.

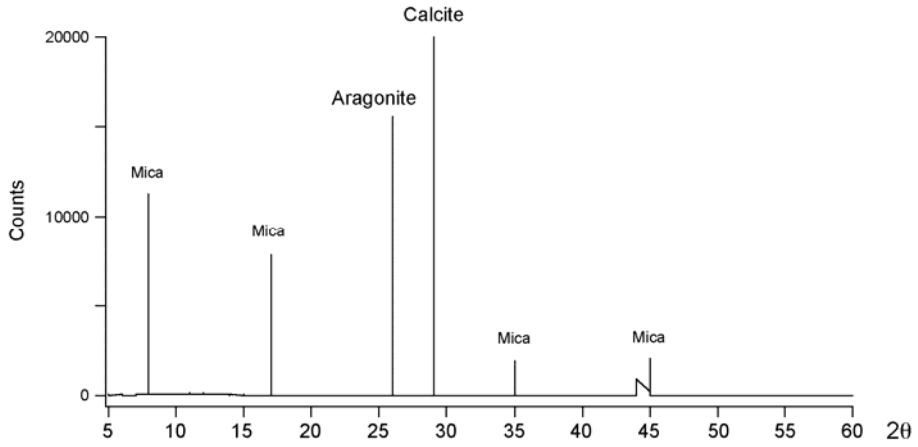

4.5.3 Discussion

The influence of perlinhibin *in vitro* on crystallization of calcium carbonate revealed that perlinhibin can strongly control the nucleation and formation of calcium carbonate crystals and it is able to induce polymorph transition. The ammonium carbonate method in parallel with AFM investigations showed that the inhibitory mechanism is very specific. Perlinhibin molecules can bind preferable to mineral edges, inhibiting the growth or the dissolution of calcium carbonate at the adhesion point.

The ammonium carbonate vapour diffusion method suggested that perlinhibin molecules, adsorbed on the calcite surface, modified the growth rate of certain faces of the precipitated crystals, which presented a cubic habit rather than rhombohedric.

The formation of aragonite on a calcite substrate took place at ambient conditions indicated that perlinhibin exerts a control over the polymorph selection. Aragonite precipitation at ambient condition does not spontaneously take place. Only the presence of metal ions, as magnesium, or additives can induce the formation of aragonite. The formation of aragonite at ambient conditions was also observed during the investigation of the intracrystalline proteins. This can suggest that perlinhibin and intracrystalline proteins can control *in vivo* the nucleation and growth of aragonite platelets or regulate the polymorph transition during mollusc shell formation.

4.6 Interactions of poly-γ-methyl-L-glutamate with calcium carbonate

The influences of poly-γ-methyl-L-glutamate (PMG) on calcium carbonate crystallization were investigated with two different techniques. The precipitation of calcium carbonate in a supersaturated $CaCO_3$ solution with PMG was monitored. In parallel the nucleation of calcium carbonate crystals in presence of PMG was investigated using the ammonium carbonate vapour diffusion technique.

4.6.1 Precipitation of calcium carbonate with poly-γ-methyl-L-glutamate

Poly-γ-methyl-L-glutamate was mixed with a supersaturated calcium carbonate solution and incubated for 5 days. Visible white crystals, formed at the bottom of reagent glasses, were collected by centrifugation and investigated by scanning electron microscopy (fig. 4.41). The crystals presented a tablet-like structure, a non-homogeneous size (approximately from less than 1 μm to 30 μm) and variable thickness. The surface of the platelets appeared mostly flat. The morphology of the crystals precipitated is roughly similar to that of purified nacre tablets (see fig. 4.1).

Fig. 4.41. (Next page) SEM images of crystals obtained after precipitation of saturated $CaCO_3$ solution supplied with PMG. A. Overview of the sample. B-C. Progressive magnification of the sample. Crystals with a platelet-like shape were found. The crystals presented a non-homogenous size distribution (from less than 1 μm to 30 μm) and a shape similar to that of purified nacre tablets (see fig. 4.1).

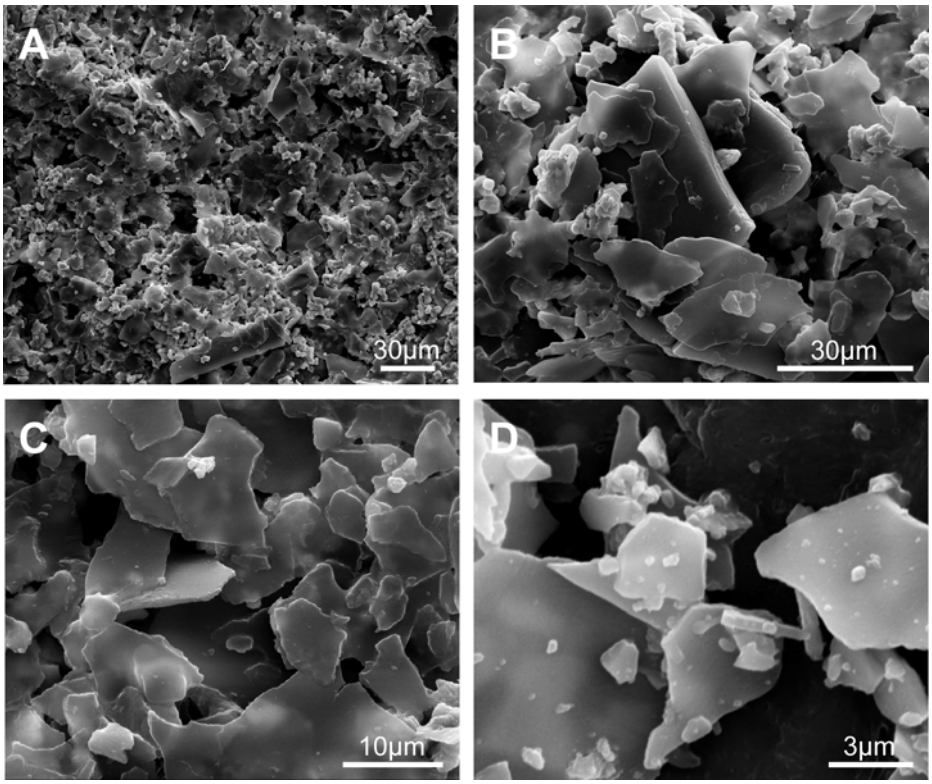

4.6.2 Cocrystallization of calcium carbonate with poly-γ-methyl-L-glutamate

The crystals grown with the vapour diffusion technique were investigated by scanning electron microscopy (fig. 4.42).

Single crystals with a size comprised between 30 and 50 µm were found, as well polycrystallites. The crystals, with a cubic habit resembling the main calcite morphology, where characterized by a step-like structure. This may indicate that the growth of the crystals was the result of progressive nucleation of new layers on the pre-existing ones (black arrows). All the layers appeared parallel to each other with the same orientation on all the three spatial directions. Crystal aggregates present a random orientation and they maybe originated by confluent grow of single crystals. The main characteristics, as cubic habit and stepped structure, were maintained.

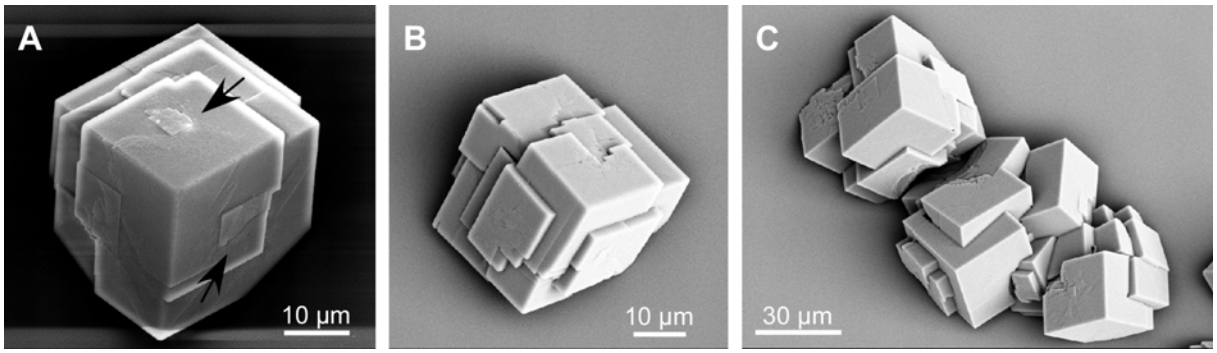

Fig. 4.42. SEM images of calcium carbonate crystals grown with ammonium carbonate vapour diffusion technique in the presence of PMG. A-B. Single crystals presented a cubic shape and a size of approximately 30 µm. Secondary step-like structures formed on the crystal faces, suggesting that the growth of the crystal may be a layer-by-layer process. The nucleation of new layers on the pre-existing ones is visible (black arrows). C. Polycrystallites. Polycrystallites are made of confluent single crystals randomly oriented. The main feature of the single crystals, as cubic shape and step-like structure, is clearly recognizable.

4.6.3 Discussion

The crystals obtained with the two different methods presented interesting characteristics. In particular the crystals precipitated from the calcium carbonate solution have a shape similar to the natural nacre platelets. The crystal precipitated with the vapour diffusion technique showed analogies with the crystals precipitated in presence of perlucin in low concentration (fig. 4.32). The stepped structure and the nucleation of mineral layer with the same orientation were the main common features.

It stated out that poly-γ-methyl-L-glutamate could be a valid candidate for the investigation and design of synthetic material with morphologies similar to that of natural nacre.

More in general synthetic polymers, now days available in large quantity can be specifically designed with selected properties of interest. Polymers with structures similar to the natural nacre proteins may help to find new straightforward ways to create new composite material and at the same time furnish a valid help to clarify of many aspects of natural nacre formation.

5 Conclusions and perspectives

5.1 Conclusions

Nacre is a fascinating biogenic material made of calcium carbonate, proteins and other organic molecules. Nacre presents mechanical properties that far exceed those of the pure components, it is highly resistant against corrosion even in seawater and it has a beautiful appearance shining in all rainbow colours. Even more fascinating is the fact that a self-organizing process guided by organic macromolecules creates nacre. Proteins specifically control and regulate the nucleation and growth of the mineral phase, influencing the crystal morphology and polymorph selection.

The aim of this thesis was a further elucidation of the mechanisms of interaction between native nacre proteins of the green lip abalone (*Haliotis laevigata)* with calcium carbonate in solution and calcium carbonate minerals.

First of all new strategies to extract and purify nacre proteins in their native and functional state had to be developed. This provided the basis for the next step, the investigation of the interaction of the nacre proteins with calcium carbonate in solution and with calcium carbonate minerals.

In particular the function of the intracrystalline proteins, a group of proteins that was characterized for the first time in nacre of *H. laevigata*, and the already sequenced nacre proteins perlucin and perlwapin were elucidated. It could be shown that each nacre protein presents a very specific and unique function. In addition to that the influence of poly-γ-methyl-L-glutamate, a synthetic polymer, which may mimic nacre proteins, on calcium carbonate mineralization was investigated.

5.1.1 Intracrystalline proteins

An important part of this thesis was focused on the search, purification and characterization of the intracrystalline proteins, a new group of proteins embedded in single nacre aragonite platelets.

By using biochemical techniques and small angle neutron scattering, it could be clearly shown for the first time that proteins are included in the aragonite platelets of nacre. With small angle neutron scattering the size of the intracrystalline proteins was determined to be 40 Å and their content at 3-4% of the platelet volume.

The best way to purify these proteins turned out to be the methanol – chloroform precipitation after dissolution of purified aragonite platelets. Three main intracrystalline proteins with a molecular weight of 6, 14 and 25 kDa were obtained. Unfortunately a further isolation of this three-protein mixture was not achieved. The behaviour of the intracrystalline proteins during gel electrophoresis and ion exchange chromatography suggested that they are possibly negatively charged. The possibly acidic nature of the proteins and the purification difficulties were also reported by other groups [Fu et al., 2005; Gotliv et al., 2003].

The investigation of the influence of the intracrystalline proteins on a growing calcite surface with atomic force microscopy revealed a strong surface modifying effect of these proteins. After the incubation of the proteins on the calcite surface it could be shown that a polymorph transition to aragonite had taken place. In contrast to that, the intracrystalline proteins showed an inhibitory effect on crystallization, when added to a supersaturated calcium carbonate solution.

It can be stated that the interaction of the intracrystalline proteins with calcium carbonate is very strong, possibly depending to their proposed acidic nature. The reason for the different behaviour of the proteins, in a supersaturated solution and on a crystal surface is unclear.

5.1.2 Perlucin

A new assay for the extraction of the nacre water-soluble protein perlucin was developed. A ball mill to prepare nacre for protein extraction was used for the first time. By using this method almost pure perlucin in its native state could be obtained.

The reason for this is unclear; a possible explanation is that during ball milling other nacre proteins get degraded, maybe due to lower temperature stability.
By cocrystallization of calcium carbonate with native perlucin, crystals characterized by a stepped morphology due to the nucleation of new layers were obtained. All newly nucleated crystal faces presented a parallel orientation to the faces beneath. This result was in accordance with previous investigations that showed that perlucin is able to nucleate flat mineral layers on a calcite surface [Treccani et al., 2003; Blank et al., 2003].

5.1.3 Perlinhibin

It could been shown that perlinhibin, a small water-soluble protein, is an inhibitor calcium carbonate crystal growth. When incubated on a calcite surface with a supersaturated calcium carbonate solution perlinibin adheres to mineral step edges and inhibits the growth of new mineral at the binding site. Further more it could be shown that perlinhibin has the capability to induce aragonite formation. The complementary ability of perlinhibin to suppress the growth of calcite and induce the formation of aragonite suggests that this small protein is maybe involved in the highly controlled polymorph regulation.

5.1.4 Poly-γ-methyl-L-glutamate

Crystallization of calcium carbonate with poly-γ-methyl-L-glutamate induces the precipitation of flat crystals, with a shape similar to that of natural aragonite platelets. The crystals precipitated with the vapour diffusion techniques presented a stepped morphology, also found in the crystals precipitated with perlucin at very low concentrations. The common features between the calcium carbonate crystals precipitated in presence of poly-γ-methyl-L-glutamate and perlucin may be an indication of some analogies between the molecular structure of poly-γ-methyl-L-glutamate and perlucin.
Because poly-γ-methyl-L-glutamate seems to interact with calcium carbonate in a way similar to that of nacre proteins, poly-γ-methyl-L-glutamate might provide a valid candidate to model the interactions taking place between native nacre molecules and

calcium carbonate minerals to gain a better understanding of the process at the atomic scale.

5.2 Perspectives

The intracrystalline proteins in nacre of *H. laevigata* need further investigation. Each single component has to be isolated and its structure as function as well should be characterized. This may lead to a more precise and detailed understanding of the protein-mineral interactions.

Besides the characterization of intracrystalline proteins, other water-soluble proteins have to be investigated. A wider amount of information about the protein structure may lead to a better understanding of their role in nacre formation. Because the formation of nacre is a result of the cooperative interaction of all its organic molecules and proteins, more information about the interplay – spatial and temporal - of the different organic components has to be obtained.

In addition to that, the interactions of the soluble organic - matrix components with the insoluble matrix, especially with chitin should be elucidated. This is of special importance because recent investigations from our lab showed that the water-insoluble matrix induces *in vitro* the formation of stacks of aragonite platelets [Heinemann et al., 2006]. It seems likely that soluble matrix components are partially bound to the water - insoluble chitin matrix during growth of nacre, maybe working as crystallization nucleators when bound to a surface and inhibitors, when dissolved.

Besides the clarification of the processes involved in the nacre formation *in vivo*, synthetic molecules which template or influence mineral formation in a desired way should be found. This may lead the way to novel composite materials with tuneable properties. On the other side the investigation of such synthetic molecules in calcium carbonate mineralization may also help to understand the principles of biomineralization.

6 Appendix

6.1 Publications

1. **Treccani L.**, Koshnavaz S., Blank S., vonRoden K., Schulz U., Weiss I., Mann K., Radmacher M., Fritz M., *Biomineralizing proteins with emphasis on invertebrate-mineralized structures*, peer-reviewed chapter in the multi-volume series: Biopolymers, volume 18, chapter 11, p. 289-321 (VCH, Weinheim) 2003

2. Blank S., Arnoldi M., Koshnavaz S., **Treccani L.**, M. Kuntz, K. Mann, G. Grathwohl, M. Fritz, *The nacre protein perlucin nucleates calcium carbonate crystals*, 2003, J. Microscopy, **212**: 280-291

3. **Treccani L.**, Mann K., Heinemann F., Fritz M., *Perlwapin, an abalone nacre protein with three four-disulphide core (WAP) domains, inhibits the growth of calcium carbonate crystals,* 2006, Biophysical Journal, in press

4. Mann K., Siedler F., Treccani L., Fritz M., *Perlinhibin, a cystein-, histidine- and arginine-rich miniprotein from abalone (Haliotis laevigata) nacre inhibits in vitro calcium carbonate crystallization*, 2006, submitted Functional surface in Biology

5. Heinemann F., **Treccani L.**, Fritz M., *Abalone nacre insoluble matrix induces growth of flat and oriented aragonite crystals*, 2006, Biochem. Biophys. Res. Comm., **344**: 45-49

6. **Treccani L.,** Gummich M., Fritz M.**,** *One step purification of perlucin*, in preparation

6.2 Abbreviations

Å	Angstrøm [10^{-10} m]
AFM	Atomic Force Microscope - Atomic Force Microscopy
°C	Centigrade
Ca^{2+}-binding proteins	Calcium-binding proteins
Da, kDa	Dalton, kiloDalton
DHB	2,5-dihydroxybenzoic acid
DSC	Differential Scanning Calorimetry
EDTA	Ethyldiethylamineacetic acid
eV	electronvolt
g, mg, µg, ng	Grams, milligrams, mirograms, nanograms
h	Plank constant [h = 6,626 10^{-34} Js]
HPLC	High Pressure Liquid Chromatography
ICP	Intracrystalline protein
IEC	Ion Exchange Chromatography
K	Kelvin
$\boldsymbol{k}_i$; $\boldsymbol{k}_f$	Wave vectors
λ	wavelength
l, ml, µl	Litre, millilitre, microlitre
M	Mass
M, mM	Molar, millimolar
MALDI	Matrix Assisted Laser Desorption Ionisation
MS	Mass Spectroscopy
MW	Molecular Weight
MWCO	Molecular Weight Cut Off
pH	Unit for [H^+] concentration
PMG	Poly-γ-methyl-L-glutamate
SANS	Small Angle Neutron Scattering
SDS-PAGE	Sodium Dodecyl Sulfate Poly-Acrylamide Gel Electrophoresis
SEM	Scanning Electron Microscope - Scanning Electron Microscopy
TCA	Trichloroacetic acid
TFA	Trifluoroacetic acid
TOF (MALDI-TOF)	Time of Flight (MALDI-TOF)
TRIS	2-Amino-2-(hydroxymethyl)-1,3-propanediol
TRIS-HCl	2-Amino-2-(hydroxymethyl)-1,3-propanediol hydrochloride
UV-VIS	Ultraviolet-visible
XRD	X-ray Diffraction
Wt	Weight
z	Charge

6.3 Amino acid codes[29]

Amino acids	Three letter code	One letter code
Alanine	ala	A
Arginine	arg	R
Asparagine	asn	N
Aspartic acid	asp	D
Cysteine	cys	C
Glutamic acid	glu	E
Glutamine	gln	O
Glycine	gly	G
Histidine	his	H
Isoleucine	ile	I
Leucine	leu	L
Lysine	lys	K
Methionine	met	M
Phenylalanine	phe	F
Proline	pro	P
Serine	ser	S
Threonine	thr	T
Tryptophan	try	W
Tyrosine	tyr	Y
Valine	val	V

[29] From [Lottspeich and Zorbas, 1998].

6.4 Ammonium sulfate saturation for precipitation at 0°C

The following table shows the amount of solid ammonium sulfate (g/l) to be added to a protein solution of known ammonium sulfate concentration (rows) to reach a higher concentration (columns). The reported values are valid for 0° C. For precipitation at higher temperatures the amount of salt to add is higher due to an increase in $(NH_4)_2SO_4$ solubility [Holtzhauer, 1997].

I= initial $(NH_4)_2SO_4$ saturation (in %); **F**= final $(NH_4)_2SO_4$ saturation (in %)															
	F →	**10**	**20**	**30**	**40**	**45**	**50**	**55**	**60**	**65**	**70**	**75**	**80**	**90**	**100**
I ↓															
0		55	107	166	229	262	295	331	366	404	442	483	523	611	707
5		26	80	139	200	232	266	300	336	373	411	450	491	578	671
10			54	111	171	203	236	270	305	342	379	418	458	544	636
20				56	84	115	145	177	210	244	280	316	392	476	565
30					57	87	119	150	184	217	253	289	328	408	495
40						29	59	90	122	155	190	225	262	340	424
50							29	60	91	125	158	193	229	306	388
60								30	61	93	127	161	197	272	353
70										31	63	96	131	204	283
75												32	66	136	212
80													32	102	176
90														68	141
															71

6.5 List of manufacturers

AFM	„Nanoscope IIIa“, Digital Instruments, Santa Barbara,
AFM cantilevers	*MSCT-Sharpened contact microlevers with backside gold coating* Veeco Instrument, Mannhein, Germany
Ball mill	Fritsch GmbH, Idar-Oberstein, Germany
Fluid cell for AFM	Digital Instruments, Santa Barbara, CA, USA
Centrifuge	Sorvall RC-SB Refrigerated Superspeed Centrifuge, Sorvall DuPont, Germany
	Biofuge primoR, Heraus, Germany
BSA IgG and albumin	Sigma Aldrich Chemie GmbH, Steinheim, Germany
Chemicals	Sigma Aldrich Chemie GmbH, Steinheim, Germany Merck KGaA, Darmstadt, Germany Carl Roth GmbH, Karlsruhe Germany
Chemicals for HPLC	Sigma Aldrich Chemie GmbH, Steinheim, Germany
Crystallization vessels	Nunc GmbH & Co. KG, Wiesbaden, Germany
Deionized water (ultrapure water)	Milli-Q® Ultrapure Water Purification Systems, Millipore GmbH, Eschborn, Germany
Dialysis membrane	Spectra/Por RC, MWCO 3500; MWCO 6 – 8000, Spectrum Laboratories, The Netherlands
Eppendorf reaction tubes	Eppendorf, Netheler, Hinz GmbH, Hamburg, Germany
Epoxy glue	Bindulin-Werk, H. L. Schönleber GmbH, Fürth i. Bay, Germany
Filter pads (0.22 µm Ø)	Durapore® Membrane filters, Millipore GmbH, Eschborn, Germany
Gels for electrophoresis	Invitrogen GmbH, Karlsruhe, Germany
HPLC-columns	GraceVydac, Hesperia, California, USA
HPLC-detector	Waters 2487 Dual λ Absorbance Detector, Waters GmbH, Eschborn, Germany
HPLC-system	Waters Delta 600 system, Waters GmbH, Eschborn, Germany
Ion exchange chromatography system	GradiFrac system with HiLoad Pump P-50, Amersham Pharmacia Biotech, Freiburg, Germany
Ion exchange chromatography columns	Amersham Pharmacia Biotech, Freiburg, Germany
MALDI analyzer	Ultraflex II TOF/TOF, Bruker Daltonic GmbH, Bremen, Germany
Mica	Plano W. Plannet GmbH, Wetzlar, Germany
Micro C-18 ZIP-TIP	Millipore GmbH, Eschborn, Germany
One-way cuvettes	Plastibrand, Brand, Wertheim, Germany
PH-meter	Sartorius AG, Goettingen, Germany
PMMA-cuvettes	Ratiolab GmbH, Dreieich, Germany
Sandblaster	Heinrich Schlick GmbH. Greven-Reckenfeld, Germany
Syringes (Injekt-F 1mL)	Braun Melsungen AG, Melsungen, Germany
Scanning Electron Microscope	Camscan Series 2, Cambridge Instruments, Cambridge, England
Sterile syringe nylon filters	NALGENE, Nalge Company, Rochester, NY, USA
Sandblasting agent	Asilikos ASIKOS Strahlmittel GmbH, Dinslaken, Germany
Sonicator	Bransonic 1510, Branson Ultrasonics B.V. Eemnes, The Netherlands
	Bandelin Sonoplus HD 70, model UW 70, Bandelin electronic, Berlin, Germany
Sputter coater	*Emitech K550*, EM Technologies Ltd., England EM Technologies Ltd., Ashford, Kent, England
Vacuum jar	NALGENE™ vacuum jar, Nalge Company, Rochester, NY, USA
Ultra Joy detergent	Procter & Gamble, Cincinnati, Ohio, USA
Ultrapure water	Milli-Q® Ultrapure Water Purification Systems, Millipore GmbH, Eschborn, Germany
UV pen ray lamp	UVP, San. Gabriel, CA, USA
UV-VIS spectrometer	Perkin-Elmer, Neuried, Germany

7 References

Addadi L., and Weiner S., *Interactions between acidic proteins and crystals: sterochemical requirements in biomineralization*, 1985, Proc. Natl. Acad. Sci. USA, **82**: 4110-4114

Addadi L., Joester D., Nudelman F., and Weiner S., *Mollusk shell formation: a source of new concepts for understanding biomineralization processes*, 2006, Chem. Eur. J., **12**: 980–987

Addadi L., and Weiner S., *Control and design principles in biological mineralization*, 1992, Angew. Chem. Int. Ed. Engl., **31**: 153-169

Addadi L., and Weiner S., *Crystals, asymmetry and life*, 2001, Nature, **411**: 753-755

Addadi L., Weiner S., and Geva M., *On how proteins interact with crystals and their effect on crystal formation*, 2001, Zeitschrift für Kardiologie, **90 (3)**: 92-98

Arnoldi, M., *Kraftmikroskopische Untersuchungen an biolologischen Material*, 2001 Shaker Verlag

Ashurst W.R., Yau C. Carraro C. Maboudian R., and Dugger M.T., *Dichlordimethylsilane as a comparison as an anti-stiction monolayer for MEMS: a comparison to the octadecyltricholrsilane self-assembled monolayer,* 2001, J. Microelectromech. Sys., **10**: 41-49

Atkins P., *Physical chemistry*, 2002. Oxford University Press

Baier R.E., and Zisman W.A., *The influence of polymer conformation on the surface protperies of poly(γ-methyl-L-glutamate and poly(benzyl glutamate)*, 1970, Macromol., **3**: 70-79

Becker A., Becker W., Marxen J.C., and Epple M., *In-vitro crystallisation of calcium carbonate in the presence of biological additives - comparison of the ammonium carbonate method with double-diffusion techniques*, 2003, Z. Anorg. Allg. Chem., **629**: 2305-2311

Belcher A.M., Wu X.H. Christensen R.J., Hansma P., Stucky G., and Morse D.E., *Control of crystal phase switching and orientation by soluble mollusc-shell proteins,* 1996, Nature, **381**: 56-58

Bimmler D., Graf R., Scheele G.A., and Frick T.W., *Pancreatic stone protein (lithostathine), a physiologically relevant pancreatic calcium carbonate crystal inhibitor?*, 1997, J. Biol. Chem. **272 (5)**: 3073-82

Binnig G., Quate, C. F., and Gerber C., *Atomic force microscope*, 1986, Phys. Rev. Lett. **56**: 930-933

Binnig G., and Rohrer H., *Scanning tunneling microscope*, 1982, Helv. Phys. Acta, **55**: 726-735

Blank S., Direkte Beobactung der enzymatische Aktivität einzelner alkalischer Phosphatasemoleküle - eine kraftmikrosckopische Studie, Doctoral dissertation

Block H., *Poly(γ-Benzyl-L-Glutamate) and other Glutamic Acid Containing Polymers*, 1983, Gordon and Breach Publishers, New York

Bradford M.A., *A rapid and sensitive method for the quantitation of micrograms quantities of protein utilizing the principle of protein-dye binding*, 1976, Anal. Biochem., **72**: 248-254

Chou L., Garrels R. M., and Wollast R., *Comparative study of the kinetics and mechanisms of dissolution of carbonate minerals*, 1989, Chem. Geol., **78**: 269-282

Churchill H., Teng H., and Hazen R.M., *Measurements of pH-dependent surface charge with atomic*

force microscopy: implications for amino acid adsorption and the origin of life, 2004, American Mineralogist **89 (7)**: 1048-1055

Cooper T.G., *Biochemische Arbeitsmethoden*, 1980, De Gruyter & Co

Covey-Crump S.J., *The normal grain growth behaviour of nominally pure calcitic aggregates*, 1997, Contrib. Mineral Petrol, **129**: 239-254

Crick R.E., *Origin, evolution, and modern aspects of biomineralization in plants and animals*, 1999, Plenum Press, New York,

Currey J.D., *Mechanical properties of mother of pearl in tension*, 1977, Proc. R. Soc. Lond. B, **196**: 443-463

Currey J.D., and Kohn A.J., *Fracture in crossed-lamellar structure of Conus shells*, 1976, J. Mater. Sci, **11**: 1615-1623

Currey J.D., and Taylor J.D., *The mechanical behaviour of some molluscan hard tissues*, 1974, J. Zool. Lond, **173**: 395-406

Dauphin Y., and Cuif J.P., *Isoelectric properties of the soluble matrices in relation to the chemical composition of some Scleractinian skeletons,* 1997, Electrophoresis, **18**: 1180-1183

Davis K.J., Dove P.M., and De Yoreo J.J., *The role of Mg* $^{2+}$ *as an impurity in calcite growth,* 2000, Science, **290**: 1134-1137

Dreybrodt W., *Process in Karst systems*, 1988, Springer-Verlag

Falini G., Albeck S., Weiner S., and Addadi L., *Control of aragonite or calcite polymorphism by molluscs shell macromolecules,* 1996, Science, **271**: 67-69

Falini G., Fermani S., Gazzano M., and Ripamonti A., *Polymorphism and architectural crystal assembly of calcium carbonate in biologically inspired polymeric matrices*, 2000, J. Chem. Soc. Dalton Trans.: 3983-3987

Falini G., Weiner S., and Addadi L., Chitin silk-fibroin interactions: relevance to calcium carbonate formation in invertebrates, 2003, Calc. Tissue Int, **27**: 548-554

Friedman G.M., *Identification of carbonate minerals by staining methods*, 1959, J. Sedim. Petrology, **29**: 87-97

Fritz M., Belcher A.M., Radmacher M., Walters D.A., Hansma P., Stucky G., Morse D.E., and Mann S., *Flat pearls from fabrication of organized composites on inorganic substrates,* 2002*,* Nature, **371**: 49-51

Fritz M., and Morse D.E., *The formation of highly organized biogenic polymer-ceramic composite materials: the high-performance microlaminate of molluscan nacre,* 1998*,* Current Opinion in Colloid & Interface Science, **3**: 55-62

Fu G., Valiyaveettil S., Wopenka B., and Morse D.E., *CaCO3 biomineralization: acidic 8-kDa proteins isolated from aragonitic abalone shell nacre can specifically modify calcite crystal morphology,* 2005, Biomacromolecules, **6**: 1289-1298

Gerbaud V., Pignols D., Loret E., Bertrand J.A., Berland Y., Fontecilla-Camps J.C., Canselier J.P., Gabas N., and Verdier J.M., *Mechanism of calcite crystal growth inhibition by the N-terminal undecapeptide of lithostathine,* 2000, J. Biol. Chem., **275**: 1057-1064

Gillgren H., Stenstam A., Ardhammar M., Norden B., Sparr E., and Ulvenlund S., *Morphology and Molecular conformation in thin films of poly-*γ*--methyl-L-glutamate at the air-water interface*, 2002, Langmuir, **18**: 462-469

Goldberg H.A., and Warner K.J. *The staining of acidic proteins on polyacrylamide gels: enhanced sensitivity and stability of "Stains-All" staining in combination with silver nitrate,* 1997, Analytical

biochemistry, **251:** 227–233

Gotliv B., Addadi L., and Weiner S., *Mollusk shell acidic proteins: insearch of individual functions,* 2003, Chem, Biochem, **4**: 522-529

Grats A.J., Hillner P.E., and Hansma P.K., *Step dynamics and spiral growth on calcite,* 1993, Geochim. Cosmochim. Acta, **57**: 491-495

Hagiwara, K., Kikuchi, T., Endo, Y., Huqun, Usui, K., Takahashi, M., Shibata, N., Kusakabe, T., Xin, H., Hoshi, S., Miki, M., Inooka, N., Tokue, Y., and Nukiwa, T., *Mouse SWAM1 and SWAM2 are antibacterial proteins composed of a single whey acidic protein motif,* 2003, J. Immunology, **170 (4)**: 1973-1979

Hammouda B., A *tutorial on small angle neutron scattering from polymers,* 1995, National Institute of Standards and Technology Materials Science and Engineering Laboratory Gaithersburg, MD 20899

Hattan S. J., Laue T. M., and Chasteen N.D., *Purification and characterization of a novel calcium-binding protein from the extrapallial fluid of the mollusc, Mytilus edulis,* 2001, J. Biol. Chem., **276**: 4461-4468

Heinemann F., *Nukleation und Wachstum von Modulierten Kalziumkarbonate Kristallen durch Biopolymere*, 2005, Diploma thesis, Institut of Biophysics, University of Bremen

Heuer A.H., Fink D.J., Laraia V.J., Calvert P.D., Kendall K., Messing G.L., Blackwell J., Rieke P.C., Thompson D.H., Wheeler A.P., Veis A., Caplan A.I., *Innovative materials processing strategies: a biomimetic approach,* 1992, Science*,* **255**: 1098-1105

Hillner P.E., Grats A.J., Manne S., and Hansma, P.K., *Atomic scale imaging of calcite growth and dissolution in real time*, 1992, Geology, **20**: 359-362

Ho R., Yuan J.Y., and Shao Z., *Hydration force in the atomic force microscope: a computational study*, 1998, Biophysical J., **75**: 1076-1083

Högfeldt E., *Stability constants of metal-ion complexes. Part A: inorganic ligands*, 1982, Pergamon, Oxford

Hofmeister F., *Zur Lehre von der Wirkung der Salze*, 1888, Zweite Mittheilung. Arch Exp Pathol. Pharmakol, **24**: 247-260.

Holtzhauer M., *Biochemische Labormethoden,* 1997, Springer-Verlag Berlin Heidelberg

Jackson A.P., Vincent J.F.V., and Turner R.M., *The mechanical design of nacre*, 1988, Proc. R. Soc. Lond. B., **234**: 415-440

Kazmlerczak T. F., Tomson M.B., and Nancollas G.H., *Crystal growth of calcium carbonate. A controlled composition kinetic study*, 1982, J. Phys. Chem., **86**: 103-107

Kevin P. Campbell, MacLennan and Jorgessen A.O., *Staining of the Ca^{2+}-binding proteins, calsequestrin, calmodulin, troponin C, and S-100, with the cationic carbocyanine dye "Stains-all"*, 1983, J. Biol. Chem., **258 (18)**; 11267-11273

Kitano Y., Kanamori N., and Yoshioka S., *Influences of chemical species on the crystal type of calcium carbonate*, In: Watabe N., Wilber K.M., *Mechanism of mineralization in the invertebrates and plants*, 1976, University of South California Press, Columbia

Kido T., *Identification of calcitic and aragonitic otoconia by selective staining methods*, 1996, Acta Histochem. Cytochem., **29**: 121-127

Klepetsanis P.G., Kladi A., Koutsoukos P.G., and Amjad Z., *The interaction of water-soluble polymers with solid substrates. Implications on the kinetics of the crystal growth*, 2000, Progr. Colloid. Polym. Sci., **115**: 106-111

King S.M., *Small Angle Neutron Scattering.* In *Modern techniques for polymer characterisation,* Pethrick R. A. and Dawkins J.V. Editor, 1999, Wiley

Knitter R., Haußelt J., and Fritz M., *Thermal behaviour of nacreous layer of the abalone shell*, 2006 Mat. Sci. Eng. C , submitted

Krampitz G.P., *Structure of the organic matrix in mollusc shells and avian eggshells.* In *Biological mineralization and demineralization* (Nancollas, G.H., ed.), 1982, pp. 219–232, Berlin, Heidelberg, New York, Springer-Verlag

Laemmli U.K., *Cleavage of structural proteins during the assembly of the head of bacteriophage T4*, 1970, Nature, **227**: 680-685

Levi-Kalisman Y., Falini G., Addadi L., and Weiner S., *Structure of the nacreous organic matrix of a bivalve mollusk shell examined in the hydrated state using cryo-TEM*, 2001, J. Struct. Biol., **135**: 8–17

Lottspeich F., and Zorbas H., *Bioanalytik*, 1998, Spektrum Akademischer Verlag

Lowenstam H.A., and Weiner S., *On biomineralization*, 1989, Oxford University Press

Mann K., Weiss I., and Fritz M., *Evidence for a bikunin (inter α-trypsin inhibitor light chain) in the nacreous layer of the abalone (Haliotis laevigata) shell,* in preparation

Mann K., Weiss I., Andre´ S., Gabius H., and Fritz M., *The amino-acid sequence of the abalone (Haliotis laevigata) nacre protein perlucin,* 2000, Eur. J. Biochem., **267**: 5257-5264

Mann S., *Biomineralization*, 2001, UK Oxford University Press

Mann S., *Molecular tectonics in biomineralization and biomimetic material chemistry,* 1993, Nature, ***365***: 499-505

Mann S., Archibald D.D., Didymus J.M., Douglas T., Heywood B.R., Meldrum F.C., and Reeves N.J., *Crystallization at inorganic-organic interfaces: biominerals and biomimetic synthesis,* 1993, Science, **261**: 1286-1292

Marin F., Corstjens P., de Gaulejac B., de Vrind-De Jong E., and Westbroek P., *Mucins and molluscan calcification,* 2000, J. Biol. Chem., **275**: 20667-20675

McGrath K.P., Fournier M.J., Mason T.L., and Tirrell D.A., *Genetically directed syntheses of new polymeric materials. Expression of artificial genes encoding proteins with repeating -(AlaGly)3ProGluGly- elements,* 1992, J. Amer, Chem. Soc., **114**: 727-733

Meldrum F.C., *Calcium carbonate in biomineralisation and biomimetic chemistry*, 2003, Int. Mat. Reviews, **45**: 187-224

Mortimer C.E., *Chemie*, 1996, Georg Thieme Verlag, Stuttgart

Nakahara H., *Calcification of the gastropod nacre*, 1983, In Westbroek P., De Jong E.W. (ed) *Biomineralization and biological metal accumulation*, D. Reidel Publishing Company: 225-230

Nakahara H., Belavender G., and Kakei M., *Electron microscopic and amino acid studies on the outer and inner shell layer of* Haliotis Rufescens, 1982, Venus, **41**: 36-46

Oaki Y., and Imai H., *The hierarchical architecture of nacre and its mimetic material,* 2005, Angew. Chem. Int. Ed., **44**: 6571-6575

Ohtaki H., *Crystallization processes,* 1998, John Wiley & Sons

Parsegian A., *Intermolecular forces,* 2001, Biophysical Society

Patel R.C., Boe R.J., Atkinson G., *The CO_2-water system. I. Study of the slower hydration-dehydration step*, 1973, J. Sol. Chem., **2 (4)**: 357-372

Patterson S.D., and Aebersold R., *Mass spectrometric approaches for the identification of gel-separated proteins*, 1995, Electrophoresis, **16**: 1791-1814

Pynn R., *Neutron scattering, a primer,* 1990, Los Alamos Neutron Science Center

Raymond S., and Weintraub L., *Acrylamide gels as a supporting medium for zone electrophoresis*, 1959, Science, **130**: 711-

Redfern S.A.T., Salje E., and Navrotsky A., *High-temperature enthalpy at the orientational order-disorder transition in calcite: implications for the calcite/aragonite phase equilibrium*, 1989, Contrib. Mineral Petrol., **101**: 479-484

Roberts C.J., Davies M.C., Jackson D.E., and Tenoller S.J.B., *Towards the low-force imaging of biological and biomedical materials by Atomic Force Microscopy*, 1993, Nanobiology, **2**: 73-79

Rousseau M., Lopez E., Stempflé P., Brendlé M., Franke L., Guette A., Naslain R., and Bourrat X., *Multiscale structure of sheet nacre*, 2005, Biomaterials, **26**: 6254–6262.

Salje E., and Viswanathan K., *The phase diagram calcite-aragonite as derived from the crystallographic properties*, 1976, Contrib. Mineral. Petrol., **55**: 55-67

Sand D.E., *Introduction to crystallography,* 1975 Dover Publications, Inc., New York, 1975

Schaeffer T.E., Ionesco-Zanetti C., Proksch R., Fritz M., Walters D.A., Almqvist N., Zaremba C.M., Belcher A.M., Smith B.L., Stucky G., Morse D.E., and Hansma P., *Does abalone nacre forms by heteroepitaxial nucleation or by growth through mineral bridges?,* 1997, Chem. Mater., **9**: 1731-1740

Snow M.E., Pring A., Self P., Losic D., and Shapter J., *The origin of the color of pearls in iridescence from nano-composite structures of nacre*, 2004, American Mineralogist, **89**: 1353–1358

Szepesi G., *How to use reverse-phase HPLC*, 1992, VHC, New York

Teng H.H., Dove P. M., Orme C.A., and De Yoreo J.J., *Thermodynamics of calcite growth: baseline for understanding biomineral formation*, 1998, Science, **282**: 724-727

Thompson J.B., Paloczi G.T., Kindt J.H., Michenfelder M., Smith B.L., Stucky G., Morse D.E, and Hansma P., *Direct observation of the transition from calcite to aragonite growth as induced by abalone shell proteins,* 2000, Biophysical J., **79**: 3307-3312

Vincent J.F.V., *Ceramics from vertebrate animals,* from *Handbook of elastic properties of solids, liquids and gases,* 2001, edited by Levy, Bass and Stern

Yvon M., Chabanet C., and Pelissier J.P., *Solubility of peptides in trichloroacetic acid (TCA) solutions. Hypothesis on the precipitation mechanism*, 1989, Int. J. Pept.Protein Res., **34 (3)**: 166-176

Walters D.A., Smith B.L., Belcher A.M., Paloczi G.T., Stucky G.D., Morse D.E., and Hansma P.K., *Modification of calcite crystal growth by abalone shell proteins: an atomic force microscope study*, 1997, Biophys. J., **72**: 1425-1433

Wang R.Z., Suo Z., Evans A.G., Yao N., and Aksay I.A., *Deformation mechanism of nacre*, 2001, J. Mat. Res., **16 (9)**: 2485-2492

Weiner S., and Addadi L., *Design strategies in mineralized biological materials,* 1997, J. Mater. Chem., **7**: 689-701

Weiner S., Talmon, Y., Traub. W., *Electron diffraction studies of molluscan shell organic matrices and their relationship to the mineral phase*, 1983, Int.J. Biol. Macromol. **5**: 325-328

Weiner S., and Traub W., *Macromolecules in mollusk shells and their function in biomineralisation*, 1984, Phil. Trans. R. Soc. Lond. B, **304**: 425-434

Weisenhorn A.L., Hansma P., Albrecht T.R., and Quate C.F., *Forces in atomic force microscopy in air and water*, 1989, Appl. Phys. Lett., **54**: 2651–2653

Weiss I., *Molecular control of natural polymer-ceramic composite material on the model of nacre biomineralization*, 2000, Shaker Verlag

Weiss I., Kaufmann S., Mann K., and Fritz M., *Purification and characterization of perlucin and perlustrin, two new proteins from the shell of the mollusc Haliotis laevigata,* 2000, Biochem. Biophys. Res. Comm., **267**: 17-21

Weiss I., Göhring W., Fritz M., and Mann K., *Perlustrin, a Haliotis laevigata (Abalone) nacre protein, is homologous to the insuline-like growth factor binding protein N-terminal module of vertebrates*, 2001, Biochem. Biophys. Res. Comm., **285**: 244-229
Wessel und Fluegge

Wheeler A.P., George J.W., and Evans C.A., *Control of calcium carbonate nucleation and crystal growth by soluble matrix of oyster shell,* 1981, Science, **212**: 1397-1398

Wessel D., and Flügge U.I., *A method for the quantitative recovery of protein in dilute solution in the presence of detergents and lipids*, (1984) Anal. Biochem. **138**: 141-143